High Current Arc Modeling for Silicon Submerged Arc furnaces

Hákon Valur Haraldsson

Thesis of 240 ETCS submitted to the Department of Engineering at Reykjavík University And Norwegian University of Science and Technology. Faculty of Natural Sciences and Technology. Department of Materials Science and Engineering in partial fulfillment of the requirements for the double doctoral degree

June 12, 2025

Thesis Committee:

Guðrún Sævarsdóttir, Supervisor
Professor, Reykjavik University, Iceland

Yonatan A. Tesfahunegn, Co-advisor
Assistant Professor, University of Iceland, Iceland

Merete Tangstad, Co-advisor
Professor, Norwegian University of Science and Technology, Norway

Quinn Reynolds, Co-advisor
Associate Professor, University of Stellenbosch, South Africa

High Current Arc Modeling for Silicon Submerged Arc furnaces

Short title: High Current Arc Modeling for Silicon Submerged Arc furnaces

Hákon Valur Haraldsson (ORCID iD 0000-0001-8308-9415)

Bibliographic information: Hákon Valur Haraldsson, 2025, *High Current Arc Modeling for Silicon Submerged Arc furnaces*, PhD Thesis, Department of Engineering, Reykjavík University, 100 pp.

ISBN 978-9935-539-82-3 (print version)
ISBN 978-9935-539-83-0 (electronic version)

Contents

List of Figures

List of Tables

List of Symbols

As a rule symbols are defined as they appear in the text but for ease of access they are listed here as well. Vectors are denoted by bold lettering and mean values by a vertical line over each symbol. Volumetric variables are denoted by small letters and integral once by big letters. We make an exception for symbols used for electrical components where we use convention for electrical engineering where the RMS values for current are Large and time dependent once are small.

Notation	*Description*	*Unit*
i_{Ti}	Current in transformer i	A
V_{Ti}	Voltage in transformer i	V
R_{Ti}	Resistance in transformer i	Ω
L_{Ti}	Inductance in transformer i	H
$M_{Ti,Ti+1}$	Mutual inductance between transformer i and i+1	H
i_{ei}	Current in electrode i	A
V_{ei}	Voltage in electrode i	V
R_{ei}	Resistance in electrode i	Ω
L_{ei}	Inductance in electrode i	H
$M_{ei,ei+1}$	Mutual inductance between electrode i and i+1	H
i_{ci}	Current in charge from electrode i	A
R_{ci}	Resistance in charge i	Ω
i_{ai}	Current in arc from electrode i	A
V_{ai}	Voltage in arc i	V
f_S	Measurement frequency	Hz
i_{phi}	Measured phase current i	A
V_{phi}	Measured phase voltage i	V
V_{pi}	Voltage over arc and charge, phase i	V
R_{ai}	Variable arc resistance i	Ω
R_{si}	Short-circuit resistance i	Ω
L_i	electrode inductance in i	V
H_a	Arc length	m

Notation	*Description*	*Unit*
$\widehat{R_a}$	Arc resistance per unit length	Ω / m
θ_a	Arc time constant	s
V_0	steady-state static arc voltage	V
V_d	Voltage per arc length	V / m
V_{an}, V_{ca}	Anode and Cathode voltage	V
P_0	Momentary arc power loss	W
G_i	Arc conductance	S
G_{min}	conductance without arc	S
σ, σ_a	Electric conductivity	S / m
p_a	Arc pressure	Pa
ρ_a	Arc plasma density	kg/m^3
r_a	Arc radius	m
r_c	Arc cathode radius	m
p_a	Arc pressure	Pa
P_{el}	Electric power that the arc generates	W
P_{loss}	Arc power loss	W
P_{con}	Convective power transfer	W
P_{rad}	radiative power loss	W
P_{an}	Conductive power loss	W
$h(T_a)$	Arc enthalpy	$kg\ m^2/s^2$
$h(T_F)$	Enthalpy of arc the surroundings	$kg\ m^2/s^2$
T_a	Arc temperature	K
T_F	Arc surroundings temperature	K
$\upsilon_a(r)$	Arc gas velocity distribution	m/s
$\upsilon_{a,max}$	maximum gas velocity is along the arc axis	m / s
K_1	CAM current density profile	
j_c	cathode current density	A / m^2
K_2	CAM velocity profile	
$\overline{u}$	mean radiation density	
r_{eff}	effective radiation radius	m
Φ_{an}	the material work function for the anode	eV
r_{ac}	dynamic arc radius	m
$\overline{T}_{ac}$	Dynamic mean arc temperature	K
M_{dc}	Dc arc mass	kg
τ	CAM arc time constant	s
P_m	Power loss due to mass transfer	W
V_{ac}	CAM dynamic arc voltage	V
$P_{el,ac}$	CAM AC electric arc power	W

Notation	*Description*	*Unit*
D	flux density	C/m
H	magnetic field density	A / m
B	magnetic field	T
E	electric field	V / m
j	current density	A / m^2
u	MHD velocity field	m / s
P	MHD pressure field	Pa
h	MHD enthalpy field	$kg\ m^2/s^2$
κ	MHD plasma thermal conductivity	kg m $s^{-3}K^{-1}$
Q_R	radiation energy loss	J
Q_m	sink term for the energy equation	J
ϕ	electric potential	V
T_c	Cathode surface temperature	K
u_c	Sheath voltage potential	V
W	material work function	eV
ΔW	is the Schottky correction term	eV
n_{e0}	the electron density	/ m^3
$n_{i\infty}$	the ion density	/ m^3
c_e	Average electron velocity	m / s
T_pl	Plasma temperature	K
H_{vap}	vaporisation enthalpy	$kg\ m^2/s^2$
C_1	is the equilibrium pressure	Pa
T_{sub}	surface temperature during sublimation	K
p_a	is the ambient pressure	bar
j_e	thermionically emitted current	A / m^2
j_i	ion current density	A / m^2
$j_{e,pl}$	counter-diffusing plasma electrons	A / m^2
$\dot{q}_{sub}$	sublimation heat flux	j / s
L	slice thickness	m
G_0	mass transfer	kg / m^2 s
ϵ_0	vacuum electric permittivity	8.8542×10^{-23} F m^{-1}
μ_0	is the vacuum magnetic permeability	$4\pi \times 10^{-7}$ N / A^2
k_B	Boltzman constant	$1.380\,649 \times 10^{-23}$ J K^{-1}
q	electron charge	C
m_i	ion mass	7.3205×10^{-26} kg
m_e	electron mass	9.1093×10^{-31} kg
k_c	thermal conductivity of carbon	140 kg m $s^{-3}K^{-1}$

Acknowledgments

First of all, I would like to thank my now wife (at the start of this work we had recently started dating) Pernille for all the patience and support during my PhD studies. It has been an exciting time with many travels abroad and other work-related events. There has been one baby born during this time and another on the way at the end of this work, and this has been trying at times to fit everything that needs to be done into each day.

I would like to thank my Supervisor Prof. Guðrún Sævarsdóttir for all the support in solving practical and numerical issues related to the project, for all the patience when it came to my sometimes oversized teaching duties and the need to work from home. We also had many very interesting discussions about politics and ideas that were always interesting even if we sometimes did not agree completely.

I would like to thank my co-supervisors, first Yonatan at RU for all the help with practical implementation when it comes to CFD modeling and assistance when numerical solutions were not converging for days on end. Second, Merete Tangstad at NTNU for all the help while I was there taking courses and simply for introducing me to everyone and making sure i fit in.

I would also like to thank Quinn Reynolds for all the help and collaboration with modeling in openFOAM, helping with implementation of boundary conditions and debugging of the main solver, as well as fun talks and discussions.

Lastly I would like to thank all the people that worked with me in smaller parts of my work or were simply there to talk and offer encouragement.

Abstract

Electric arcs are a necessary heat source in many industrial processes that take place in Submerged Arc Furnaces (SAFs). Arcs exhibit non-linear electrical characteristics and behave in a complex manner. Therefore, an improved understanding of their behavior enables better control of furnace operation.

Modeling of industrial arcs is a multiphysics process that involves simultaneously solving several coupled physical phenomena, such as electromagnetics, fluid dynamics and heat transfer, including a radiative heat transfer from the plasma arc. Coupling fluid dynamics and electromagnetics is known as Magnetohydrodynamics (MHD). However, there are also simpler approaches to arc modeling, either based on simplified physical principles or empirical behaviour. Direct measurement of the arc characteristics is impossible due to hostile conditions inside the SAF, so controlling the heat dissipation is both a science and an art. The arcs exhibit non-linear electrical characteristics and behave in a complex manner.

We start by discussing a DAQ system gathering data from a FeSi SAF, the data is processed and used to determine various furnace conditions including arc and charge current as well as harmonics.

In this work, several computational models for arc are implemented. First a combined Cassie-Mayr model (CMM) and a channel arc model (CAM), are implemented and coupled with a submerged arc furnace electrical circuit model. The complete circuit model parameters such as resistances and inductances are estimated using measurements conducted on an operational furnace which are also used to validate the models. Both models are then used to estimate harmonic distortion in a SAF for different arc power ratios.

Secondly a MHD model implemented by the author is used to simulate alternating current arcs with different plasma gas compositions, and compared to second MHD model. The thermophysical properties of each composition are calculated using specialized code as well as gathered from literature. We investigate the dependence of the results on both the MHD models used and the input plasma data for three argon data sets and compare the results to data obtained from laboratory experiments. Finally, we investigate furnace conditions using different ratios

of SiO to CO gases.

Finally a new implementation of a special sub model for cathode and anode surface conditions is presented. The models is first used with the channel arc model and then integrated into the MHD model as a module. This model is used to investigate the electrode erosion as well as the sheat voltage present close the the plasma wall.

List of Publications

This work has also been published in papers as the work has progressed. The full papers are available in the abstract at the end of this thesis.

1. H. Haraldsson, Y. A. Tesfahunegn, M. Tangstad, *et al.*, "Modelling of Electric Arcs for Industrial Applications, a Review," *SSRN Journal*, 2021, ISSN: 1556-5068. DOI: 10.2139/ssrn.3927158

2. H. V. Haraldsson, H. Traustason, Y. A. Tesfahunegn, *et al.*, "Measuring and processing of electrical parameters in a submerged arc furnace," in *Materials Processing Fundamentals 2023*, 2023, pp. 161–170, ISBN: 978-3-031-22657-1. DOI: 10.1007/978-3-031-22657-1_14

3. H. V. Haraldsson, H. Traustason, Y. A. Tesfahunegn, *et al.*, "Modeling and comparison study of industrial AC-arcs," *Metallurgical and Materials Transactions B*, Jul. 24, 2024, ISSN: 1543-1916. DOI: 10.1007/s11663-024-03214-y. [Online]. Available: https://doi.org/10.1007/s11663-024-03214-y

4. H. V. Haraldsson, Q. Reynolds, Y. A. Tesfahunegn, *et al.*, "Modeling of industrial electric arcs using different plasma gas compositions," *Metallurgical and Materials Transactions B*, vol. 56, no. 2, pp. 1208–1217, Apr. 1, 2025, ISSN: 1543-1916. DOI: 10.1007/s11663-024-03397-4. [Online]. Available: https://doi.org/10.1007/s11663-024-03397-4

5. H. Haraldsson, Y. A. Tesfahunegn, M. Tangstad, *et al.*, "Modelling of industrial electric arcs with changing plasma compositions and arc lengths," *SSRN Electronic Journal*, 2024, ISSN: 1556-5068. DOI: 10.2139/ssrn.4942616. [Online]. Available: https://www.ssrn.com/abstract=4942616 (visited on 06/09/2025)

It is also important to note the contribution of a couple of people for, first, the Measuring paper [2] where Halldór Traustason did all the actual measurements and the initial data processing. And second in [4] where Quin Reynolds created the base boundary conditions that were later modified in this work.

Chapter 1

Introduction

The aim of this research project is to develop a magnetohydrodynamics (MHD) numerical model for application in metallurgical industries, mainly for submerged arc furnaces (SAFs) for Silicon/Ferrosilicon production. MHD is the study of the interaction between electromagnetic fields, heat transfer, and the flow of conducting fluids such as liquid metals in SAF. The project will be presented in as linear of a manner as possible, the various models are explained all together as well as the results for each model. There were also new developments to the MHD model that still have to be published which are also very promising and are presented here but have not been published in a journal.

The models developed in this work are used to simulate a furnace that produces silicon alloys and is called submerged arc furnaces, because the electrodes that carry the electric current are submerged in the raw materials used in the production process. Usually the electrode currents for a three-phase SAF producing silicon or ferrosilicon metal have electrode currents of around 100 - 150 kA, phase voltages around 100 - 130 V and a total furnace power of about 20 - 60 MW. For this type of production, the presence of an arc is essential. In this case, much of the current will at some point pass through an electric arc, which burns in a gas-filled volume at the bottom of the electrode. The gas present will be a mixture of SiO and CO. The extremely hostile environment inside SAFs and especially in the arc area makes any direct observation of the arc impossible. This means that an accurate numerical simulation model of the electric arc is important for improved understanding and improved furnace operation. Three different arc simulation models have been selected for this purpose.

The first and simplest model is a Cassie-Mayr model (which is fully numerical), examples of uses are in [6], [7] and in [3]. They are easy to implement and have a low computational cost, but are not physically based. The second, which is based on simplified physical principles, is a channel arc model, similar to the one

described in [8] and [3], where the arc is implemented as a cylindrical conductor and the arc characteristics are calculated based on power balances between electric input and various output losses. The third and final model is the most complete and complex an is a magnetohydrodynamics (MHD) model. These models provide highly detailed and accurate results, but are computationally formidable - some examples for direct current (DC) arcs are [9] and [10], and for alternating current (AC) arcs [11], [8] and, [12].

A new MHD model was implemented in OpenFOAM using a transient compressible solver called *"rhoPimpleFoam"*. The model was then verified by simulating arcs in an argon furnace for which we had measurements to compare too and then using different SiO + CO ratios for the plasma gas in an Industrial furnace it is shown that the change in composition does not impact the arc behavior significantly. To further investigate this the arc length was changed while also varying the composition and it showed that the arc length has a larger impact in the behavior of the arc.

The first two models were coupled to a three phase electric circuit. The circuit model can predict the voltage and current waveforms that are present in a SAF and can estimate the harmonics based on them. A method is presented for extracting arc measurements from voltage and current data for a live SAF which we then use to compare to simulations run with the three-phase model for verification of those models. We got a good fit between the simulations and the arc measurement and then carried out simulations on varying the charge material resistance to investigate the impact on harmonics in the furnace, which showed that more arc current leads to more harmonics.

Finally the Cathode / Anode model previously developed in [13] and [14] was implemented for both the Channel arc model and the new MHD model so that now the different currents and voltage present in the space charge sheath next to the electrode and bottom material can be estimated as well as the electrode erosion across the respective surfaces.

Chapter 2

The Submerged arc furnace

A submerged arc furnace is a fairly large construction usually spanning a few floors in the building its situated in. In simple terms the furnace converts electricity and internal energy of carbon materials to heat which melts the raw materials, thus creating usable metals. A diagram of a SAF can be seen in figure 2.1 below.

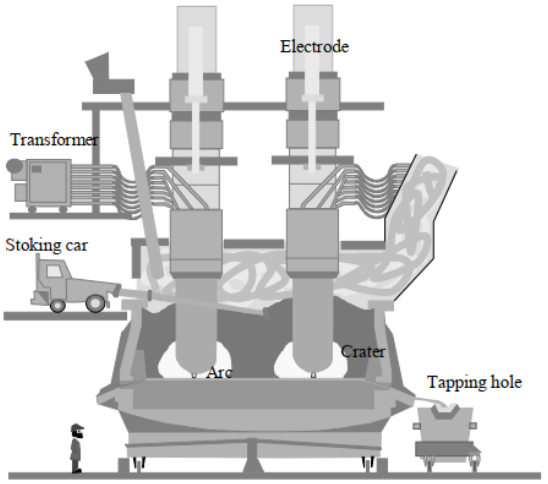

Figure 2.1: A schematic drawing of a SAF in operation.

The furnace itself is circular and varies from approximately 5 m to 11 m in diameter and from 3 m to 5 m in height. Raw materials are added from the top and will descend slowly in the furnace while they are heated. A 3-phase SAF is generally served by 3 transformers ideally placed concentrically around the furnace

with 120 degrees between them, this is done to minimize mutual inductance between them and any asymmetry that can affect the operation of the furnace. The transformers are connected to 3 electrodes that conduct electric power to the furnace trough bus bars and flexibles. This setup is called a knapsack configuration and is shown on figure 4.1.

Inside the furnace the electrodes are submerged in the raw materials, below each electrode there is a cavity where the arc is burning. This cavity or crater is filled with gas rather than solid materials, this is thought to be due to the high viscosity of the SiO_2 and the formation of a SiC crust around the cavity. Liquid silicon forms and collects at the bottom of the furnace and is tapped into lades using tap holes.

2.1 Furnace reactions

For silicon the overall process that occurs in the furnace can be in the ideal case written as:

$$SiO_2(s) + 2C(s) \rightarrow Si(l) + 2CO(g) \tag{2.1}$$

Carbon monoxide then reacts with the oxygen in the air further forming carbon dioxide:

$$CO(g) + O(g) \rightarrow CO_2 \tag{2.2}$$

This is a large simplification of what is going on in an actual furnace but it gives an idea of the total process. by adding quarts and carbon materials into the furnace, heat it up with electricity and then receive Silicon and carbon dioxide. Sounds rather simple but there are, however, a few extra steps that need to be explained so that we can see what exactly is happening inside the furnace, both to the materials and the electric current we supply to it. Generally the furnace is divided into two zones, the first is the outer zone where most of the reactions are exothermic and the temperature is around 700 - 1600 °C and, the second is the inner zone where the reactions are endothermic and the temperature is around 1800 - 2000 °C.

2.1.1 Outer zone

At the top of the outer zone the raw materials (Quartz and carbon) are added into the furnace by the feeding system. The incoming materials are heated by SiO and gas rising from the inner zone and low in the zone by electric current passing through it as it travels down in the furnace. The SiO gas reacts with the carbon to form SiC and CO gas, this is one if the most important reactions in this zone and has a large impact on the silicon yield of the furnace. It is very important that as

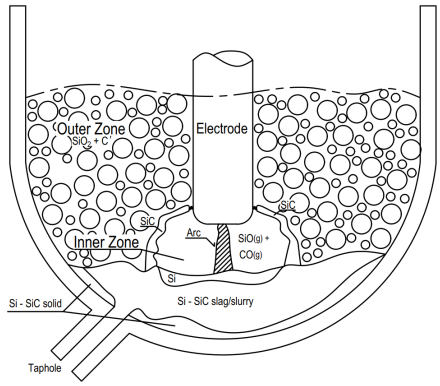

Figure 2.2: A schematic drawing of the zones and main materials present in a SAF.

much as possible of the SiO gas reacts with the carbon materials so that it does not leave the furnace as off-gas in the exhaust. The reactions for this is:

$$SiO(g) + 2C(s) \rightarrow SiC(s) + CO(g) \tag{2.3}$$

There are also two other reactions that occur in this zone, these are condensation reactions which have a smaller impact on the yield. Due to cooling the SiO gas from the inner zone condenses to SiO_2 and Si and then also along with CO to SiO_2 and SiC

$$2SiO(g) \rightarrow SiO_2(s,l) + Si(l) \tag{2.4}$$

$$3SiO(g) + CO(g) \rightarrow 2SiO_2(s,l) + SiC(s) \tag{2.5}$$

The reactions happening in the outer zone release the chemical energy in the carbon and are exothermic, so they heat up furnace materials when they occur.

2.1.2 Inner zone

The inner zone is mostly made up of the cavity where the electric arc burns, however, the SiC crust around the cavity and the bottom of the furnace are also included in this zone. Here SiO gas and SiC react to form liquid Si and CO gas, this is the main Silicon generating reaction in the furnace and is the most energy consuming reaction present in the furnace.

$$SiO(g) + SiC(s) \rightarrow 2Si(l) + CO(g) \tag{2.6}$$

The SiO in this reaction is supplied by the reverse SiO condensation reaction (2.7) as Si and SiO_2 react to form SiO. The rate of both reactions grows with temperature, but faster for reaction (2.6) than (2.7). Therefore, temperatures close to 2000 °C are required to get the partial pressure ratio of SiO and CO to be close to one ($P_{SiO}/P_{CO} \simeq 1$), which is required for optimal silicon yield, reaction (2.6) determines this ratio.

$$SiO_2(s,l) + Si(l) \rightarrow 2SiO(g) \tag{2.7}$$

The reactions happening in the inner zone are the reactions that consume the most electric energy, this is partly from the arc but a the rest is from the current traveling in the SiC crust. In order to produce ferrosilicon iron oxide is added to the charge materials which reacts with the CO to form liquid iron which then mixes with the silicon.

$$Fe_2O_3(s) + 3CO(g) \rightarrow 2Fe(l) + 3CO_2(g) \tag{2.8}$$

2.2 Energy considerations on reactions

As mentioned above in 2.1.2 the reactions occurring in the inner zone require a high temperature and are endothermic so they consume a lot of energy to happen. This energy comes from the electric arc that is burning between the tip of the electrode and the materials below it, and smaller arcs that form on the side of the electrode. The energy travels from the arc in the form of radiation and convection of the gas present in the cavity. The reactions present in the outer zone, section 2.1.1, are exothermic and thus release heat to the surrounding materials, this is due to the chemical energy of the carbon.

Table 2.1: Molar enthalpy for the reactions occurring in the furnace [15].

Reaction	ΔH T > 1512 °C [kW/mol]
$SiO + 2C \rightarrow SiC + CO$	-21
$2SiO \rightarrow SiO_2 + Si$	-397
$2SiO_2 + SiC \rightarrow SiO + 2CO$	-189
	ΔH T > 1800 °C
$SiO + SiC \rightarrow 2Si + 2CO$	47,5
$SiO_2 + Si \rightarrow 2SiO$	166

2.3 Furnace Yield

A very important parameter in the overall production of the furnace is the silicon yield which is the ratio between the amount of silicon added as SiO_2 in the raw materials and the amount tapped out as Si-metal. The main way for silicon to be lost out of the furnace is in the form of SiO gas that escapes. The SiC accumulation is low compared to the SiO gas escaping which can be up to 5 - 15% of the total silicon added, there is also some SiO_2 lost as slag during tapping.

$$\eta = Si - yield = \frac{Si_{tapped}}{Si_{added}} = \frac{Si_{tapped}}{Si_{tapped} + SiO_{leaving} + SiC_{accumulation} + Si_{in\ slag}} \tag{2.9}$$

There are a few factors that govern the rate of gas escaping:

- The SiO reactivity of the carbon materials. It needs to be high so that the SiO gas is captured in the upper region of the furnace before it gets out of the top. This is achieved by using the correct carbon materials.
- Having a higher temperature in the inner zone will shift the equilibrium for reaction (2.6) to the right, thus making more SiO react to Si.
- Having a low temperature in the outer zone will make condensation reactions (2.4) and (2.5) faster and reduce the amount of SiO gas escaping.
- By minimizing the void that forms next to the electrodes by stoking the furnace. The void shortens the path to the open air making the outer zone smaller for the SiO gas reaction to occur in. This is solved by mechanical stoking of the furnace.

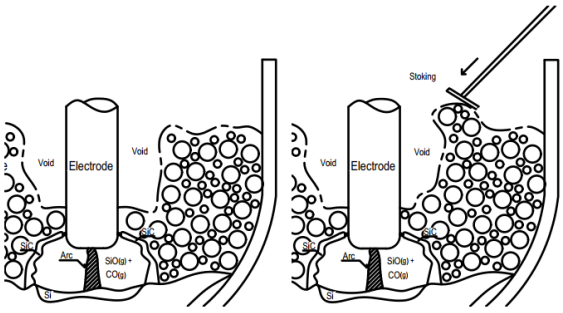

Figure 2.3: Schematic view of the stoking process.

2.4 Electrode currents

The electrode current or phase current is the total current that travels down the electrode from the transformers, before it diverges to different paths. To understand what is happening we must examine the total electrical characteristics of the SAF. Industrial high current arcs are generally present within the electric arc furnaces. To determine the behavior of the furnace and the arc itself, a complete electric circuit must be implemented. A more detailed description of a circuit model can be found in section 4.1 later in this work.

The electrode current is usually considered to split up into two parts, the current going into the arc and the current passing through the charge material, which is represented by the charge resistance R_c. The arc is represented by a voltage drop V_a rather than a resistance and is usually calculated using an arc model [1], this is not always the case, however, [8]. The physical properties of the charge materials differ with location in the furnace, as intermediate reactions change their composition and temperature changes with depth.

To show how the current in an operating SAF behaves for one period figure 2.4 shows us the actual measurements from a ferrosilicon plant in Iceland. Using a special form of signal analysis, based on a so called "arc footprint [16]" it is derived that of the maximum total current, which is around 150 kA, the arc current is 100 kA and then 50 kA go into the charge. We assume that the charge resistance is constant, and from that assumption, and additionally assuming that the arc has a very high resistance at zero current, we can calculate the share of current bypassing the arc through the charge.

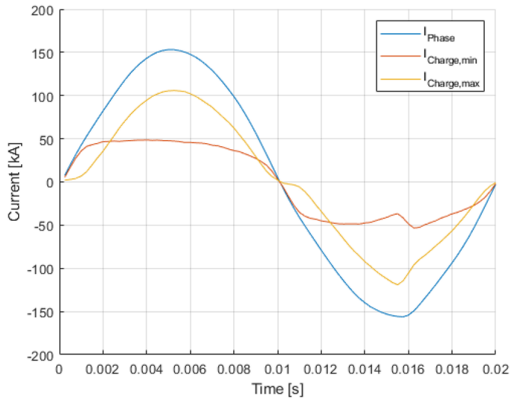

Figure 2.4: The electrode current in an operational SAF for one 50 Hz time period.

2.4.1 Arc current

The electric arc supplies most of the energy to drive the main reactions in the lower part of the furnace. The arc current is the current that travels directly from the tip of the electrode to the bottom of the arc cavity. Electric arcs are defined as an electrical discharge sustained by a current flowing through ionized gas, which forms plasma, between two electrodes [17]. In this case the furnace electrode and the material below which is usually the liquid silicon at the bottom of the cavity.

The arcs we observe in a silicon SAF are alternating current arcs [ACAs] which makes them very non-linear due to the alternating nature of the voltage supplied. To estimate ACAs we use the "arc footprint" method, see chapter 3. It is based on measuring the voltage and the current at the electrode and then extracting the voltage and current vales for the arc by estimation of the charge resistance [16]. Figure 2.5 below shows us an arc footprint from an actual arc furnace after this method is applied, for the same data shown in figure 2.4. We can see how variable voltage and resistance must be.

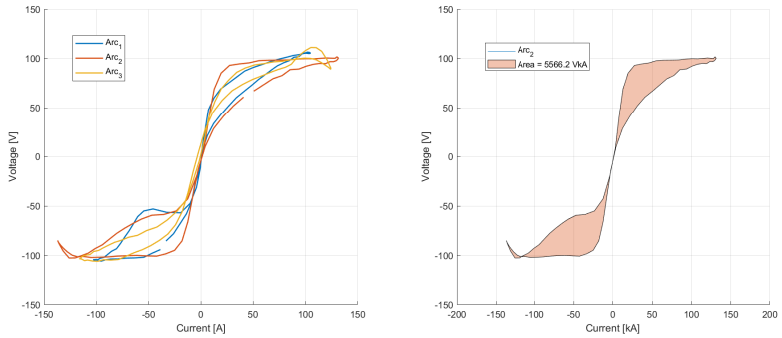

Figure 2.5: The arc footprints for all three arcs and the footprint area for arc 2.

The current in the arc is determined by the plasma gas composition, the thickness of the SiC crust on the crater sides [18], the arc length and, the charge resistance. The lower resistance in the charge or the SiC crust allows more current to pass through it and thus bypass the main arc. Generally the plasma composition is considered to be SiO(g) + CO(g) in about 50/50 % quantities at optimal conditions. This composition is, however, not exactly known since it can't be measured and will vary to a large degree during furnace operation mainly based on reaction speeds, which are dependent on the temperature, but also on the composition of the charge material. The arc length is dependent on electrode position and should be around 5 to 10 cm as the system does not have a high enough voltage to sustain a much longer arc [12].

2.4.2 Charge current

The charge current is a collection of all the current that does not go into the arc. Or a collection of currents traveling through the main charge material, which is mostly composed of SiO_2, SiC and C particles. The total charge current is more constant than the variable arc current and is mostly dependent on the electrode voltage and the charge composition. The current density does, however, changes with depth, this is both due to compression of the charge material as well as the conductance increasing with temperature.

As the material travels down in the furnace it compresses and its bulk density increases, this will create more current paths and reduce the resistance accordingly like a parallel resistor. It was explained above the temperature gets higher the closer we get to the arc cavity. Most of the materials present in the furnace have an increasing conductivity with temperature [19], figure 2.6, which will lead to more current lower in the furnace.

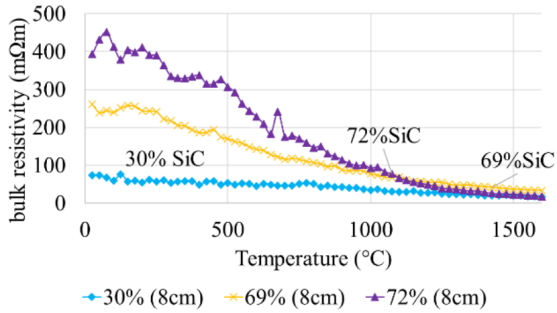

Figure 2.6: Bulk resistivity of carbon transformed to 30% SiC, 69% SiC and 72% SiC with increasing temperature over the range of 0-1600 °C [19].

Another part that can be considered a hybrid between arc and the charge current is the current going trough the SiC crater crust. This current starts out as side arcs, which are small arcs on the sides of the electrode that burn between it and the crust. There can be many side arcs at any one time but the main parameter is the crust thickness [18].

2.4.3 Eddy currents in the steel shell

The final current that is present in the furnace is in the outer shell of the furnace. Usually constructed from steel it is therefore magnetic and this leads to an induced current when the main current flows down the electrode. This current should be included even if it is not directly flowing from the electrode, since it can be a noticeable portion of the electrode current [20]. These types of currents are called eddy currents since they travel in a circular pattern in the material when an external magnetic field is applied on it. The eddy current will form three loops and is densest between the electrodes at the top of the steel shell [21], figure 2.7.

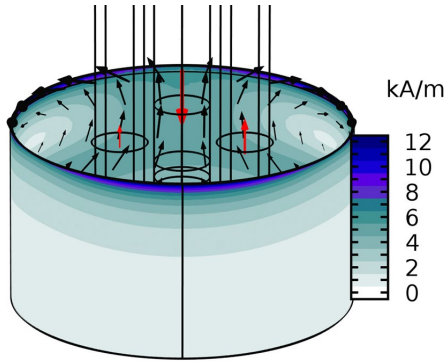

Figure 2.7: Typical patterns of induced eddy currents in the the steel shell [21]

.

Chapter 3

Estimating SAF parameters

When developing a model to mimic or estimate some physical behavior, the most effective way to verify its accuracy is by comparing it to actual measurements of that behaviour. If direct measurements are not possible, the second best approach is to use known benchmark cases or do a cross-validation between different modeling methods. The focus of this work is to model industrial arcs and their behaviour and to be able to compare the results to actual measurements. The first step is to identify a method for measuring an arc, whether directly or indirectly. To accomplish this we have recreated and improved work done by Halldór Traustason in his masters thesis [22], this was also done so that this work could be published openly in [2].

In an operating furnace we estimate the current going into each electrode from the current measurements implemented on the primary side of the transformer windings, more details on transformer configuration are a available in [23]. The voltage and current going into each electrode, but by creating a complete electric circuit model of the furnace and knowing its parameters, either by simulation or measurements. We can use the total voltage and current measurements in each electrode to indirectly measure the arc. There are not many studies on measuring arc parameters, but previous work on this has been done in [24] and [16], and in [25] measurements are used to model the effects of electrode position on arc currents. All measurements on any type of furnace require some sort of data acquisition (DAQ) system to collect and process the data. For industrial applications, reliable and accurate equipment is essential so selecting the correct equipment can be a challenge, in [26] Lorenzo et al. details this for a Spanish ferroalloy company and, [27] Gerritsen et al. details some of the methods used and impact of error in the measurements. These are necessary to obtain data to verify the validity of any models that are derived.

Here we will describe a DAQ system that was implemented on a FeSi SAF at

Elkem Iceland. We will discuss the SAF properties required for data processing to estimate actual SAF parameters. Finally we will describe how the data is processed from raw measurements to actual useful parameters that are used to estimate current distribution, arc footprint and arc harmonics in the furnace.

3.0.1 The DAQ system

The data acquisition system for SAF samples both the voltage and current in each electrode as well as a few of the higher harmonics that are present in the signal. The measurement frequency f_S 3000 Hz gives about 60 samples per period. This sampling rate allows for the estimation of harmonics up to 1500 Hz which is the 30th harmonic of 50 Hz. The DAQ system consists of three voltage sensors that measure the electrode voltage through step-down modules since it is too high to measure directly. The current sensors measure the current on the transformer primary side of each electrode using the Hall effect. A detailed description can be found in [22] where the DAQ systems design and implementation are described in detail.

3.0.2 Data processing methods

A method has been developed to estimate the current that passes through the arc and charge material. The simplified circuit presented in figure 3.1 shows the model used to process the measured current and voltage waveforms. The model is similar to the section surrounding the arc in figure 4.2 but most circuit elements have been combined and the furnace resistance is included. Current and voltage measurements for each electrode are defined as i_{phi} and V_{phi} here the subscript i is the electrode numbering. The total phase voltage V_{phi} is a combination of the voltage induced in the furnace V_{Li}, the voltage over the arc V_{pi} (which is over the time varying arc resistance R_{ai} and the assumed constant charge resistance R_{ci} connected in parallel) and, finally the voltage over the furnace short-circuit resistance R_{si},the liquid metal resistance and, the base resistance in the furnace. V_{pi} can be considered as the power producing voltage or load voltage that contributes to the actual silicon production.

Now the equivalent phase resistance R_{ph}, the arc resistance R_a and, the charge resistance R_c can be defined using Ohms law as:

$$R_{ph} = \frac{1}{\frac{1}{R_a} + \frac{1}{R_c}} + R_s \tag{3.1}$$

The induced voltage present in the phase voltage causes a phase shift in the current, this results in the current lagging the voltage by 30° to 45°. The magnitude of the phase mostly depends on the size and amperage of the furnace (high

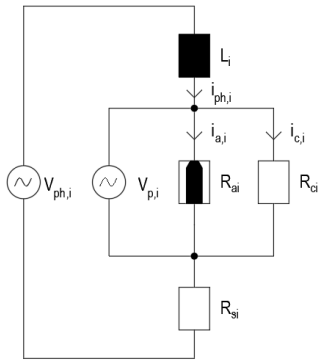

Figure 3.1: The simplified circuit model used to estimate arc characteristics from the measurements.

current > large ϕ), but the electrode position also slightly affects the phase shift. The induced voltage V_{Li} must therefore be removed from the total phase voltage V_{phi} before the resistances can be calculated. This is done by a simple time dependent differentiation of the current signal to estimate the induced voltage:

$$V_{pi} = V_{phi} - L_i \frac{di_{phi}}{dt} \tag{3.2}$$

Here L_i is the total inductance present in the electrode, this value is found by iteration until the phase shift is negligible, when the current and voltage pass zero at the same time. With the phase shift removed the total phase resistance for each electrode R_{phi} can be determined. The phase resistance or zero crossing resistance is the resistance when both the phase current and the power producing voltage cross the zero point simultaneously. R_{phi} is found by plotting the Lissajous curve for i_{phi} and V_{pi} and then the slope is estimated as the curve passes zero. To find R_c we need both R_s and R_a, the short-circuit resistance is either known from the modeling, such as in [18], or can be assumed to be around 5% of the phase resistance similar to what is done in [22]. Determining the arc resistance R_a can be difficult since you need measurements from when only an arc is present with out any charge materials present, this is important since different furnaces will have different parameters. Previous measurements carried out in the same furnace when a pure arc was present were used and determined the arc resistance to be around 2.5 to 4 mΩ at zero passage [16]. This will give an upper and lower limit for the charge resistance R_c, and consequently both the arc resistance R_a and the arc current i_a will have similar limits, here we will show the upper limit only

for simplisty of the graphs. Now all that is needed to determine the range for the arc current i_a which is the voltage over the arc V_a given as:

$$V_{ai} = V_{pi} - i_{phi}R_s \quad \Rightarrow \quad i_{ai} = \frac{V_{ai}}{R_{ai}} \tag{3.3}$$

3.1 Measuring the arc

The data used in this work for all three electrodes can be seen in figure 3.2 where the RMS values for current and voltage have been averaged over one second periods. From these figures, we can easily observe the intensely variable nature of the furnace's electric properties.

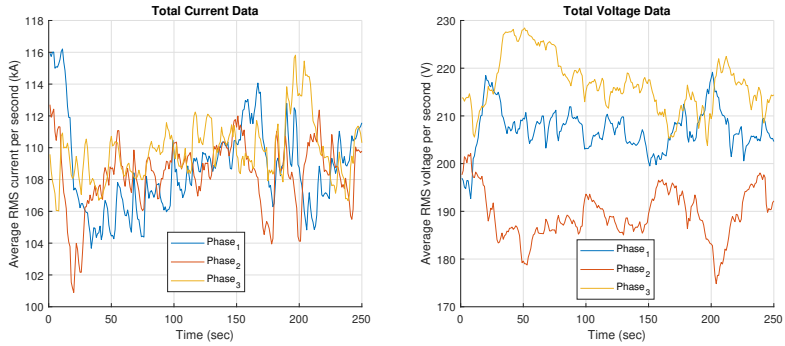

Figure 3.2: Total RMS electrode current and voltage data averaged over one second periods.

Now we can pick a piece of the data to investigate in more detail, this can be any point but we chose one where the current is about equal for each phase. First, we need to remove the induced voltage in the electrodes; figure 3.3 shows the voltage vs. current profile before and after the induced voltage is removed and the fit used to estimate the zero passage resistance using equation 3.2.

Now we can determine the charge resistance R_c using equation **??** and, since it is assumed constant over each period the change in the phase resistance must be due to the arc resistance R_a. We can now dived the electrode current into charge and arc currents and in figure 3.4 we can see all three current for two periods. Two thirds of the current is going into the arc, this indicates that it is rather short.

We have now got data for both the arc voltage and current and can start to look at it in more detail. Another factor of interest is the arc footprint or the voltage and current graph area. This area has the units kVA so it tells us how much power is present in the arc over a whole period but the shape of the curve can also be

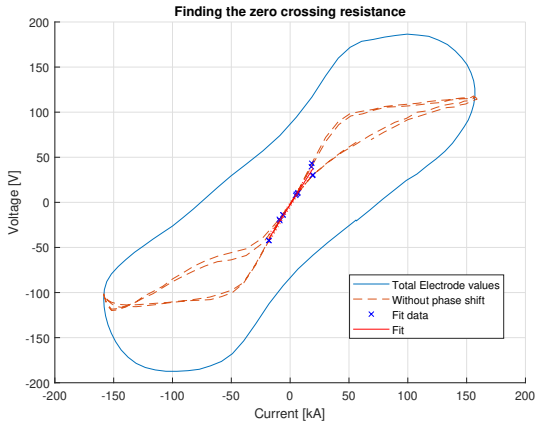

Figure 3.3: To find the zero crossing phase resistance we do a linear fit around the center of the voltage vs current curve.

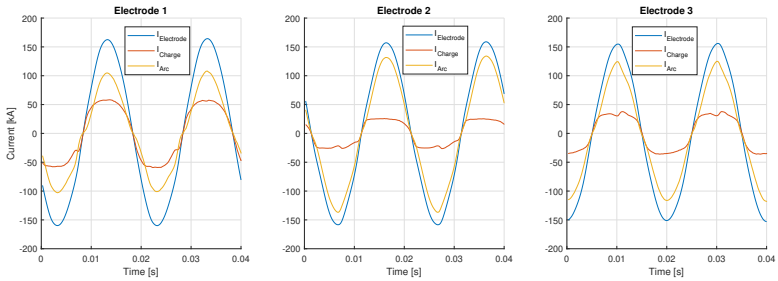

Figure 3.4: Current distribution for all three electrodes. The arc and charge currents vary somewhat between them.

connected to furnace operations. Theses can be tapping, how the charge material is distributed and so forth. Figure 3.5 shows all three arc footprints and the area for arc 2 is 5566.2 kVA.

More data during various furnace operations is needed to connect these footprints to what is actually happening in the furnace, ideas would be to properly observe during tapping, charge refilling and electrode operation and to catalog the arc footprints to get a better understanding of the electric behaviour during these events.

The final aspect examined in this work is the harmonics. These are very important to consider because, when used alongside other parameters, they can provide

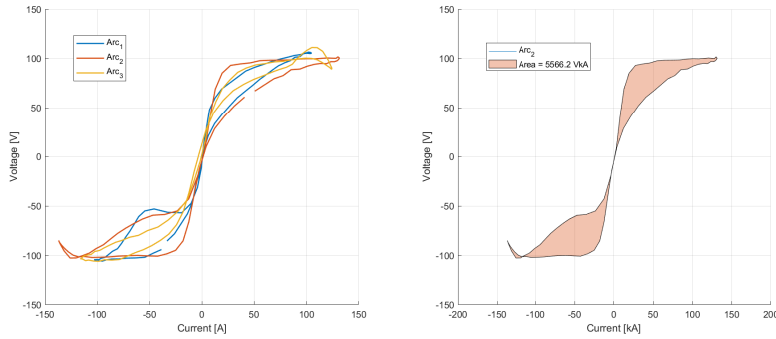

Figure 3.5: The arc footprints for all three arcs and the footprint area for arc 2.

a better picture of the furnace's behavior. Additionally, harmonics are significant in their own right for better understanding the system's performance, as an absence of harmonics can be an indicator of insufficient arc activity, and thus bad Si-yield. However, minimizing the total electrode harmonics on the high voltage side is important so that the total harmonic distortion (THD) doesn't go over the limit allowed by the electric utility supplying power to the furnace. Seeing what frequency components are present in which current can also give an idea of the situation at each electrode and in the charge material. This can be arc length and material properties in the charge and metal bath below the electrodes. Figure 3.6 shows the current harmonics in the furnace for electrode 2 and all the arcs, we can see which frequency components are present in the furnace currents in the given period.

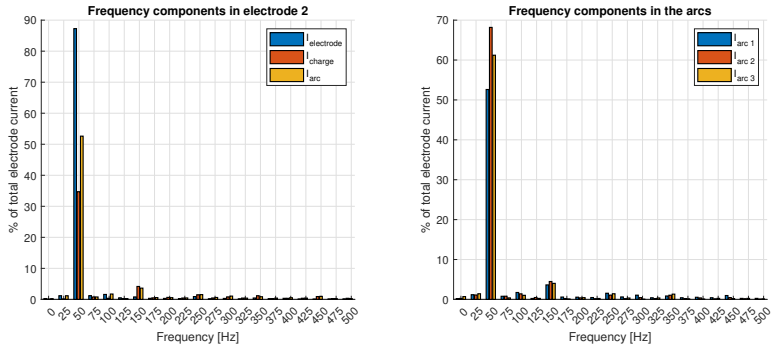

Figure 3.6: The frequency components present in electrode 2 and in all three arcs as a percentage of total current in each electrode.

Chapter 4

Modeling of Electric Arcs

Modelling industrial arcs is a multiphysics process that generally involves solving several coupled physical phenomena, including electromagnetics, fluid dynamics, and heat transfer. Coupling fluid dynamics and electromagnetics is known as Magnetohydrodynamics (MHD). There are also simpler approaches to arc modelling, either based on simplified physical principles or empirical methods. A more detailed list of literature is given in chapter1 at the start of this work.

In this chapter a complete three phase circuit model of the furnace and three arc models are presented. One is a combined Cassei-Mayr model (CMM) that numerically simulates dynamic arc behavior based on certain parameters, the second is an improved channel arc model (CAM) based on an older model created in [8] and presented in [3], and the third is a full MHD model implemented in OpenFOAM®.

The CAM uses pre-tabulated physical values to estimate the dynamic behavior of an AC arc. Both the CMM and CAM models are simulated in a three phase electric circuit model of a submerged arc furnace (SAF) modeled in SIMULINK [28]. The values of the circuit elements are estimated using modeling as well as actual measurements from an operational silicon plant in Iceland. These measurements are then used to validate the arc models by comparing the current and voltage waveform. The MHD model is the most detailed and solves a complete set of physical equation to estimate the arc. It also uses precalculated values for the various material properties needed for the simulation. The first two models are coupled to the circuit model and then used to simulate a furnace in operation.

4.1 Electric circuit description of a SAF

The behavior of a SAF can be estimated from its electrical characteristics. Industrial high current arcs are generally present within the electric arc furnaces. There-

fore, a complete electric circuit must be implemented to determine the behavior of the furnace and the arc itself. A 3-phase SAF generally consists of 3 transformers placed concentrically around the furnace with 120° between them; as a result, the mutual inductance is minimized. The transformers are connected to 3 electrodes that conduct electric power to the furnace through bus bars and flexibles. This setup is called a knapsack configuration and is shown in figure 4.1. The location of the DAQ system is also marked.

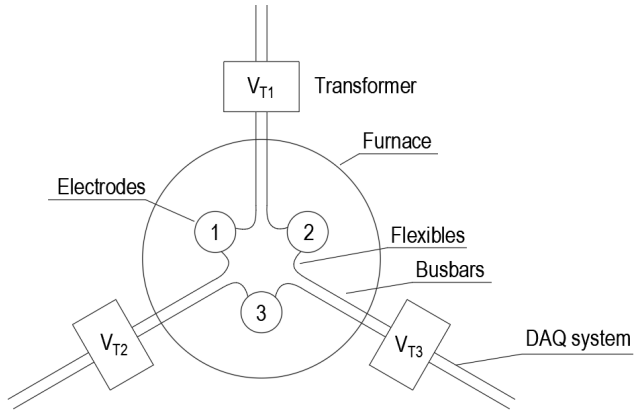

Figure 4.1: A SAF in knapsack configuration.

The model presented in [16] was recreated and added to, the parameters were also changed to fit with our other work [1]–[3]. The circuit model should include most of the components, transformer currents i_{Ti}, voltages V_{Ti}, resistances R_{Ti}, inductance L_{Ti} and mutual inductance between them ($M_{Ti,Ti+1}$ and $M_{Ti,Ti+2}$), as well as the resistances of the electrodes (R_e) and the phase inductance including the mutual inductance (L_e and $M_{ei,ei+1}$ and $M_{ei,ei+2}$). Mutual inductance due to currents in the bus bars and flexibles are not included in this model. The current i_{ei} that passes between the electrodes in a SAF mostly travels through the arc. There is, however, some part that goes into the raw material charge filling up the furnace (R_c), we call this current the charge current i_{ci}, figure 4.2 shows the electric circuit of a three-phase SAF and where each of the components mentioned before are located in it. Throughout this paper we will use i as a stand in for the electrode numbers 1 - 3 since writing all the numbers every time will become repetitive and is unnecessary since the models can work for any electrode. The physical properties of the charge materials differ with location in the furnace, as intermediate reactions change their composition and temperature changes with depth. However, this variation is not considered in the model.

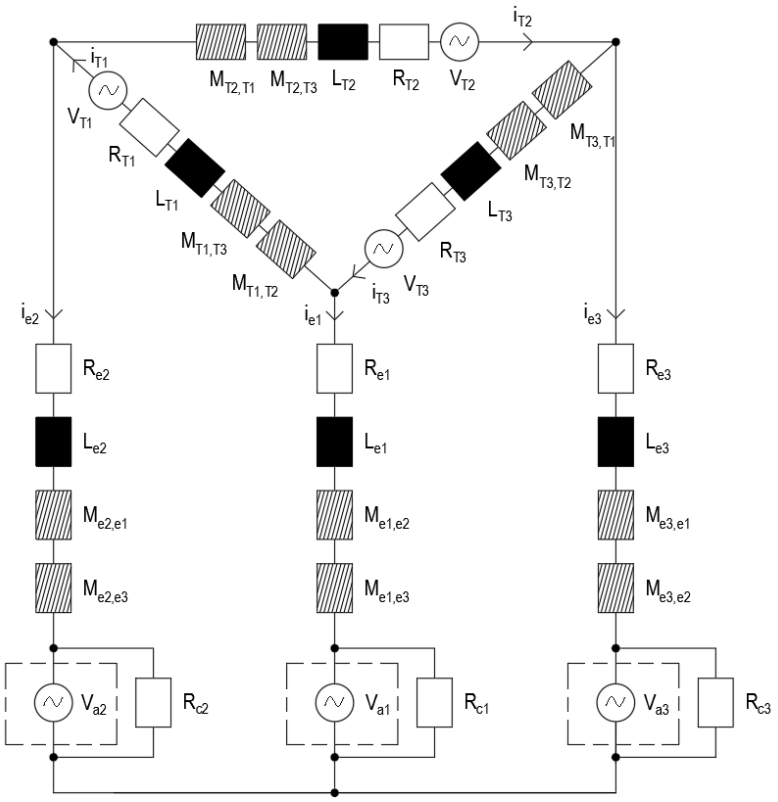

Figure 4.2: Electric circuit used for the dynamic models [8]

The purpose of the model is to determine the electric conditions in a SAF, particularly the arc and charge current, as well as the harmonics generated by the arc. The complete dynamic electrical model then consists of a three phase electrical- and arc model. We determine the phase current equations by applying Kickoff's current law and summing up the voltage drop in the three current loops T_1e_1, T_2e_2 and T_3e_3. To find the transformer current we have to solve three coupled equations, written in matrix form as:

$$\begin{bmatrix} -L_{T1}-L_1-L_2 & L_2-M_{T1,T2} & L_1-M_{T1,T3} \\ L_2-M_{T2,T1} & -L_{T2}-L_2-L_3 & L_3-M_{T2,T3} \\ L_1-M_{T3,T1} & L_3-M_{T3,T2} & -L_{T3}-L_3-L_1 \end{bmatrix} \begin{bmatrix} \frac{di_{T1}}{dt} \\ \frac{di_{T2}}{dt} \\ \frac{di_{T3}}{dt} \end{bmatrix} = \begin{bmatrix} V_{T1}-V_{a1}+V_{a2}+(R_{T1}+R_{e1}+R_{e2})i_{T1}-R_{e1}i_{T3}-R_{e2}i_{T2} \\ V_{T2}-V_{a2}+V_{a3}+(R_{T2}+R_{e2}+R_{e3})i_{T2}-R_{e2}i_{T1}-R_{e3}i_{T3} \\ V_{T3}-V_{a3}+V_{a1}+(R_{T3}+R_{e3}+R_{e1})i_{T3}-R_{e3}i_{T2}-R_{e1}i_{T1} \end{bmatrix} \quad (4.1)$$

Where the inductance L_{1-3} include the mutual inductance between the electrodes as well as the electrode inductance itself:

$$\begin{aligned} L_1 &= L_{e1} - M_{e1,e2} - M_{e3,e1} + M_{e2,e3} \\ L_2 &= L_{e2} - M_{e2,e3} - M_{e1,e2} + M_{e3,e1} \\ L_3 &= L_{e3} - M_{e3,e1} - M_{e2,e3} + M_{e1,e2} \end{aligned} \tag{4.2}$$

Now it uses the current law to find the electrode currents i_{e1}, i_{e2} and i_{e3}:

$$\begin{aligned} i_{e1} &= i_{T3} - i_{T1} \\ i_{e2} &= i_{T1} - i_{T2} \\ i_{e3} &= i_{T2} - i_{T3} \end{aligned} \tag{4.3}$$

Notice how the arc voltages V_{ai} are used in the coupled equations but not arc resistance R_a and charge resistance, this is because we assume that the voltage is the same over both these resistances. The arc voltages are estimated by a dedicated arc model and this allows us to investigate the charge current in more detail later, this model can be any arc model that uses electrode current as input since that allows us to use the model to solve the circuit equations above.

4.1.1 Multiple arcs sub-model

In previous work it was observed that the furnaces electrodes have more than one arc per electrode [12], [18], [29]. To include multiple arcs we implemented a new multi arc sub-model, where the resistance from an arc is calculated for each time step using the arc model. The arcs are assumed to be identical and parallel connected to each other as well as the charge resistance, see figure 4.3. This setup allows for only one instance of the chosen arc model to be run at a time since the current is determined by simple current division for both the arc and charge currents. Future improvements of this sub model should include a more detailed method for estimating multiple arcs. This is a feasible configuration as at the high currents this system, the arcs will exhibit a rising characteristic.

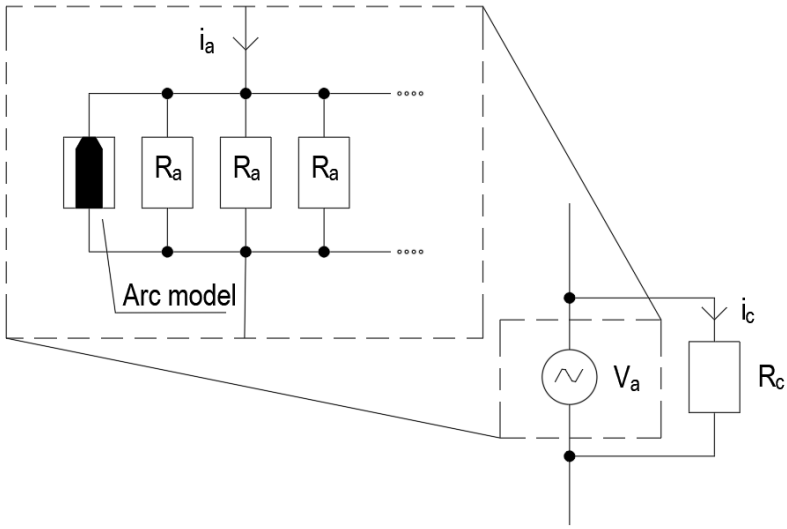

Figure 4.3: The current is divided between arcs by modeling them as a parallel resistances connected to the charge resistance.

4.2 The Cassie-Mayr model

Both Cassie and Mayr models include the electric arc as a non linear electrical circuit element, characterized by the arc voltage V_a, the arc height H_a, the arc current i_a, and the arc resistance per unit length $\widehat{R_a}$

- The Cassie model is suitable to describe high-current AC arcs and can be applied to the simulation of arcing in an electric furnace
- The Mayr model is best suitable for descriptions of low-current AC arcs or investigations of arc conditions near current-zero-passing.

The derivation of Cassie's model and Mayr's model is based on the assumption that the change with time in the arc's inner energy is equal to the difference between the electrical power input and the power dissipation in the arc column. The characteristic arc resistance per unit length for the Cassie model is [7]:

$$\frac{d\widehat{R_a}}{dt} = \frac{R_a}{\theta_a}\left[1 - \left(\frac{V_a}{V_0}\right)^2\right] \tag{4.4}$$

Where θ_a is the time constant that characterizes the arc dynamics and, V_0 is steady-state static arc voltage defined here as $((V_{an} + V_{ca}) + V_d * H_a)$, where V_d is the chosen voltage per arc length, V_{an} and V_{ca} are the anode and cathode sheath voltages respectively, and H_a is the arc height or length. And for the Mayr model its very similar:

$$\frac{d\widehat{R_a}}{dt} = \frac{R_a}{\theta_a}\left[1 - \left(\frac{V_a i_a}{P_0}\right)\right] \tag{4.5}$$

Here P_0 is the momentary arc power loss, The total arc resistance is then given by:

$$R_a = H_a\widehat{R_a} \tag{4.6}$$

In this thesis a new combined Cassie-Mayr model was developed to estimate the conductance of the arc and thus the arc voltage and current. The change in arc conductance G_i is given by [30]:

$$\frac{dG_i}{dt} = \frac{G_{min} - G_i + \left[1 - exp\left(-\frac{i_{ai}^2}{I_0^2}\right)\right]\frac{V_{ai} i_{ai}}{(V_0)} + \left[exp\left(-\frac{i_{ai}^2}{I_0^2}\right)\right]\frac{i_{ai}^2}{P_0}}{\theta_a} \tag{4.7}$$

where: G_i is the arc conductance, G_{min} is the conductance between any two electrodes when the electric arc is absent and, I_0 is a current value used to determine which model is dominant. We now have a model that can be inserted into the 3-phase circuit model.

4.3 The channel arc model

The second model developed was a channel arc model [CAM] it is a reconstruction of the model in [8]. However, we will explain the model in detail here, as both the notation and method have been modified slightly from the original. The first part of the model is a DC model and it is assumed that the arc is an ionized gas channel, which is symmetrical around the central arc axis. This allows for a variety of simplifying assumptions to be made within the channel. The simplest is to assume homogeneous current distribution throughout the channel diameter, but other distributions such as parabolic or gaussian can also be used. There is also an area where the arc expands from the cathode towards the arc channel. In the region where the current expands, it will have a radial component, which interacts with the magnetic field and forms a Lorentz force component directed towards the anode. This generates flow, contributing to convection in the arc. Figure 4.4 visually shows the model parameters and the variables used in the model.

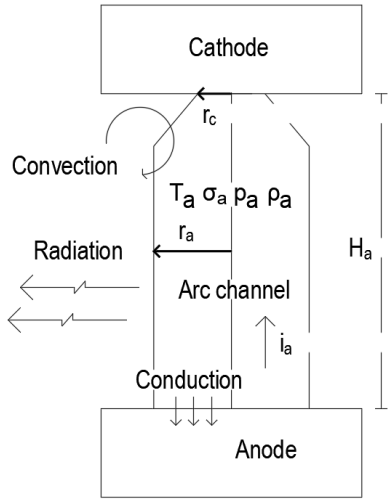

Figure 4.4: A visual representation of the parameters present in the channel arc model.

The variables used in the model are the arc temperature T_a, electrical conductivity σ_a, pressure p_a and mass density ρ_a. The radiative heat transfer, convection and conduction to the anode from the arc plasma is included as well. These variables then vary based on the type of heat distribution assumed for the arc. r_c is the arc radius at the cathode and r_a is the arc radius in the main arc area. While the arc is in a steady state, the electric power P_{el} that the arc generates must be

transferred completely to the surroundings, P_{loss}, of the arc and it can be assumed that:

$$P_{el} = P_{loss} \tag{4.8}$$

The electric power delivered to the arc must both include the energy loss in the arc column and the cathode anode layers and is given as [8]:

$$P_{el} = \frac{H_a {i_a}^2}{\sigma_a \pi r_a^2} + (V_{an} + V_{ca}) i_a \tag{4.9}$$

As mention above the arc then dissipates power by three mechanisms, i.e. radiation, convection, and conduction. The convective heat transfer to the arc surroundings is then given as:

$$P_{con} = 2\pi \int_0^{r_a} r \rho_a \left(T_a\left(r\right)\right) \; v_a\left(r\right) \; \left[h\left(T_a\left(r\right)\right) - h\left(T_F\right)\right] \; dr \tag{4.10}$$

Where $h(T_a)$ is the specific enthalpy of the arc, $h(T_F)$ is the enthalpy of the surroundings and $v_a(r)$ is the gas velocity distribution. The maximum gas velocity is along the arc axis and is given by:

$$v_{a,max} = \frac{i_a}{\pi r_a} \sqrt{\frac{K_1 \mu_0}{2\rho_a} \left(\frac{r_a^2}{r_c^2} - 1\right)} \tag{4.11}$$

The constant K_1 determines the current density profile, $K_1 = 1$ is a uniform profile while $K_1 = 5/3$ is a parabolic one [31]. The cathode spot radius is estimated with $r_c = \sqrt{i_a / \pi j_c}$ where j_c is a preselected current density. And then the mean velocity distribution is found with:

$$\overline{v_a} = K_2 v_{a,max} \tag{4.12}$$

Here K_2 decides the velocity profile. Finally the radiative heat loss from the arc is given by:

$$P_{rad} = \pi r_a^2 H_a \, \overline{u}\left(r_{eff}, \overline{T}_a\right) \tag{4.13}$$

Here $\overline{u}\left(R_{eff}, \overline{T}_a\right)$ is the tabulated mean radiation density as function of the mean arc temperature $\overline{T}_a$ and effective radiation radius r_{eff} based on the radiative properties for the plasma composition. Heat transfer to the anode due to conduction is given by:

$$P_{an} = i_a \left(\Phi_{an} + \frac{5 k_B \overline{T_a}}{2e} + V_{an}\right) \tag{4.14}$$

Φ_{an} is the material work function for the anode, k_B is the Boltzmann constant and e is the electron charge. In the end we will need a final relation to add to the energy balance (4.8) so we can determine the arc radius and mean temperature. We assume that the power loss P_{loss} will be minimized which means that the arc will find the path of least resistance:

$$P_{con} + P_{rad} + P_{an} = P_{loss} = P_{el} = V_a i_a \rightarrow Minimum \tag{4.15}$$

4.3.1 Dynamic channel arc model

To make the model capable of simulation alternating current arc we use the already discussed DC model as a sub model for the new dynamic model, where the instantaneous arc current $i_a(t)$ is used to calculate the dynamic arc radius r_{ac} and mean temperature $\overline{T}_{ac}$. This is done by first estimating the DC arc radius r_{dc} and the mean temperature $\overline{T}_{dc}$, the mass of the DC arc can then be calculated by:

$$M_{dc} = \pi r_{dc}^2 H_a \overline{\rho}_a \tag{4.16}$$

Since the AC arc will always attempt to approach the temperature and radius of the steady state DC model for any given current i(t), the change of mass over time can be estimated by:

$$\frac{dM}{dt} = \frac{1}{\tau}(M_{dc} - M) \tag{4.17}$$

here τ is a time constant, around 1 ms. The change of mass can both be positive and negative since the arc can both lose and gain mass. The surrounding gas, which is pulled into the arc, has a temperature T_F, estimated around 2300 K. The gas released from the arc has the mean temperature $\overline{T}_{ac}$. The change of arc energy due to mass change P_m is then:

$$\frac{dM}{dt} > 0 \Rightarrow P_m = h(T_F)\frac{dM}{dt} \tag{4.18}$$

$$\frac{dM}{dt} < 0 \Rightarrow P_m = \overline{h}(\overline{T}_{ac})\frac{dM}{dt} \tag{4.19}$$

here the $\overline{h}(\overline{T}_{ac})$ is the mean enthalpy of the arc for the mean instantaneous temperature $\overline{T}_{ac}$. The energy balance for the AC-arc can then be defined as:

$$\frac{dE}{dt} = P_{el} - P_{loss} + P_m \tag{4.20}$$

Where P_{el} and P_{loss} are the arc losses calculated for the current AC-arc time step using the DC submodel. The arc mass M(t) and energy E(t) can then be found

by explicit integration over time. When the total mass and energy are known they can be used to find the mean enthalpy of the arc and from that the mean ac-arc temperature $\overline{T}_{ac}$ is estimated:

$$\frac{E(t)}{M(t)} = \overline{h}(\overline{T}_{ac}) \quad \Rightarrow \quad \overline{T}_{ac} \tag{4.21}$$

Then the AC-arc radius is found using:

$$r_{ac}(t) = \sqrt{\frac{M(t)}{\pi H_a \overline{\rho}_a}} \tag{4.22}$$

The final step is then to find the dynamic arc voltage V_{ac} for the circuit model we use equation (4.23) by equating the new AC values and finding the new electric power in the arc:

$$P_{el,ac} = \frac{H_a {i_a}^2}{\sigma_a \pi {r_{ac}}^2} + (V_{an} + V_{ca}) i_a \rightarrow V_{ac} = \frac{P_{el,ac}}{i_a} \tag{4.23}$$

4.4 Magnetohydrodynamics arc models

Detailed electric arc models are generally based on MHD, as this approach incorporates most of the relevant physics. To capture the momentum and heat transfer as well as the effect of the electromagnetic fields, Maxwell's equations are solved together with Navier Stokes and energy conservation equations. This results in a total of seven coupled partial differential equations.

The electromagnetic fields are governed by Maxwells equations:

$$\nabla \cdot \mathbf{D} = q \tag{4.24}$$

$$\nabla \times \mathbf{H} - \frac{d\mathbf{D}}{dt} = \mathbf{j} \tag{4.25}$$

$$\nabla \cdot \mathbf{B} = 0 \tag{4.26}$$

$$\nabla \times \mathbf{E} + \frac{d\mathbf{B}}{dt} = 0 \tag{4.27}$$

Where $\mathbf{D} = \epsilon_0 \mathbf{E}$ is the flux density, $\mathbf{H} = \mathbf{B}/\mu_0$ is the magnetic field density, $\mathbf{B}$ is the magnetic field, ϵ_0 is the electric permittivity, q is the electric charge, $\mathbf{j}$ is the current density, and μ_0 is the vacuum magnetic permeability.

Fluid flow is described using the Navier-Stokes equations for momentum conservation, and the continuity equation for mass conservation:

$$\frac{\partial \rho \mathbf{u}}{\partial t} + \nabla \cdot (\rho \mathbf{u} \otimes \mathbf{u}) + \nabla P = \mu \nabla^2 \mathbf{u} + \mathbf{j} \times \mathbf{B} \tag{4.28}$$

$$\frac{\partial \rho}{\partial t} + \nabla \cdot (\rho \mathbf{u}) = 0 \tag{4.29}$$

Here ρ is the plasma density, $\mathbf{u}$ is the velocity field, P is the pressure field, and $\mathbf{u}$ is the viscosity.

Heat transfer is described by the energy conservation equation. As most of the thermophysical properties of plasmas are strongly temperature dependent, this couples the energy equation tightly to the other components in the model. The general equation is:

$$\frac{\partial \rho h}{\partial t} + \nabla \cdot (\rho \mathbf{u} h) = \nabla \cdot \kappa \nabla T + \nabla \cdot \left(\frac{5 k_B T \mathbf{j}}{2q} \right) + \frac{\mathbf{j} \cdot \mathbf{j}}{\sigma} + Q_m - Q_R \tag{4.30}$$

Here h is the enthalpy field, κ is the plasma thermal conductivity, σ is the plasma electrical conductivity, k_B is the Boltzmann constant, and Q_R is the radiation energy loss term. Q_m includes all additional terms related to the mechanical contribution to the energy from compressibility effects.

4.4.1 Finite volume method

Before going into the details of the models we will briefly explain the basics of the finite volume method for CFD. The finite volume schemes are principally different from the classical finite difference schemes in the way they are derived. Instead of discretizing the partial differential equations, we start with the physical conservation laws in the integral form, such as equation 4.31 below. Discretization is applied directly to the integral equations written for small control (finite) volume, figure 4.5. For a generic conserved variable ϕ, the integral form for a control volume Ω_i is:

$$\frac{\partial}{\partial t}\int_{\Omega_i}\phi d\Omega_i = -\int_{S_i}\phi V_i \cdot n_i dS_i + \int_{S_i}\chi\nabla\phi \cdot n_i dS_i + \int_{\Omega_1} Q d\Omega_i \tag{4.31}$$

where n_i outward facing normal and expresses the 'conservation' of the scalar field within Ω_i, S_i is the surface of the control volume, and χ is a constant of diffusion. The left-hand side represents the rate of change of the total amount of ϕ within. Each integral in the right-hand side represents a certain typical way by which this amount can be changed. The first shows the *convective flux* through the boundary S_i, the second is the *diffusive flux*, and finally represents the rate of change of the amount of ϕ due to internal sources of intensity Q per unit volume.

The algebraic discretization equations that constitute a finite volume scheme are derived by approximating the integral equations written for the finite volume cells. The surface integrals are generally approximated using fluxes calculated at the cell faces. For a face shared by two adjacent cells, the flux is typically interpolated from the values at the cell centers. Convective fluxes are often discretized using upwind schemes, central differencing, or higher-order schemes to improve accuracy and stability. Diffusive fluxes are discretized using gradients approximated from neighboring cell values.

The discretization process converts the integral conservation equations into a system of algebraic equations for each control volume. These equations are typically linear or nonlinear depending on the nature of the PDEs being solved. Solve the resulting system of algebraic equations using appropriate numerical solvers. Common methods include iterative solvers like Gauss-Seidel, Conjugate Gradient, and Multigrid methods.

4.4.2 Axi-symmetric MHD

Older MHD models generally used axi-symmetry to simplify the model domain and save on computing costs. This is done in [11], [31], and [8]. These models were developed in NTNU and the model presented here is a continuation and an upgrade to them. This method assumes the modelling domain is a cylinder with

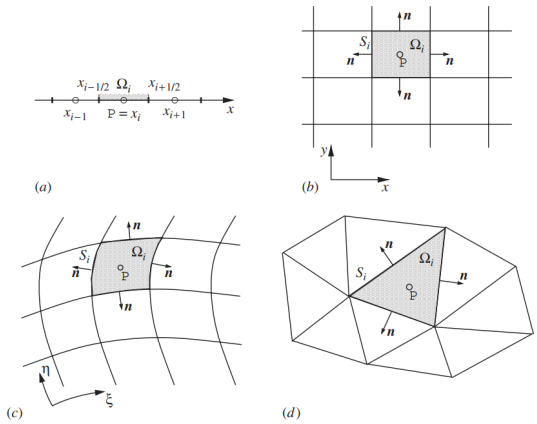

Figure 4.5: Examples of finite volume grids. (a) One-dimensional grid; (b) Two-dimensional Cartesian structured grid; (c) Two-dimensional curvilinear structured grid; (d) Two-dimensional unstructured grid [32].

a certain radius r and a height/length z, they also include Φ to estimate the radial magnetic field, figure 4.6. Besides from having a smaller amount of control volumes the simulation also benefits greatly from being only two dimensional. The MHD and CFD equations listed before are simplified considerably, mass conservation shown as an example:

$$\frac{\partial \rho}{\partial t} + \nabla \cdot (\rho \mathbf{u}) = 0 \rightarrow \frac{\partial \rho}{\partial t} + \frac{1}{r}\frac{\partial}{\partial r}(r\rho u_r) + \frac{\partial}{\partial z}(\rho u_z) = 0 \tag{4.32}$$

Here r is the radius, u_r, and u_z are the velocity components for each direction. At first glance it may seem like the axial equation is longer but the elimination of whole dimension decreases the computing time by a large margin. These models were shown to give a very acceptable result for the arc problem they were applied to but they can only be used for processes that allow for the results to be simplified to a circular domain.

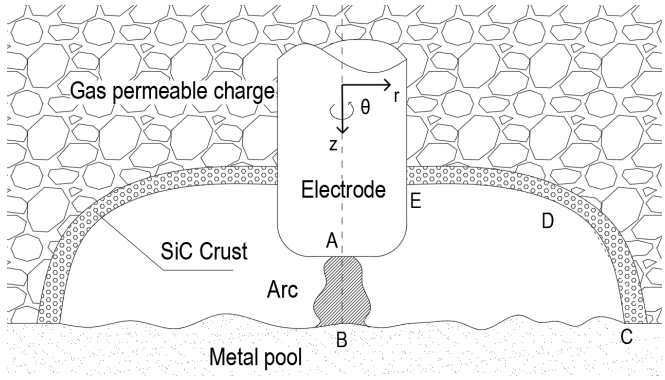

Figure 4.6: An schematic figure of the axi-symmetric modeling domain

4.4.3 3D - MHD model

In the present work, a new MHD model has been implemented in the OpenFOAM-v2012® [33] open-source computational fluid dynamics framework. A modified version of the standard *rhoPimpleFoam* solver was used as a base for the solver, given its existing capabilities for transient turbulent flow and heat transfer. A new MHD solver loop was added to the base code of the standard solver. For the implementation in OpenFOAM® simplifications for equations 4.24 - 4.27 can be made by using the electric scalar potential ϕ and magnetic vector potential $\mathbf{A}$:

$$\nabla \cdot \mathbf{j} = 0 \tag{4.33}$$

$$\mathbf{j} = -\sigma \left(\nabla \phi + \frac{\partial \mathbf{A}}{\partial t} - \mathbf{u} \times \mathbf{B} \right) \tag{4.34}$$

$$\nabla^2 \mathbf{A} = -\mu_0 \mathbf{j} \tag{4.35}$$

$$\mathbf{B} = \nabla \times \mathbf{A} \tag{4.36}$$

We do this to both eliminate certain stability problems inherent in calculating the magnetic field $\mathbf{B}$ directly close to boundaries [34] and make the equations better suited to be used in OpenFOAM®. The utility of this is evident when the equations are applied in the solver. OpenFOAM® directly handles the discretization while you can pick the scheme and the solver used. Below are a few of the most important math operators used:

$$\nabla A \ : \ \nabla \times A \ : \ \nabla \cdot A \ : \ \nabla^2 A \ : \ \frac{dA}{dt} \tag{4.37}$$

OpenFOAM® has a very robust way of adding user made equations. First the system of equations is put into the correct format, then you add them to a solver loop, and finally specify if its a vector or a scalar. We started by solving for the electric voltage potential ϕ and the magnetic vector potential $\mathbf{A}$ by inserting equation 4.34 into equation 4.33:

$$\nabla \cdot -\sigma \left(\nabla \phi + \frac{\partial \mathbf{A}}{\partial t} - \mathbf{u} \times \mathbf{B} \right) = 0$$

then we use equation 4.36 to elimate $\mathbf{B}$:

$$\nabla \cdot -\sigma \left(\nabla \phi + \frac{\partial \mathbf{A}}{\partial t} - \mathbf{u} \times (\nabla \times \mathbf{A}) \right) \Rightarrow \nabla^2 (\phi\sigma) + \sigma \nabla \cdot \frac{dA}{dt} - \sigma \nabla \cdot (\mathbf{u} \times (\nabla \times A)) = 0$$

and then we do a final simplification and get:

$$-\nabla^2 (\phi\sigma) - \sigma \nabla \cdot \frac{dA}{dt} + \sigma \left((\nabla \times \mathbf{u}) \cdot (\nabla \times A) + \mathbf{u} \times \nabla^2 \mathbf{A} \right) = 0$$

and finally moving the ϕ term we have equation 4.38. Next we insert equation 4.34 into 4.35:

$$\nabla^2 A = -\mu_0 \sigma \left(\nabla \phi + \frac{dA}{dt} - (\mathbf{u} \times \mathbf{B}) \right)$$

then we insert equation 4.36 to get equation 4.39:

$$\nabla^2 (\phi\sigma) = -\sigma \left((\nabla \times \mathbf{u}) \cdot (\nabla \times A) + \nabla \cdot \frac{dA}{dt} - \mathbf{u} \times \nabla^2 A \right) \tag{4.38}$$

$$\nabla^2 A = -\mu_0 \sigma \left(\nabla \phi + \frac{dA}{dt} - (\mathbf{u} \times (\nabla \times A) \right) \tag{4.39}$$

With $\mathbf{B}$ and $\mathbf{j}$, it is then possible to calculate the Lorentz force and the Ohmic heating source terms for the Navier-Stokes equation and the energy conservation equation. For each time step the electromagnetic calculation loop is iterated multiple times to increase the accuracy of the solution.

To account for the radiation heat transfer term we currently use OpenFOAM®'s built-in P1 radiation model, but due to the modular nature of the solver it is possible to implement more detailed radiation models in the future.

4.4.4 Boundary conditions

Boundary conditions [BCs] are an essential part of any modeling. They are needed to make the main simulation possible by using simplifying assumptions at the boundary surfaces that are either known values or educated guesses of the conditions present outside. Figure 4.7 shows an overview of the BCs used.

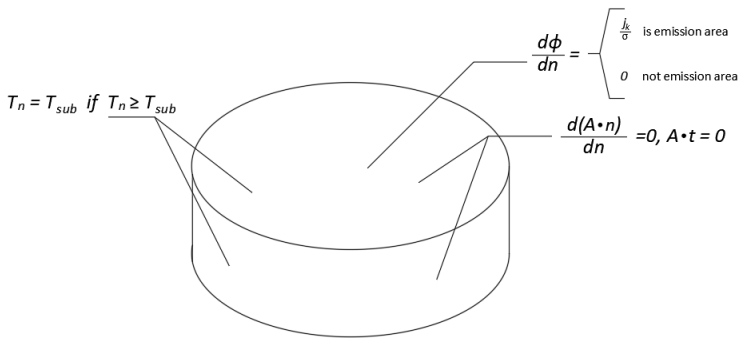

Figure 4.7: The new boundary conditions for the MHD simulation.

4.4.4.1 Boundary conditions for ϕ

The boundary condition for the electric potential ϕ has been largely improved from previous works, such as in [35]. A new boundary condition was developed for the MHD solver, which accurately identifies the surface from which electrons are emitted at any point in the AC cycle. The electric potential is based on a set current density j_c and the electrical conductivity σ on the emitting surface. Two methods are available when using the BC, the first is to fix the center of the arc and the second is to allow it to start where the highest electrical conductivity is found, to allow for mobility of the cathode spot.

Both use the same base method, where by looping over a list of all surface elements on the cathode ordered by surface conductance, and assigning each to the attachment spot until the total required area for the current at that time is reached. The boundary condition per control volume is then assigned as $\frac{d\phi}{dn} = 0$ except where the emission occurs then we have:

$$\frac{d\phi}{dn} = -\frac{j_k}{\sigma} \tag{4.40}$$

In the new boundary condition, the arc is reversed by switching the emitting surface between the electrode and the work surface in order to simulate the change in voltage polarity at different points in the AC cycle. Figure 4.8 below shows the boundary conditions for ϕ:

More accurate cathode and anode boundary conditions are possible, such as those developed later in this work and should be used for future work.

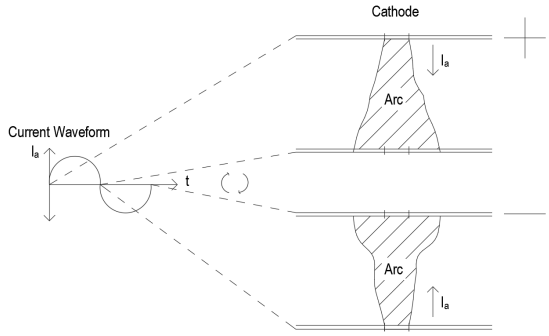

Figure 4.8: The arc changes direction using the new boundary conditions for the voltage potential Φ.

4.4.4.2 Boundary conditions for A

The magnetic vector potential in equation 4.39 needs a spatial boundary condition to be specified. These are usually difficult to determine in complex geometries, Andreas Westermoen, in his thesis [34], reported that acceptable accuracy could be obtained by setting the derivative of A in the normal direction of the surface to zero and at the same time forcing the tangential components at the surface to zero as well. This can be thought of a having the boundary magnetically insulating or not allowing the magnetci field lines to cross the boundary:

$$\frac{d(A \cdot n)}{dn} = 0, \quad A \cdot t = 0 \tag{4.41}$$

4.4.5 Boundary conditions for T

The final special boundary conditions is for the temperature T. Both the anode and the cathode surface are subject to very high levels of heat flux from the plasma by conduction, convection, and radiation from the arc. If allowed to heat up in the simulation it would take the surface temperature well over the sublimation temperature T_{sub} of the surface material, generally carbon. Here we have decided to simply limit the surface temperature to the sublimation temperature of the material. Any excess heat flux is used to sublimate or erode the surface:

$$\text{if } T_n < T_{sub} \text{ then } T_n = T_n, \quad \text{if } T_n \geq T_{sub} \text{ then } T_n = T_{sub} \tag{4.42}$$

Here T_n is the temperature for in each surface volume. This is of course is a simplification but it becomes useful later when we start to develop the cathode/anode model.

4.4.6 OpenFoam implementation

We have mentioned in 4.4.3 that the model was created in OpenFOAM but we have not gone into any specific details. Since this was a considerable part of this work we would be remiss if we did not describe this model and its development in at least some detail. To start with there is no MHD model available in OpenFOAM that handles magnetic and conductive fluids at high temperatures. The initial idea was to use the *simpleFoam* solver but this was quickly abandoned due to lack of an energy equation [33], in the end we decided to use *rhoPimpleFoam* which is a transient solver that includes turbulence, density and the energy equation by default. To start with the implementation of the geometry had not been decided upon, if it should be axi-symmetric or fully three-dimensional, as was described in section 4.4.3 a completely three-dimensional geometry was chosen.

Initial steps were to implement small changes to the base solver while at the same time learn how the internal structure of OpenFOAM operated. The first step was to add the Lorentz force as a set value field in a 2D mesh, the results can be shown below in fig 4.9:

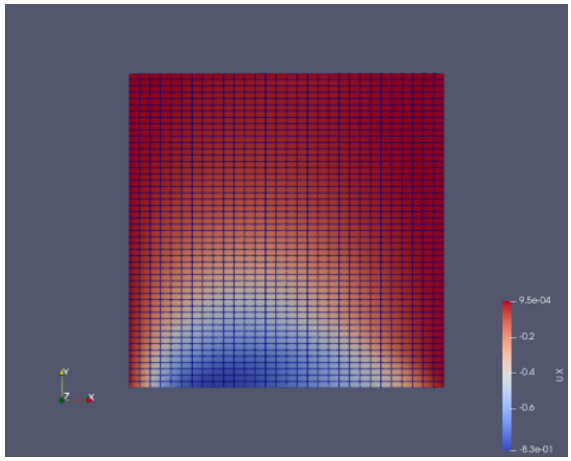

Figure 4.9: The effects on the velocity field of a otherwise still fluid after adding the Loretz force to the solver.

These results were not accurate in any physical respect but were the start to implementing the rest of the changes. With equations 4.38 and 4.39 already on the correct format as described in 4.4.3, we could start figuring out how to integrate them in to the existing solver. The *rhoPimpleFoam* solver is rather straight forward when you have started to understand how openFoam works, below is a the basic structure show in a very simple way:

...
Create Fields
while $t < t_{end}$ **do**
    solve $\rho(T, \mathbf{u})$, eq (4.29)
    solve $\mathbf{u}(\rho, P)$, eq (4.28)
    solve $T(\mathbf{u}, \rho)$, eq (4.30)
end while
...

In order to be a able add the new source terms to equations 4.28 and 4.30 we must start by solving the MHD equations, 4.38 and 4.39, that we defined in 4.4.3. The first step is to estimate the electric conductance σ in each element. The conductance is tabulated and is simply assigned by a look-up function based on the temperature. Next we implement the new equations in between where the solver calculates the density ρ and the momentum $\mathbf{u}$ as a sub-model.

The timescale for electromagnetic physics is a lot smaller than for the material interactions we need to account for it when estimation them. This is done by iterating the MHD equations several times to make them converge sufficiently before going forward in a given time step. This makes sure that we have as accurate of a result as possible. After adding the MHD sub model the solver looks like this:

...
Create Fields, here
while $(t < t_{end})$ **do**
    solve $\rho(T, \mathbf{u})$, eq (4.29)
    ... Start of MHD ...
    assign σ(T,P)
    while $(i < num\_it)$ **do**
        solve ϕ($\mathbf{u}$,$\mathbf{A}$,σ), eq (4.38)
        solve $\mathbf{A}$($\mathbf{u}$,ϕ,σ), eq (4.39)
        calculate $\mathbf{j}$, eq (4.34)
        calculate $\mathbf{B}$, eq (4.36)
        if (ϕ and $\mathbf{A}$ is converged) **then**
            break loop
        end if
        i++
    end while
    ... End of MHD ...
    solve $\mathbf{u}(\rho, P)$, eq (4.28)
    solve $T(\mathbf{u}, \rho)$, eq (4.30)
end while
...

The new source terms can now be added to the relevant equations and the

whole set of MHD equations is solved for each time step. We call this new MHD solver *mhdRhoPimpleFoam*.

Adding to an existing solver is a difficult task. The starting point should always be to learn how the chosen solver works, what is it doing when and where can the additions be implemented. One of the most important parts is to be sure the scientific units of the additions are correct and match the ones being solved already. Then the equations have to be solved correctly by putting them on the correct format and then finally the mesh need to fit the simulation requirements.

4.5 The industrial arc modeling domain

In this work we have focused on the arcs present inside submerged arc furnaces and thus the modeling domain, the region we need to model, must reflect that. We focus on the area directly under the electrode where the arc burns between the electrode and the bottom material, figure 4.10 shows a schematic drawing for one electrode and where the modeling domain is located.

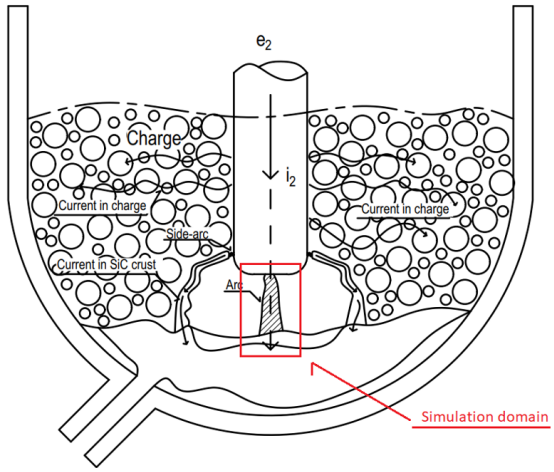

Figure 4.10: The simulation domain for our MHD models is directly below the electrode in a SAF.

During this work *blockMesh* has been used to create the main mesh. It is the simplest tool for meshing in openFOAM and only relies on a set of coordinates that contain the corners of the modeling domain sections. When those have been identified the domain can be split into blocks and then each block will have a defined mesh type, the amount of elements in each direction, and a grading scheme.

In the early stages of the solver development this was done with a 2D domain which was only used for a very short time. The second iteration of the domain was a full 3D mesh in the shape of a cube that had a slightly smaller mesh in the center, this was later developed into a cylindrical mesh, figure 4.11 shows these meshes. Both of theses had serious issues, the cube was to course and the cylinder had crippling issues with how the MHD model assigned the voltage potential to the cathode surface due to large variations in the surface are of the control volumes.

The end of this development led to the final mesh that was used for all the industrial simulations that are presented later in this work. It is sort of a combination of the two shown above. We kept the outside boundary as a cylinder but the

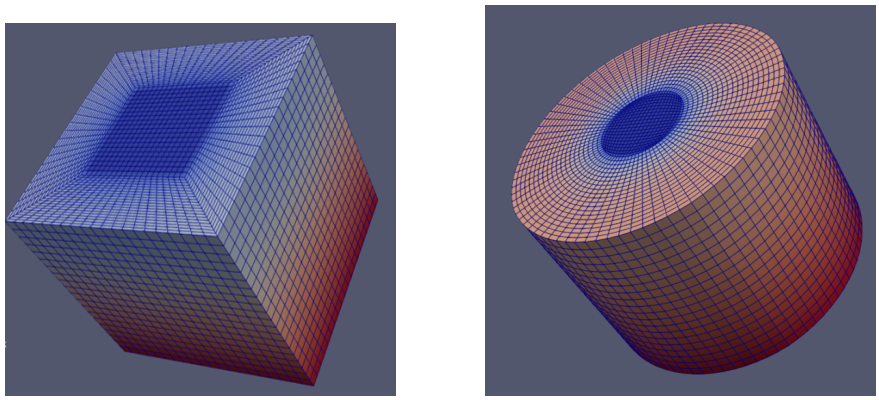

(a) (b)

Figure 4.11: (a) The initial 3D mesh cube used for the model (b) The cylindrical mesh for the model

central area was reverted to a square so that the surface area of the volumes would be constant.

We called this the industrial case geometry and it has a height of 7 cm and a total radius of 30 cm. The domain height was chosen to represent a typical arc length for an operating furnace [8], [24]. The mesh has a total of 306250 elements and consists of 5 blocks. A 5 x 5 cm central block has a denser mesh size to increase simulation accuracy in the arc area. This is important due to the rapid spatial and temporal changes in the temperature field in and around the arc column during the simulation. In the center at the bottom boundaries elements are 1.43 x 1.43 x 0.35 mm (length, breadth, and height), with the element height smaller close to the boundary to create inflation layers. The mesh inflation layers near the upper and lower boundaries permit better evaluation of local variations in the magnetic vector potential A in the electromagnetic field solution.

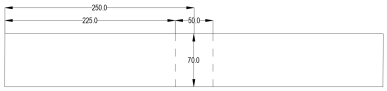

(a)

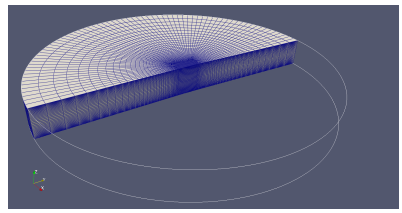

(b)

Figure 4.12: (a) The Industrial furnace geometry in mm, (b) A visual representation of the mesh used in the simulation of the industrial case.

Chapter 5

Cathode / Anode sub model

One of the most important aspects of arc modeling is the boundary conditions at the cathode and anode, where the arc spot is attached. In the model we described previously in 4.4.3 we impose a set current I and distribute it over the cathode surface using ϕ and a set current density J_c, this is usually what has bee done for most arc published models, however, it is not exactly accurate and a better method is needed to estimate the current density and at the boundary. This chapter will discuss more details on the layers that border the plasma and how they are treated, what estimations are made there, and then what models have been used before, finally it will introduce the model that is under development and has been integrated into the MHD model as a sub-model.

5.1 The Sheath layers

We can divide the arc into 5 zones or regions based on the electrical potential distribution, figure 5.1. In the border regions, (1 2) near the cathode and (4 5) near the anode, the electrical field strength increases sharply. In contrast, in the central region (3), the field remains relatively constant. In low current arcs, the electron emission is generally started by field emission, however, in high current arcs thermionic emission dominates due to the large amount of current flowing through the electrodes.

The regions closer to the electrode (1 and 5) are usually called the sheath or space charge layers. These are the transition regions between metallic and gaseous conduction and are made up of positive ions. The regions next to the plasma column (2 and 4) are called pre-sheath or ionization layers, where charged species are created by ionization [17]. In high-current industrial arcs these layers are less well defined, as the energy impacting anode and cathode surfaces produces a surplus of electrons through thermionic emission [13]. This allows us to treat them

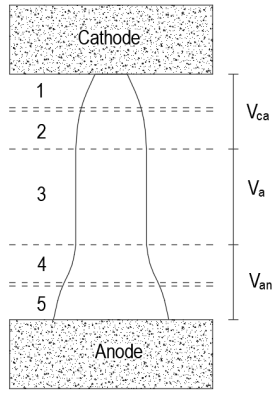

Figure 5.1: The arc regions and simplified voltage drop in an industrial arc.

as a single region for the purpose of creating the cathode anode model.

5.2 Modeling description

This model is cathode / anode sub-model [CASM] is based on the one presented by Seavarsdottir et al. in [13], [14] and [36]. Which are in turn based on ideas appearing in Neumanns theory [37] and Benilovs model [38], [39] for low-current DC arc cathodes. The behavior of the arc at the electrode is crucial when estimating its impact on electrode erosion. This behavior is highly sensitive to the boundary conditions at both the cathode and anode, which is why significant effort has gone into developing cathode submodels tailored for high-current AC arcs. However, different assumptions apply to high-current arcs compared to low-current arcs. The model used in this analysis treats both the anode and cathode similarly, as the large energy input from the arc causes both surfaces to emit and absorb a significant amount of electrons. The energy balance in the ionization layer does not need to be strictly maintained because the arc provides a large energy surplus that enters this layer. The cathode fall voltage is considered constant in each finite-volume cell across the cathode surface, determined by the condition that the total current from the electrode matches the imposed arc current.

If a large plasma at local thermodynamic equilibrium (LTE) is suddenly enclosed by an insulating wall, the wall will initially be bombarded by fast-moving plasma electrons and become negatively charged. This negative charge repels incoming plasma electrons and attracts ions, creating a space charge sheath that shields the plasma from the wall's influence. Plasma electrons only begin to feel the wall's presence once they enter this sheath. As they pass through the ion layer,

the shielding effect weakens, and they slow down due to the electric field. For an insulating wall, the potential drop across the sheath is just enough to maintain zero total current. When a net current is applied to plasma confined between two walls, it's reasonable to assume that the potential drop adjusts to allow a net charge exchange between the plasma and the wall, consistent with the applied current.

We also assume that the electrons and ions are at LTE since this makes things a lot simpler and is not perhaps to far from the truth. But we still have to estimate the temperature of the electrons T_e and ions T_i, we will use T_e for both here. We use the same method as in [14] where we use a ratio of the wall and plasma temperatures T_{pl}:

$$T_e = \frac{3T_c + 4T_{pl}}{7} \tag{5.1}$$

As we discussed in section 4.4.3 we assign the surface potential ϕ based on the conductance at the surface σ and the imposed current density j_c this makes the voltage at the surface vary based on the conductance in the plasma next to it. This is perhaps not the most accurate assumption but electrodes are not strictly a perfect conductor and will therefore also have a slightly different potential in reality.

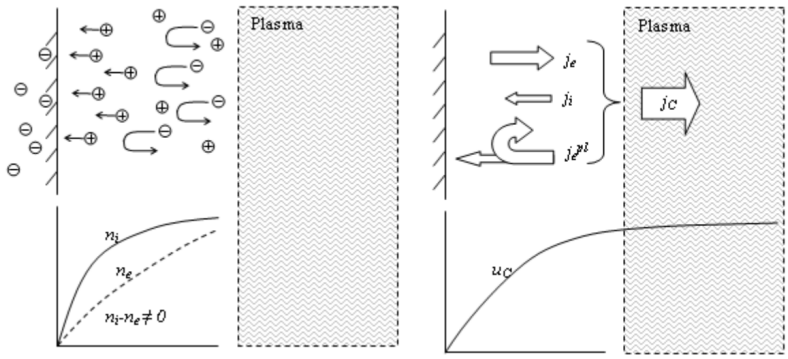

Figure 5.2: Schematic drawing of a space charge sheath and the current components in the Cathode anode sub model.

The current density at the cathode and anode is composed of three distinct components, figure 5.2. The first is the thermionically emitted current, which is when electrons inside a material posses enough kinetic energy (heat) to overcome the potential barrier of the material or work function W. This is governed by the Richardson-Dushman's equation:

$$j_e = f A_R T_c^2 \exp\left(\frac{q(W + \Delta W)}{k_B T_c}\right) \tag{5.2}$$

A_R is a universal constant given by:

$$A_R = \frac{4\pi q m_e k_B^2}{h^2} = 1.2 \times 10^6$$

where T_c is the cathode surface temperature (a fixed value based on the material), q is the electron charge, m_e is the electron mass, W is the work function, ΔW is the Schottky correction term usually around 0.5 eV for carbon, k_B is the Boltzmann's constant, and h is Planck's constant. f is a scaling factor used since the theoretical maximum thermionic emitted current of $f = 1$ has never been observed experimentally, thus set to $f = 0.5$ in this work.

The plasma gas also contributes electrons that diffuse over the sheath voltage potential u_c and those that are not repelled by the potential enter the electrode. We call theses electrons *counter-diffusing plasma electrons* and the current density for them is given by:

$$j_e^{pl} = \frac{q n_{e0} c_e}{4} \exp\left(\frac{q u_c}{k_B T_e}\right) \tag{5.3}$$

$$c_e = \sqrt{\frac{8 k_B T_e}{\pi m_e}}$$

here n_{e0} is the electron density at the edge of the sheath and, c_e is the average electron velocity.

Thirdly we have the ion current, in [40] Benilov put forth a solution for the current density of plasma ions traveling through the sheath towards the electrode surface for low current arcs. A more simple version is proposed in [14] for high current arcs where the ionization degree has reached saturation:

$$j_{i,sat} = \frac{q n_{i\infty}}{\sqrt{2\pi}} \sqrt{\frac{k_B (T_c + T_e)}{m_i}} \tag{5.4}$$

where m_i is the ion mass, $n_{i\infty}$ is the ion density at the edge of the sheath. We assume the electron densities are identical next to the wall and at the sheath edge, figure 5.2, so $n_{e0} = n_{i\infty}$ In the model here we assume the ion current is fully saturated. We use precalculated values for $n_{i\infty}$, they are shown in figure 5.3 for SiO + CO:

The total current at the surface is then:

$$I(t) = \sum^{n} (j_{e,n} A_n + j_{i_{sat},n} A_n - j_{epl,n} A_n) \tag{5.5}$$

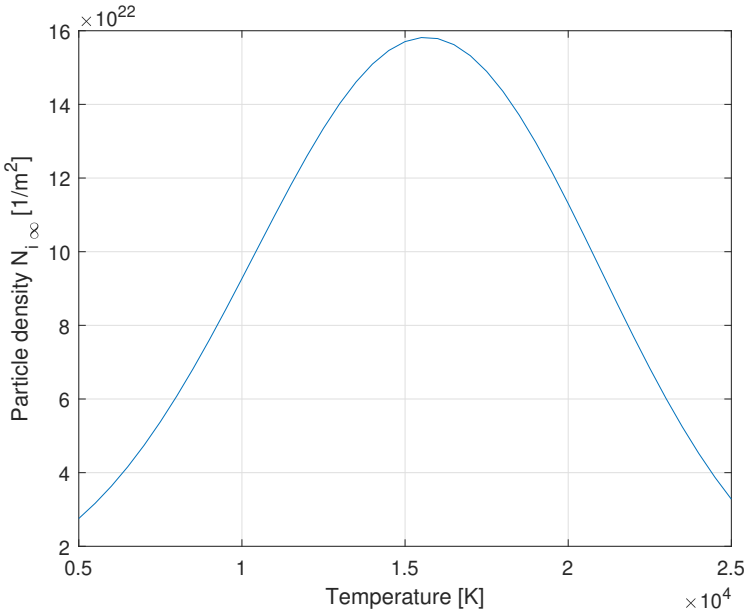

Figure 5.3: Precalculated values for ion/electron density.

where n is the ID number of each control volume surface and A is the surface area of the volume. We assume that the cathode and anode both thermionically emit electrons based on their respective temperatures, and they are both bombarded by electrons and icons from the plasma. Only the orientation of the surfaces in respect to the current density direction separates how the emission behaves for each one.

For each surface we solve equation 5.5 in each control volume surface to get the local value of u_c, this essentially means that it will vary based on plasma temperature T_{pl} and the voltage potential ϕ (which is turn is based on conductance and current density) in each volume. We impose AC current condition by using the boundary condition described in 4.4.3 above.

In order to estimate the electrode erosion we assume that all the heat flux $\dot{q}_{sub}$ generated by these currents as well as from radiation to the surface goes to sublimation:

$$\dot{q}_{sub} = -j_i\Big(2\frac{k_B T_e}{q} - 2\frac{k_B T_c}{q}\Big) + j_e\Big(2\frac{k_B T_c}{q}\Big) - j_{e,pl}\Big(2\frac{k_B T_e}{q}\Big) + j_c u_c + S_{rad} \quad (5.6)$$

Here S_{rad} is the radiation source term. We then calculate the sublimation according to the Clausius-Clapeyron equation for the equilibrium vapour pressure of carbon as a function of temperature given in equation 5.7, and then we use the Hertz-Knudsen equation for the maximum evaporation rate from the surface in equation 5.8 which provides the mass flux.

$$P_{eq} = C_1 e^{\frac{-H_{vap}}{RT}} \tag{5.7}$$

$$G_0 = C_2 \sqrt{\frac{m_C}{2\pi k_B T}} (p_{eq} - p_a) \tag{5.8}$$

Where H_{vap} is the vaporization enthalpy, C_1 is the equilibrium pressure, and T is the temperature estimated for the erosion calculation. We do not solve the transport equations for carbon leaving the electrode in the arc area. Equation 5.8 was therefore simplified to where we have the factor C_2, can between 0 and 1 but we use 0.1, which is a measure of the mass transfer resistance from the surface. p_a is the ambient pressure which we use here instead if the partial pressure p^* since it will be close to the ambient pressure while the temperature is over the sublimation temperature.

5.3 Model implementation

To implement the model we decided to use at first the channel arc model previously described here since it gives the plasma temperature of the arc for a given current and current density, see figure 4.4. This implementation was similar to the one described below for the MHD model and was mostly used to test out new changes and debug since it was easier to do for the simpler CAM. For the channel arc cathode anode sub model we continue to use the pre-calculated DC model as a base, we use an imposed current and assume a flat temperature profile across the cathode spot. We also assume that the sheath voltage u_c is constant in that area, otherwise the implementation is the same as below.

Implementing the cathode anode sub model into the new MHD model was more complex than for the channel arc model. Initially a boundary condition was used to calculate the sheath voltage u_c at the boundaries, this turned out to be rather unwieldy in practice, so a submodel inside the solver code structure was used instead of a boundary condition.

The benefit of the simulation domain being three dimensional control volumes and not a 2D cylinder are that there is no need to integrate the current over the cathode surface, we can simply look at each volume in series and run the model for each one. This gives us all of the current components, the sheath voltage and, mass transfer across both cathode and anode.

The already discussed MHD model gives us all the values for the plasma and surface temperature that we need to calculate the current densities. The first step in the sub-model involves accessing the temperature field and current density close to the surface of the cathode and anode. The main goal of the model is to estimate the sheath voltage u_c to do that we use equation 5.5, since we impose a set total current and the current density for each volume is used to initialize the electric potential we can estimate u_c in a mostly straightforward manner, we start by calculating the thermionic and ionic current densities j_e and j_i and then we set up a balance:

$$j_{epl} = j_c - j_e - j_i \tag{5.9}$$

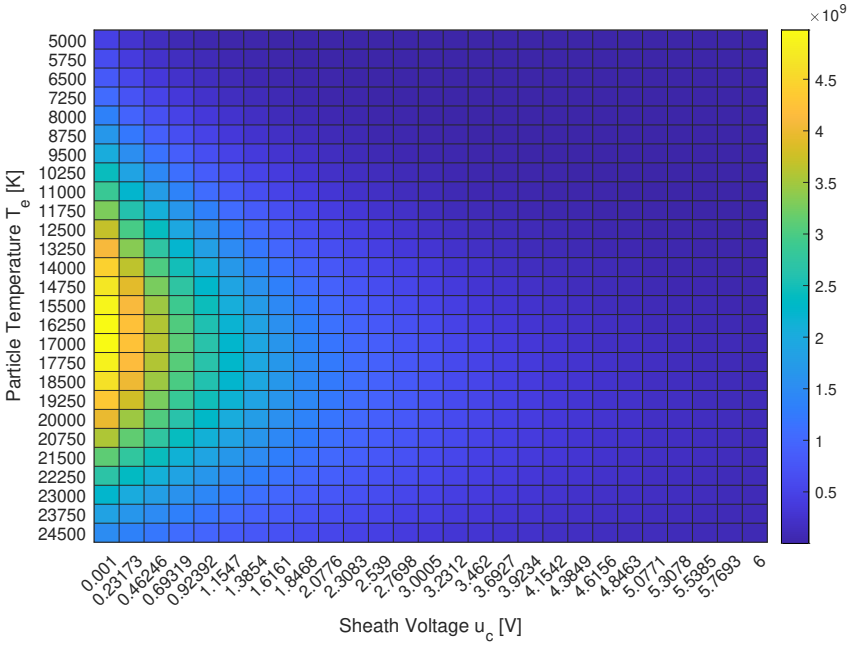

Figure 5.4: The counter diffusing plasma electron current density $j_{e,pl}$ over a range of particle temperatures and sheath voltages.

From this relation of current densities we can start to calculate the voltage, figure 5.4 shows how varied the plasma electron density $j_{e,pl}$ can be for different values of particle temperature T_e and sheath voltages u_c. The previous method described in [14] and [13] where voltage is estimated by an iterative method where equation 5.3 is solved by varying the value of u_c until equation 5.9 is fulfilled. This

can be a bit computationally heavy especially when you also have to take into account the anode where the current has a negative sign, this method was the first implemented in this work and is shown with *"pseudo code"* below:

...
$u_c = 0$
while $(i < 10000)$ **do**
    calculate j_e, eq (5.2)
    calculate j_i, eq (5.4)
    if $i = 5000$ **then**
        $u_c = 0$
    end if
    if i < 5000 **then**
        calculate j_{epl}, eq (5.3)
        $u_c = u_c + 0.002$
    else
        calculate $-j_{epl}$, eq (5.3)
        $u_c = u_c - 0.002$
    end if
    if $j_e + j_i - j_{epl} \geq j_c$ **then**
    end if
end while
...

This could sometimes also deliver numerical errors in the model developed here when the u_c steps were to large and then j_{epl} would overshoot the desired value by a large margin. To fix both of theses issues a new model was developed where we calculate the voltage directly after first determining the needed plasma electron current, this allows us to save a lot of computing time and and also get an exact value for the sheath voltage. The new sudo code is below and figure 5.5 shows a comparison between the two methods:

...
calculate j_e, eq (5.2)
calculate j_i, eq (5.4)
$j_{e,pl} = j_i + j_e - j_c$
if $j_{e,pl} < 0$ **then**
    calculate $-u_c$
else
    calculate u_c
end if
...

When the sheath voltage and the current densities have been determined we next have to find out the heat flux to the surface and then the sublimation and

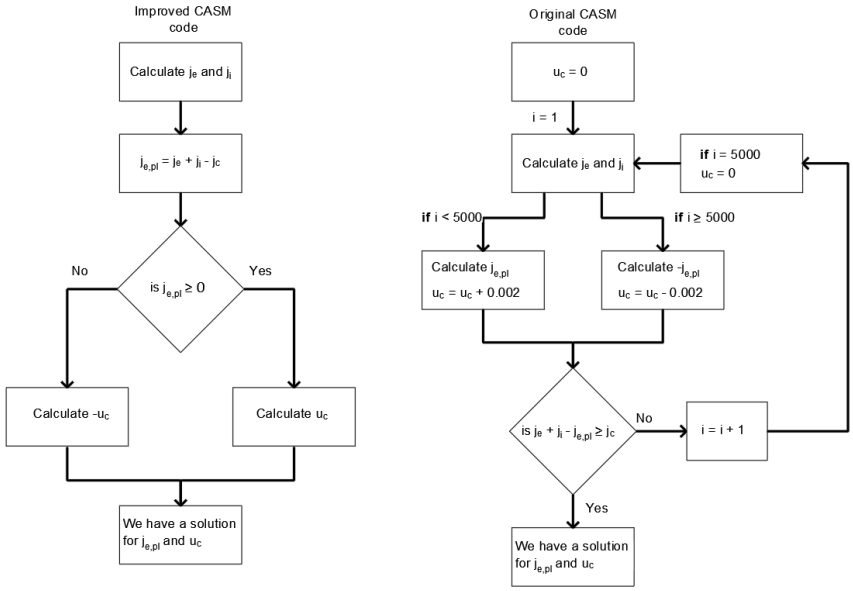

Figure 5.5: Block diagram of the two different solution methods for the the Cathode anode sub model.

mass transfer. We start by using equation 5.6 to calculate the heat flux. Since the MHD model already fixes the temperature at the boundary to the sublimation temperature of the surface material we can assume that this heat flux all goes to sublimation like we mentioned previously. We now need to estimate how much the surface would heat up if the model would allow it, for this purpose and due to some time constraints a simple thermal conductivity model, figure 5.6, was used to estimate what we will call the erosion temperature T_{ero}, we assume each control volume is connected to a small slice of carbon material that conducts heat to a cooler part of the electrode:

$$T_{ero} = T_c + \frac{\dot{q}_{sub} L}{k_C A_n} \tag{5.10}$$

where k_c is the thermal conductivity of carbon, L is the slice thickness. We now have all we need to calculate the equilibrium vapor pressure P_{eq} and mass transfer G_0 using equations 5.7 and 5.8.

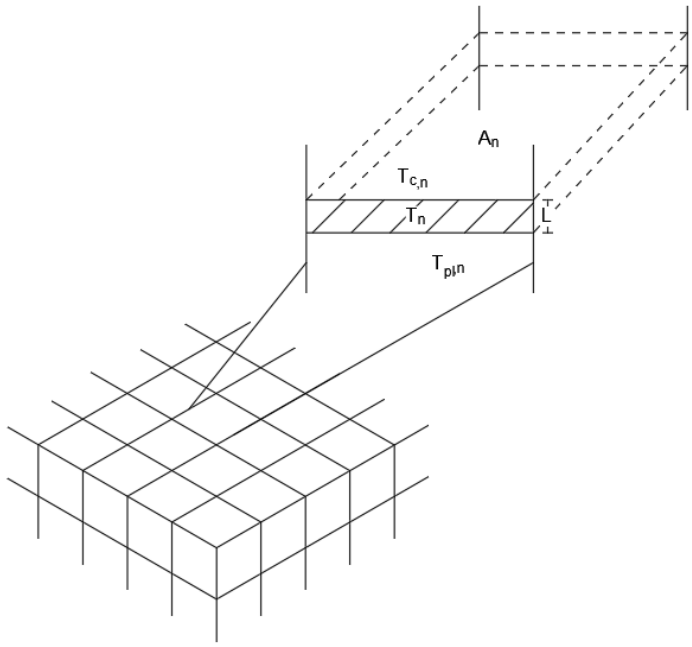

Figure 5.6: Schematic drawing of the erosion tempereature sub-model used in the Cathode anode sub model.

Chapter 6

Results

In this chapter the parameters and results for the many models will be presented in the same order they were described previously. We will show how the models were validated and what assumptions are made for them. Generally the models are validated using either other modeling, previous works that are considered to be correct or actual measurements.

First the circuit model is shown along with the results for the two coupled models CMM and CAM. Theses models are validated using values extracted from a SAF in operation and show a good fit to the actual data. Harmonic analyses is then done on the arc and electrode currents for different values of the charge resistance. Next we show the full MHD modeling results were we vary the plasma composition and then the length of the arc to see the effect it has on the arc voltage. Finally the results from the new cathode anode sub model are presented and we estimate the fall voltage and erosion of the electrode and bottom material.

6.1 Three phase Cassi-Mayr and Channel arc model results

In chapter 4 we have described the models we used and their methodologies. Setting up the simulation is a bit complex since we have a total of three models (CAM, CMM and, MHD), with varying degrees of complexity and amount of input needed. In this section, we will describe these inputs as much as possible and then how the needed parameters were estimated.

6.1.1 Circuit model parameters

The circuit model requires quite a few parameters to run, some are easier to get than others. The transformer resistances and inductance's can be measured by conventional means. In the current model the distributed resistances and induc-

tances in the furnace are lumped into circuit elements L_i, R_i, based on a complete furnace model reported in [18] and [14].

We assume for this study that the transformers are symmetrical and thus have the same resistances and inductances, same for the electrodes. This is probably not the case in a live SAF but will give a good starting point and makes the setup easier. The values are presented in table 6.1 below:

Table 6.1: Parameters for the SAF circuit model.

Parameters	Values
V_{Ti}	230 V
R_{Ti}	0.03 mΩ
L_{Ti}	2.25 μH
$M_{Ti,Ti+1}$	0.375 μH
R_{ei}	0.09 mΩ
L_{ei}	2.09 μH
$M_{ei,ei+1}$	0.349 μH
R_c	2.1 mΩ

6.1.2 Model verification

As we have discussed the previous sections there are many parameters that have to be chosen for each of the arc models so that they can simulate a real arc. Those used in the CMM are not physically based but serve as fitting parameters to be adjusted to obtain the desired result. For the CAM you need a complete set of material properties and radiation energy absorption data for the desired arc plasma composition (SiO + CO in this case) for the model to work. The parameters for the arc models are in table 6.2 below. The arc height is set to 7 cm since that industrial arcs in Si-furnaces are thought to be around 5 - 10 cm and the number of arcs was 2 in the model since the simulations did not fit well if more or less were used.

The simulations were validated with measurements in an industrial furnace. In One of Elkem Icelandt's ferrosilicon furnaces was equipped with a data acquisition system [DAQ] [22]. This system measured the three phase current and voltage waveforms, independently for each electrode of the furnace. One of the most interesting factors is how much current goes through the arc and the charge material respectively. The method used in [16], was implemented to estimate both current and voltage in each electrode. The implementation used in this paper is explained in detail in [2]. We tried to pick a time period where the currents in the three electrodes were the same since we had already set the circuit model to be symmetric, we chose the time at 141 seconds for this purpose, figure 3.2.

Table 6.2: Parameters for the Cassi-Mayr model and the Channel arc model [3].

CMM		CAM		Used in both	
V_d	13 V/cm	j_c	25 MA/m^2	V_{an}	5 V
I_0	1 kA	K_1	1	V_{ca}	5 V
G_{min}	3 S	K_2	1/2	H_a	7 cm
P_0	50 kW	Φ_{an}	4.75 eV	Number of arcs	2
θ_a	0.1 ms	T_F	2273 K		
		τ	1 ms		

We compared the electrode, arc and charge currents for both models and the SAF measurements [MEAS], figure 6.1 left, the model parameters were adjusted for a better fit, table 6.2. All the modeled currents fit very well to the measured values, the total electrode current is around 150 kA while the arc and charge currents are 100 kA and 50kA respectively. The general shape is also a very good fit. The second thing to compare is the arc voltage waveform, figure 6.1 right, which also conforms to an acceptable level with the arc voltage being around 100 V and slightly square. For the case in question, around 2/3 of the phase current passes through the arcs, dissipating heat at extremely high temperatures.

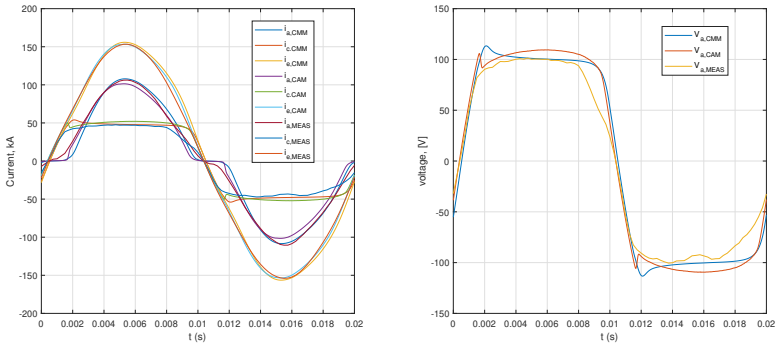

Figure 6.1: Electrode, arc and charge current (left), and arc voltage (right). Model data is marked CMM and CAM are the models and the measurements are marked [MEAS].

Finally it can be interesting to look the I-V curve of the arc or the arc footprint. We can see from figure 6.2 how the footprints for the models and the SAF look. There is a good comparison for the models but we can also see that the real arc behaves a lot more erratically, but this is normal. We can now say that both the circuit model and the two arc models are working as desired.

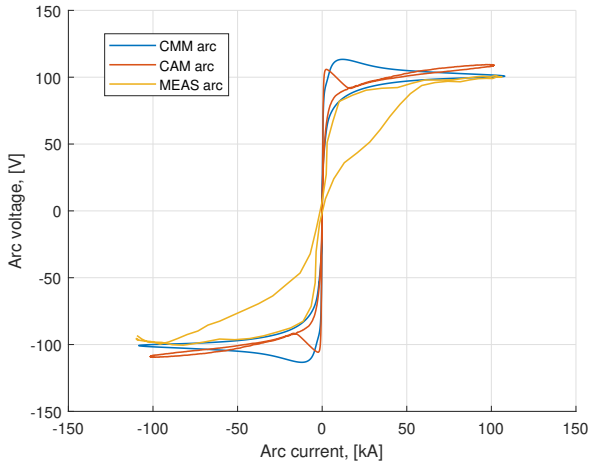

Figure 6.2: Arc footprints for the arc voltage and current from the SAF measurements and both simulation models.

6.1.3 Harmonics in the electrode

The electrical control of a SAF consists of a combination of Power control, where the power dissipation is managed by changing transformer tap position. The phase current and/or resistance is changed by adjusting electrode holder position and thus moving the electrode tip up and down. The electrode tip position determines how power dissipation is distributed in the furnace. When the electrode is moved up or down, the contact area between the electrode and surrounding materials change, and the availability of potential arcing sites, as well as the resulting length of the arc, changes accordingly [41].

The question is then when to lower or raise the electrode so that we can keep the correct balance between the arc and charge current. Since the arc is the main generator of furnace harmonics, figure 6.3, we should see a change in the total harmonic distortion [THD] as more or less current goes through the arc. So we propose here that by measuring the THD should give you an idea of the amount of current going through the arc and thus inversely the charge.

To investigate the variations in the harmonics, we used both models to simulate different vales of the charge resistance R_c. This was done by scaling the charge resistance from a low to a high value. It changes the current that goes through the arc from about 0 % to 90 % in several steps. To estimate the harmonics we decided to use the standard THD % generally used for power systems, given by:

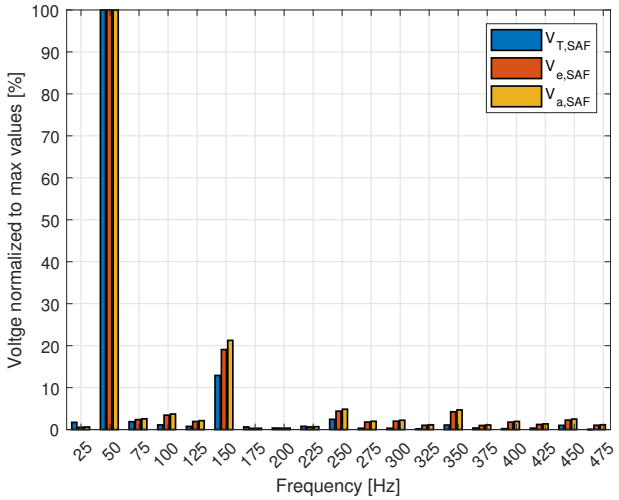

Figure 6.3: Normalized frequency components for the transformer, electrode and arc voltages for the measured values from the SAF. The arc can be observed to have the highest amount of over tones.

$$THD = \frac{\sqrt{H_2 + H_3 + H_4 + ... \quad H_n}}{H_1} \tag{6.1}$$

Where H_i is the harmonic component number i and i is the multiple of the base frequency, in this case 50 Hz. The results from both models for the voltage harmonics are shown in figure 6.4.

We can observe that as more power goes through the arc the THD_V % increases, almost linearly from 0% to 22 - 24%. This simple figure shows us where we want to have the voltage THD in order to have the desired arc current ratio, this will in turn ensure that the right amount of power goes into driving reactions to make silicon and in to melting the furnace charge materials. So if we would want to keep the ratio at 0.6 for example and we see that the THD is getting above 17% we can raise the electrode and thus increase the arc resistance.

6.2 MHD Modeling Results

To validate the model we have described in section 4.4.3, a cross validation study with Quinn Reynolds, the author of the model in [35], was conducted. We also did a study into the effects of varying the composition data that is used for the plasma

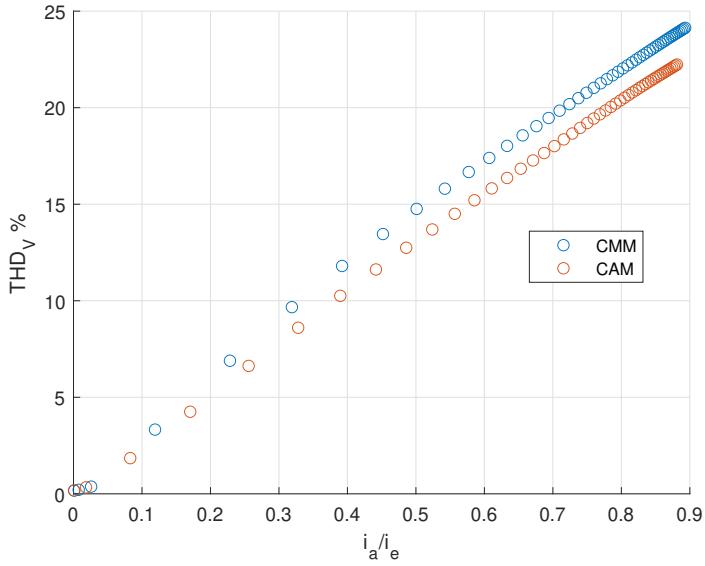

Figure 6.4: Total harmonic voltage distortion as a function of the current going to the arc for both models.

parameters. We started by comparing the two models using three different plasma property data sets for Argon, in a geometry that corresponds to a known laboratory furnace for which experimental measurements are available. This allowed us to assess the effect that different plasma property data sets have on the final results, and how well they fit the experimental data.

To simulate an industrial case we used a high current and two plasma data sets. The data sets were for a 50/50 mixture of SiO and CO gas and a 50 kA current was used. We investigated the effect that the different property data sets had on large-scale arcs since this is the likely composition present in the crater region. Finally we simulated industrial arcs in plasmas generated from different mixtures of SiO and CO gas, and investigate how the arc conditions change as the crater gas becomes more CO- or SiO-rich.

6.2.1 Plasma gas composition

One of the main challenges in simulating the arc furnaces is the lack of precise data on the compositions of the plasma gas that makes up the arc. Another is the lack of thermodynamic and transport property data for said plasma gas. In many

simulations and experiments, Argon is used as the plasma gas due to its ease of use and a very complete knowledge of its thermophysical properties. The main gases present inside an industrial furnace are SiO(g) and CO(g), and these can be in different ratios depending on conditions in the furnace interior.

For this work we used we used two different calculation procedures to estimate the plasma gas properties. The first is the open source *minplascalc* Python package [42] developed at Mintek and the second is an internal code developed at NTNU 30 years ago in [43]. We then studied the effect of the different data sets on the overall simulation results. The plasma property data used as input for the simulations was the enthalpy h, density ρ, electric conductivity σ, thermal conductivity κ and, specific heat C_p. We began by comparing three different data sets for Argon, followed by a comparison of two data sets for a 50/50 mixture of SiO and CO gases. In the end we varied the ratios of SiO to CO from 0 to 100 % in order to give an overview of how the properties change with different gas compositions.

6.2.1.1 Argon properties

For the argon we used the two different calculation procedures as well as previously tabulated data from calculations by Boulos et al [28]. The benefit of using Argon for verification is that its properties are well understood even at the temperatures present in an arc, and it is often used as a plasma gas in arc experiments which provide measured data for model validation. The three data sets for Argon are surprisingly different but follow a similar trend, see figure 6.5 below:

6.2.1.2 Industrial furnace gas properties - 50/50 mixture

For the industrial case studies, a SiO + CO gas with an equimolar mixture ratio was chosen. This is the most likely composition of the gases present in the crater. The data sets conform for density, enthalpy and electric conductivity but are fairly divergent for the rest except for specific heat at lower temperatures, see figure 6.6 below. This should give us different results for the arc voltage.

6.2.1.3 Industrial furnace gas properties - all mixtures

To further investigate the effects of changing plasma composition on the industrial scale, thermophysical property data for a range of plasma compositions from 0 % to 100 % SiO (the rest being made up of CO) were calculated. In figure 6.7 below we can see how the enthalpy-temperature curves change as the SiO fraction is increased. The corresponding variation in the specific heat capacity curves is quite extreme, particularly at low to moderate temperatures, and this can be expected to have an appreciable impact on the thermal behavior of the arc.

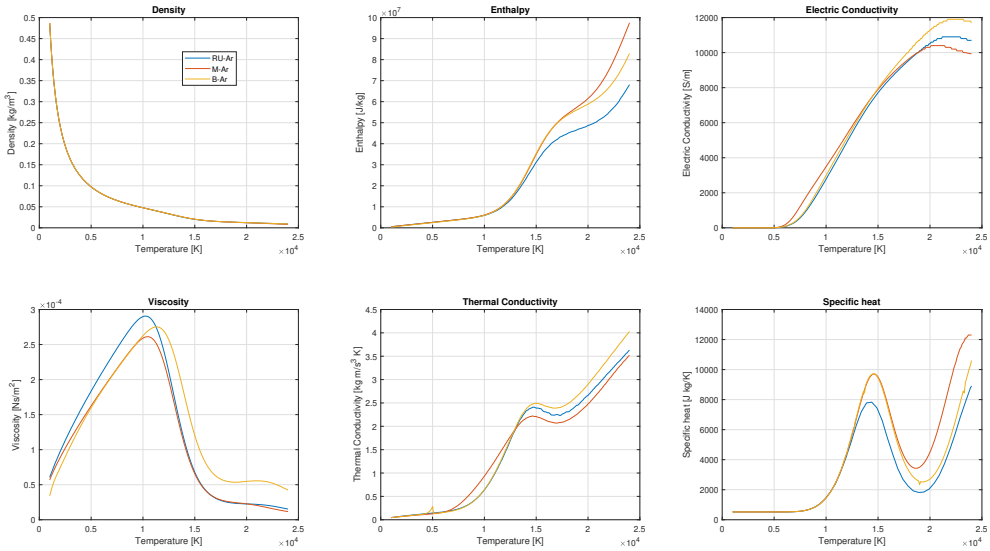

Figure 6.5: Plasma properties for different argon plasma compositions.

6.2.2 Verification and validation between solvers for Argon experiments

As discussed earlier, in order to verify and cross-validate our models, experimental data from pilot furnace experiments were used. We compared measurement data from [8] obtained from the pilot furnace experiment described in [31] to simulations conducted with the two MHD models and the three Argon plasma property data sets. We observed minimal differences between the two solvers, but there was some significant variance between the different data sets. The results are shown in figure 6.8 below. The measurements from the actual furnace show somewhat more chaotic behaviour than all the simulations, but a similar trend can easily be observed. We can therefore say that the solvers are working as desired and conform acceptably well to measurements and to each other for this known case. We can, however, see that the different data sets give slightly differing results. The voltage varies from around 40 V to 30 V for different data sets, or approximately 25%.

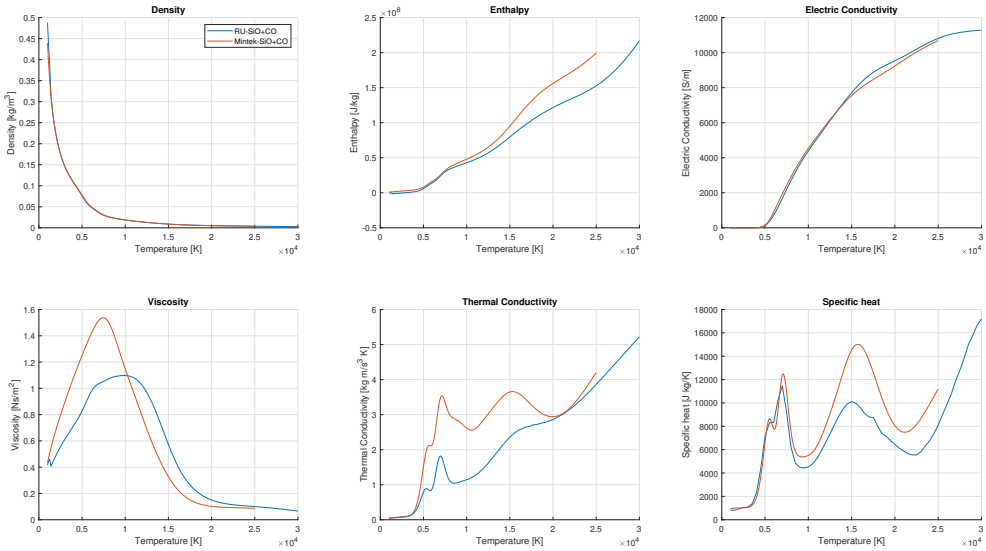

Figure 6.6: Plasma properties for the industrial plasma compositions.

6.2.2.1 Mesh dependence for the industrial case

The simulations for the industrial case were observed to have a large amount of noise during the transition from zero to top current. We therefore decided to do a small mesh dependence study to see if this was due to numerical or physical issues. We both reduced and increased the mesh density from 2 mm to 1.1 mm respectively to see if that would be a noticeable change in the behaviour of the noise as well as the final result. Figure 6.9 show the results for the mesh study and we can see that the noise is a mesh issue and not a physical one and that the final values of the arc voltage vary only a little.

6.2.2.2 Verification between solvers for industrial case

Here we are trying to see if the different solvers get similar results at higher currents at an industrial level and using the most likely plasma composition, half and half SiO and CO. The current has an 50 kA amplitude and for the boundary condition of ϕ we use the current density $j_k = 2.5\ A/m^2$. We can see on figure 6.10 bellow the arc voltage for both solvers and both data sets. We observed a good fit between the solvers and the data but with small differences, somewhat less than

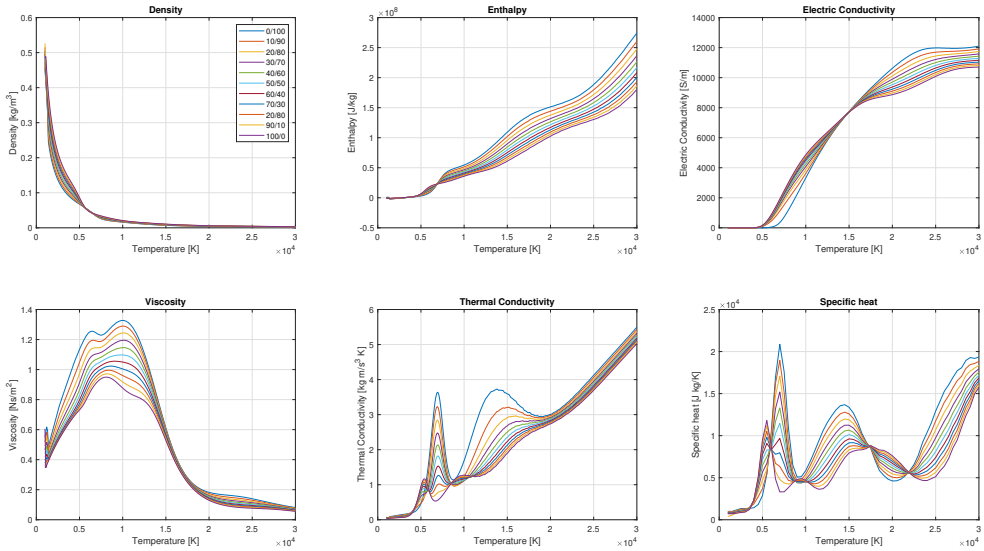

Figure 6.7: Plasma properties for the different industrial plasma compositions, the ratio of SiO to CO varies from 0 to a 100%.

for the previous argon case. The Mintek data gives a slightly lower voltage than the RU one and the same goes for the solvers, this results in the solver converging in the middle when the RU solver is running on Mintek data and then the oposite for the Mintek solver runnig RU data. The voltage is a bit high from what we should be expecting but we think it might be the lack of a proper cathode model as seen in [36] and the simplicity of the radiation model used, this might be causing the plasma not to heat up properly leading to the conductance to be lower than it should be.

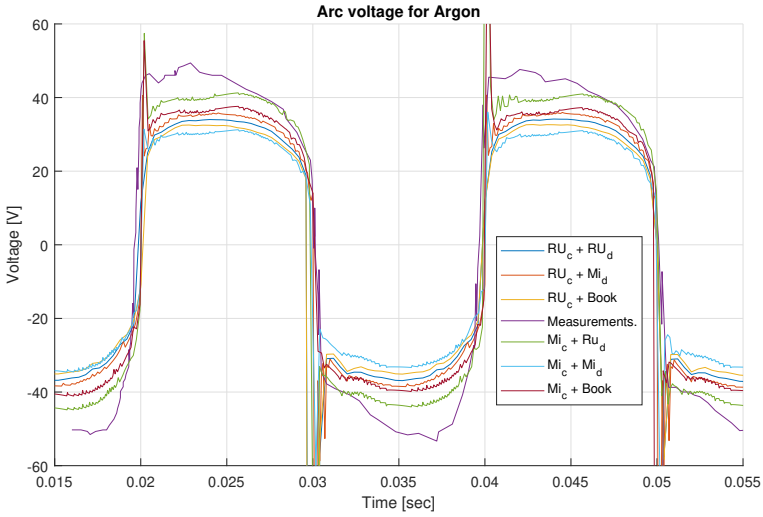

Figure 6.8: Arc voltage of the three different argon plasma data sets, run with both solvers. Measurements data is plotted in purple.

6.2.2.3 Effect of plasma composition in the industrial case

Now we wanted to see how the arc voltage would change with different plasma compositions for the industrial case. As mentioned a above we varied the composition from 0 - 100% SiO to CO ratio, to get an idea of how the arc voltage would change and that could then be used to estimate furnace conditions in a real furnace. Running pure CO crashed the simulation so we did not get any results from that part but the rest of the composition arc voltages are shown in figure 6.11. We can see that the voltage changes from around 263 V to 240 V this is around 8% so not very much but still notable. We can then say that changes in the composition of the arc plasma will not significantly impact the voltage in a operating silicon SAF.

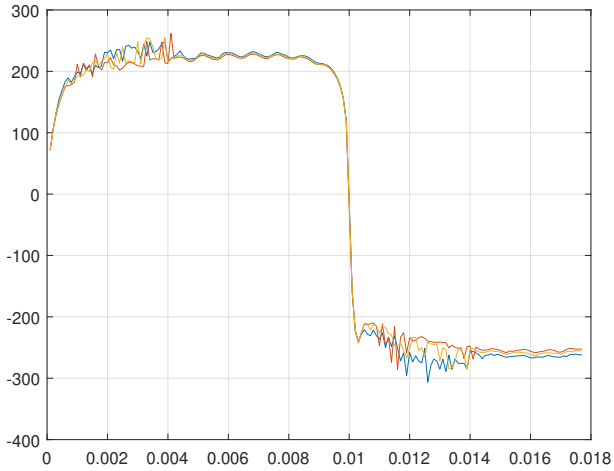

Figure 6.9: Arc voltage of the three different mesh densities. The noise seems to be dependent on the mesh not the physical parameters and the final result changes little between meshes.

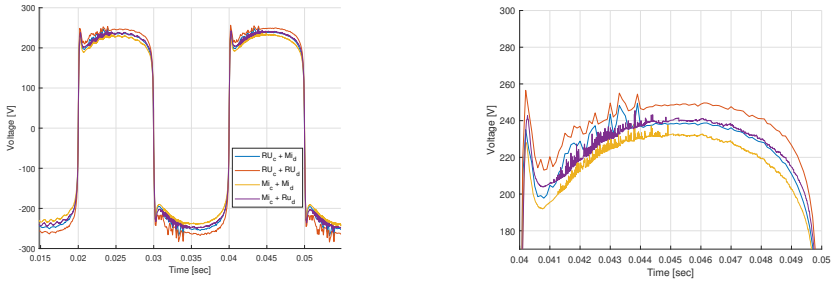

(a) (b)

Figure 6.10: Arc voltage for the industrial case where the SiO to CO ratio is 50/50. Here both solvers are used and both data sets for the plasma. (a) shows the larger waveform and (b) shows a close up of on of the tops.

6.2.3 Changing plasma compositions and arc lengths

The above results for the arc behavior showed that the composition did not have a very strong affect on an industrial arc behaviour so we decided to also look into the

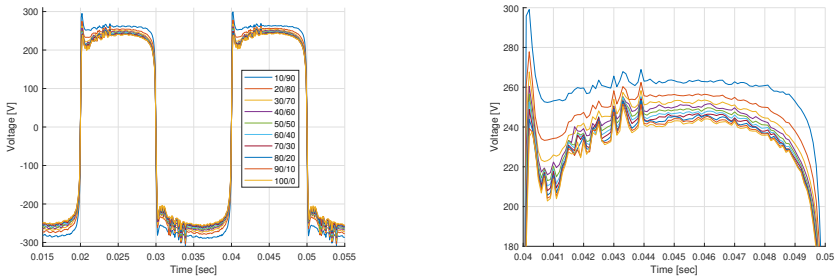

(a) (b)

Figure 6.11: Arc voltage of the ten different SiO / CO ratios of plasma data sets, run with the RU solver. (a) shows the larger waveform and (b) shows a close up of on of the tops.

effects of the arc length. We ran a total of 15 cases where the arc was simulated for a total of 0.08 seconds in simulation time, or 4 periods for 50 Hz AC current. The arc current is set to 50 kA peak to peak AC like before. We observed that the arc voltage seams to be most dependent on the arc length, but the plasma composition does also have a small effect on the outcome. Figure 6.12 below shows the results for the arc voltage for all the runs. We can see that the different composition runs cluster around each other for each length.

To make some practical sense of the results normalized the RMS voltage for all the runs, see figure 6.13. The voltage is normalized to the centre value or 50% SiO(g) and 7 cm arc length since this is the simulation case that is in the middle of the chosen parameters. We can then observe how much the voltage varies from that value; this should help in estimating what conditions are present in any furnace as long as the normal operating value for the arc voltage is known. This will of course vary from furnace to furnace.

What we can see from the results is that the voltage increases with length and decreasing SiO amount in the cavity. The arc length changes the voltage by about 50% while the composition changes it by about 10 % to 15 %. Thus we may conclude that the length has much more impact on the voltage than the SiO:CO ratio.

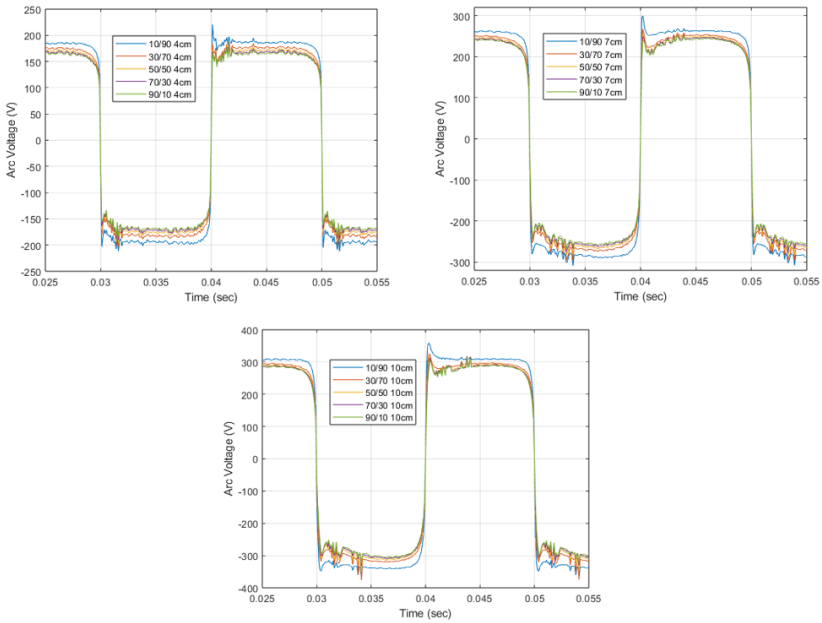

Figure 6.12: Arc voltages for the 15 simulations for all 5 compositions and 3 lengths. Sorted based in arc length.

6.3 Cathode / anode sub model results

The cathode anode model promises some very interesting results, especially the electrode erosion. We will start by showing the results from the model coupled to the channel arc model and then move on the MHD one. Here we only look at the cathode since it will be a mirror of the anode except the total current density would be a little higher. We use I(t) = 50 kA, same as for the previous simulations, the cathode spot radius r_c is assumed fixed at 3.0 cm, the arc length H_a is 7cm, and the surface temperature is 4100 K. The imposed current and the spot radius set the current density j. The model was run for a total of 10 ms in a 100 steps, or for a half a AC period. If we look at the current density over that period we can see how the model estimates different current densities in figure 6.14 below:

We can see that the thermionic emission is constant at $j_e = 1.2927 \times 10^7\ A/m^2$ as fits a fixed surface temperature, the ion current density j_i is varying with the plasma temperature from about 4.2×10^6 to $7.3 \times 10^6\ A/m^2$, and finally we can see how the plasma electron current density $j_{e.pl}$ compensates so that the total current density fits to the imposed value. If we look at the sheath voltage u_c we can see

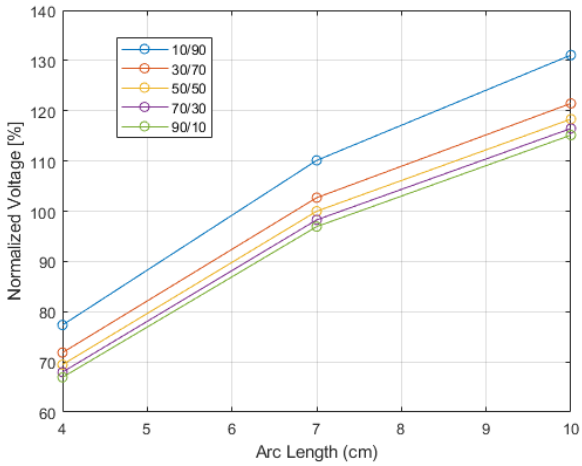

Figure 6.13: The normalized RMS arc voltages for all simulations, shows the effect of length and composition on the results.

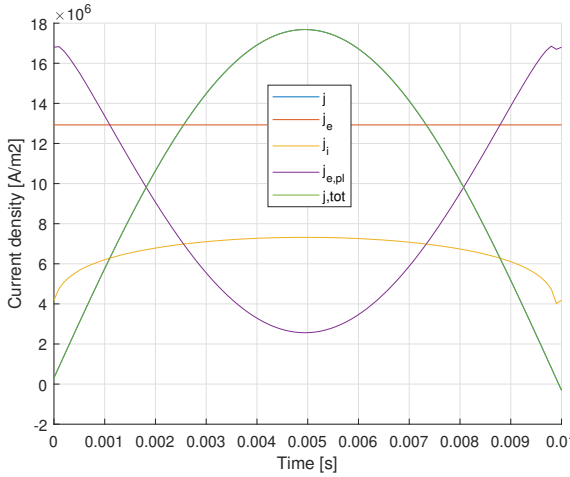

Figure 6.14: The estimated current densities for the CAM. j is the imposed current density, j_e, j_i and $j_{e,pl}$ are the calculated current components, and j_{tot} is the total of the estimated currents, and same as j.

how it behaves:

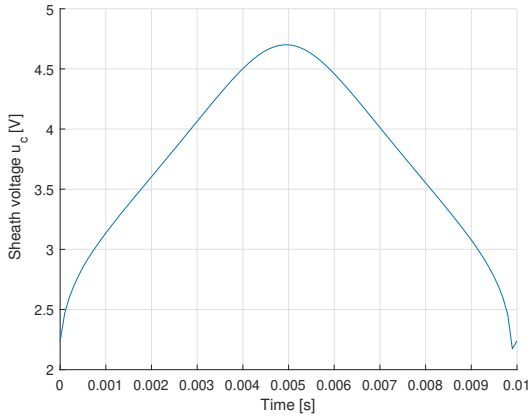

Figure 6.15: The sheath voltage u_c calculated by the CASM.

We can see how the voltage goes from around 2 to 4.7 V at the top, this fits well within expectations as this voltage is usually thought to be around 5V. Next we look at the heat flux, figure 6.16, sublimation temperature figure 6.17 and the erosion, figure 6.18. We can see that the erosion is 6.6 kg / m^2 s, and with our arc spot it would amount to 0.3897 tones over 24 hours.

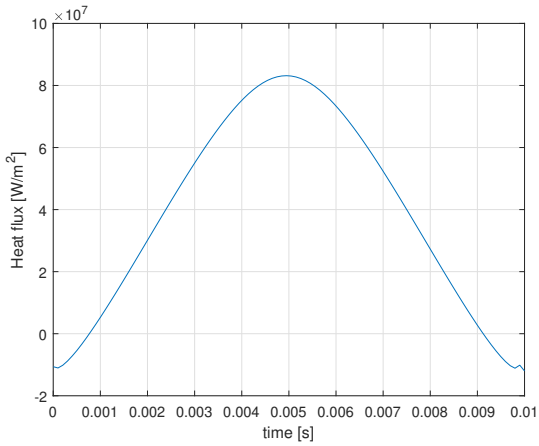

Figure 6.16: The heat flux estimated using the cathode / anode model.

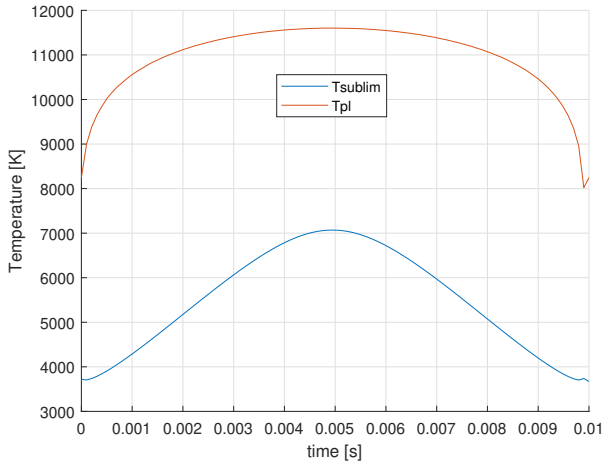

Figure 6.17: The plasma temperature T_{pl} and temperature estimated for the sublimation T using the cathode / anode model.

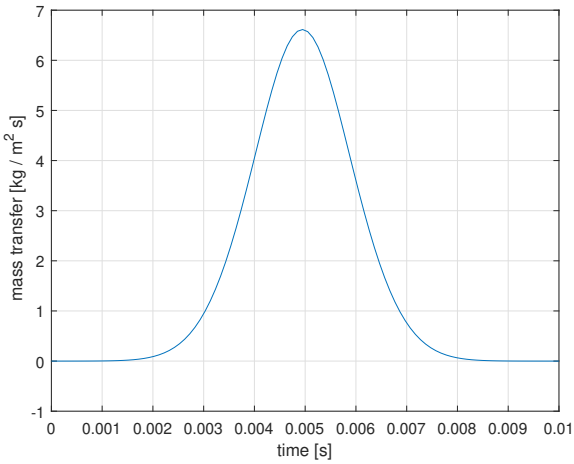

Figure 6.18: The mass transfer estimated using the cathode / anode model.

6.3.1 MHD CASM results

We decided to use Argon arcs since they run a lot faster and smother than silicon arcs. All the parameters are the same as for the previously discussed MHD simulations. The arc length was set to 4 cm since that length seemed to fit best to actual voltages observed, see section 6.2.3. To start we do a quick visual validation to see if the sub-model is behaving correctly, we look at the current density, temperature, Lorentz force, and velocity during the peak of the AC curve. We can see in figure 6.19 that the current distribution looks natural and is converging on the anode at two main points, normal for an arc to slit up. Next we look at the temperature in figure 6.20, here the temperature field follows the arc current well. Figures 6.21 and 6.22 show the Lorentz force that drives the velocity and the velocity it self, the velocity is strongest around the arc where the magnetic field is strongest.

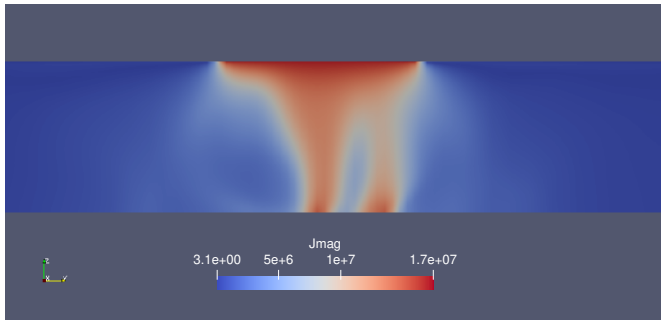

Figure 6.19: Surface plot of the current density [A/m^2] magnitude for the peak current in a section of the MHD simulation.

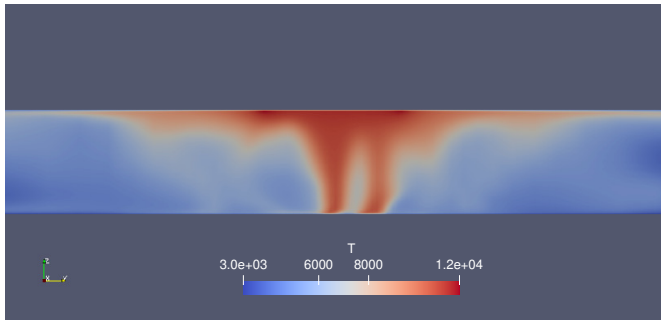

Figure 6.20: Surface plot of the Temperature [K] for the peak current in a section of the MHD simulation.

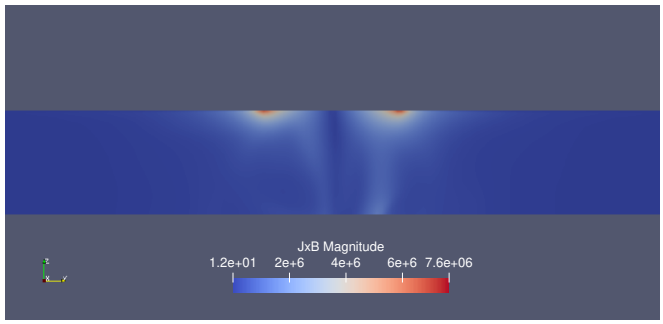

Figure 6.21: Surface plot of the Lorentz force (j x B) for the peak current in a section of the MHD simulation.

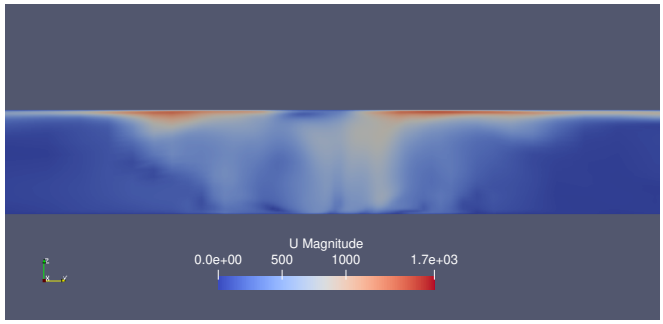

Figure 6.22: Surface plot of the velocity magnitude [m/s] for the peak current in a section of the MHD simulation.

If we then look at the estimated current density parts, figure 6.23 and 6.24, we can see how they behave. For the cathode we have a constant thermionic current density j_e the same as for the CAM case, we can see how the ion current density j_i increases as we get closer to the arc spot, as expected since it is very temperature dependent, we can then finally see how the electron current $j_{e,pl}$ compensates to keep the sheath at a constant charge. j_{mag} is the imposed current density and j_{tot} is the total difference between the calculated values and the imposed current, should be zero.

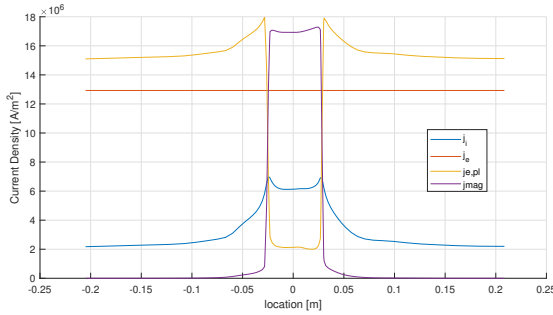

Figure 6.23: The different cathode current densities estimated using the MHD cathode / anode model.

As we mentioned the current is converging at two points on the anode, it is very interesting to see how the model estimates this. On figure 6.24 we can see the two current peaks, and how $j_{e,pl}$ compensates. There are some key differences happening for the anode since we have set the temperature here to 3000 K, this translates to there being both less ion and thermionic current coming from the surface.

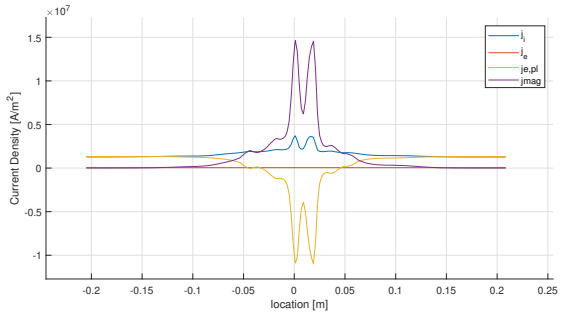

Figure 6.24: The different anode current densities estimated using MHD the cathode / anode model.

So far the model looks to be running as intended and if we look at the sheath voltage u_c for both anode and cathode. The sheath voltage at the cathode is around 4.5 V in the spot but just below 1.5 V across the electrode. What we see for the anode is that the voltage is negative where the arc is hitting the surface, this is very interesting since usually it is assumed positive.

Finally we will look at the electrode erosion or mass transfer from the sur-

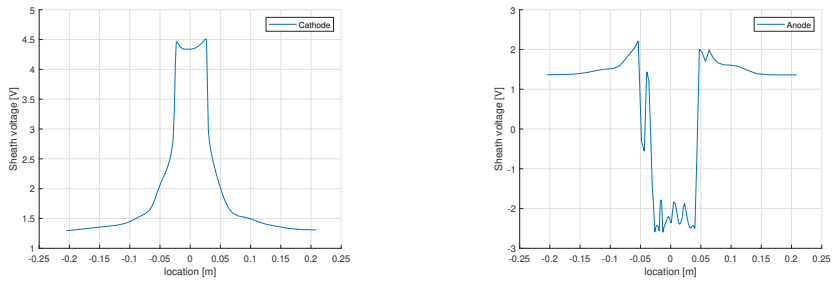

(a) (b)

Figure 6.25: Sheath voltage u_c estimated using the MHD cathode / anode model. (a) Cathode (b) Anode

face, the cathode is of most interest here since it is the electrode that has to be continually extended to keep the furnace running. Since the model is fully three dimensional we can see the erosion across the electrode 6.26, for the positive part its mostly centered on the cathode spot, but during the negative period, we gain look at the peak current, it is more spread out to where the arc hit the surface.

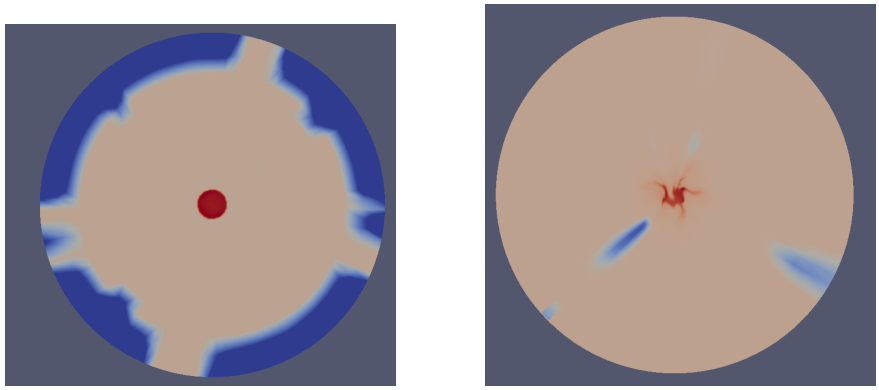

(a) (b)

Figure 6.26: The electrode erosion estimated using the MHD cathode / anode model. (a) At a positive peak (b) At a negative peak

If we look at a cross section through the surface we can see in more detail how the erosion looks. We marked the legend in such a way to show where the arc is coming from, cathode or anode. We start looking at the heat flux, figure 6.27, and it is highest in the center during the cathode period and where the arc hits

during anode period. The sublimation temperature, figure 6.28, then follows the heat flux and then in turn the mass transfer or erosion, figure 6.29, of the electrode. The erosion is measured in kg/m^2s, equation 5.8, but if summed up for the whole electrode and accounting for the negative period we can get a value in tonnes per hour , which is around 0.2748 tonnes/h which is lower than the values reported in [13] and the previous guess of the CAM model. These lower values are probably a result of the simplified radiation model used in the MHD implementation.

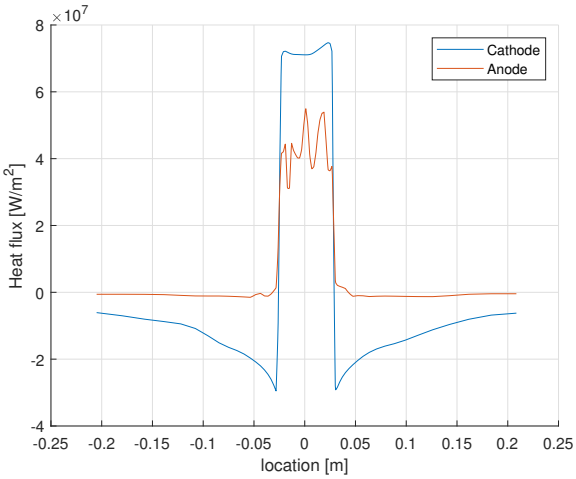

Figure 6.27: The heat flux estimated using the MHD cathode / anode model.

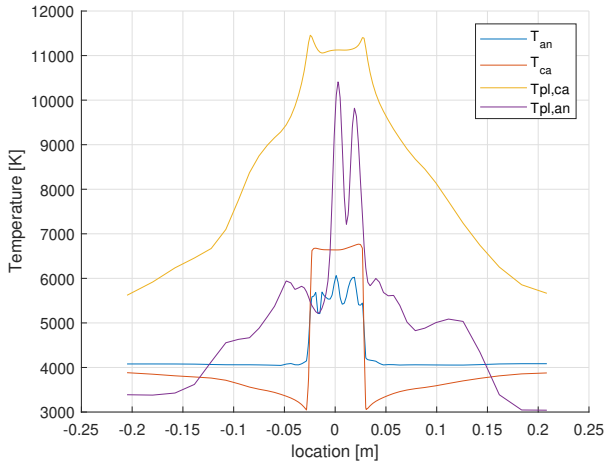

Figure 6.28: The plasma temperature and the temperature used to calculate the mass transfer estimated using the MHD cathode / anode model.

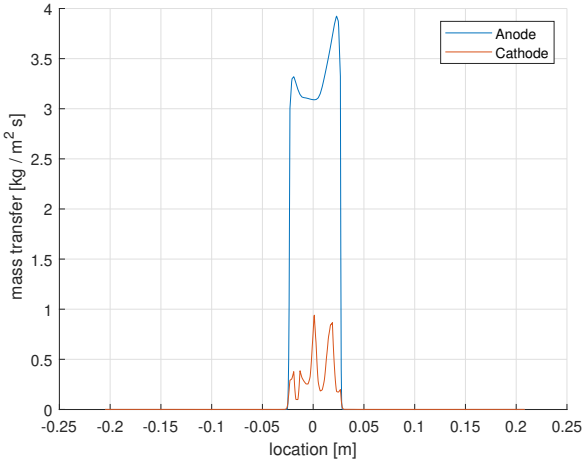

Figure 6.29: The mass transfer estimated using the MHD cathode / anode model.

Conclusions and Further Work

Measuring and processing of SAF parameters

We used data gathered using a DAQ system implemented in the Elkems FeSi plant in Iceland to estimate various furnace parameters. The data is initially a set of voltage measurements that must be converted to actual voltage and current values based on the selected furnace, and measurement equipment. Using this data and previous measurements done on the furnace we have devised a method of estimating the furnace current distribution profile for arc and charge currents.

The method described allows us to estimate all electrode current and voltage parameters for each time period. Using reference data for a pure arc, we can find the constant charge resistance based on each electrode's slope of the Lissajous curve. This, in turn, allows us to estimate the arc resistance, which is very variable during each period.

By having a better idea of what is going on inside the furnace in relation to the arc and charge currents should allow for smother furnace operation. Which should improve silicon yield and lower the specific energy consumption. However, more measurements are needed during operations to collect more data on current behavior, preferably during tapping, filling, and general electrode operation.

Modeling and comparison of industrial arcs

Two highly simplified fast-running models, Cassie-Mayr and a channel arc model, were constructed to simulate electric arcing in a submerged arc furnace. They were validated with industrial data, indicating that around 2/3 power dissipates in the arc for the case considered. The models were connected to a complete three-phase AC circuit, which represents a SAF and includes a new multiarc submodel. The model uses parameters from a full-scale SAF electrical model and from actual measurements conducted in a ferro-silicon plant in Iceland. This allows for verification of the model presented by estimating most of the model parameters with the ones measured in the SAF.

The models can simulate a wide range of arcs present in many industrial applications, and this is possible for both DC- and AC-arcs. The circuit used to represent the SAF also has the ability to use any arc model as well as multiple arcs, this allows for an easy comparison between different arc models using the same base electrical conditions. The models seem to conform acceptably to the actual arcs measured, after the arc model parameter have been determined.

An investigation into the effects of varying charge resistances was conducted by changing the appropriate parameter in the circuit model (R_c) from very low to high. The results show that total harmonic distortions increase with a higher portion of total current going into the arc and should give operators and idea of how the current distribution can be estimate based on the harmonics.

Magnetohydrodynamic arc model for OpenFOAM

A fully three dimensional MHD simulation model in OpenFOAM was implemented, that we call *"mhdRhoPimpleFoam"*. This model is implemented on top of an existing solver *rhoPimpleFoam*, which is compressible, turbulent, and transient. The MHD model is implemented as a new EM loop inside the solver structure, fields calculated there are then used to estimate additional source terms in the existing solver. A simple P1 radiation model was used, but that can be changed out later for a more complex option.

The model iterates the MHD solution several times during each time step of the main simulation to increase both accuracy and stability. The model allows for full MHD calculations for any geometry and any set of material properties. It can be used for modeling of various process that require simulation of conducting liquids at high temperatures and rapidly changing electric conditions.

Industrial arcs and Changing plasma compositions

We investigated the effect of changing compositions on the plasma gas present in a silicon submerged arc furnace using a selection of different plasma property data sets and MHD models. We have validated the models using a known geometry of an Argon furnace for which measurement data was available, we use three different data sets for argon gas for this purpose. All model and data set combinations gave qualitatively acceptable results for the argon furnace geometry, although some differences in predicted voltage were observed. This is most likely due to discrepancies in the Argon plasma electrical conductivity between data sets.

To test the models at industrial current levels we used a 50/50 mixtures of SiO and CO plasma gas, and compared the results obtained from various combinations of MHD models and plasma property data sets. The results were found to be

acceptably close to each other, although we did observe the voltages to be somewhat high compared to what we would expect from real furnace operations. This is likely due to lack of detail in the modeling used, in particular the simplified thermal radiation sub-model or the arc might be to long.

Finally, the models were used to study how different mixtures of the two gases in the furnace can impact the electrical behaviour of the arc. A variation of 8% in the peak voltage was observed, with CO-rich compositions producing more resistive arcs with higher voltages.

Some problems were encountered with the models, especially related to the formulation of the cathode boundary conditions and the radiation sub-models. Inconsistencies in the plasma data sets were also observed, and can produce significant differences in the end results. These issues will need to be given attention in future work, but overall the two MHD models tested were seen to be acceptably consistent and accurate for simulating arcs in industrial processes. We also have an improved understanding of the importance of input parameters when simulating electric arcs, and that care is needed when choosing plasma property data sets for such high temperatures.

Industrial arcs at variable compositions and lengths

We have simulated an industrial arc of 50 kA by using a MHD model for five different plasma gas compositions and three arc lengths. We observed that the arc voltage varies mostly due to the length of the arc but also slightly based on the composition of the plasma.

It seems that industrial arcs operating under ideal conditions are not very affected by the exact composition present in the plasma, this is perhaps due the high current that drives the arc. Further investigation into the reason for this should be conducted and further simulations at both higher and lower currents are warranted, as well as more detailed modelling of the anode material.

Cathode / Anode model for industrial arcs

The cathode / anode model had previously been implemented 22 years ago for a axi-symmetric arc model in fluent 6. This model was almost integrated completely into the MHD model but time constraints prevented further work at the time. Now similar progress has been made where the model works mostly as expected and has been mostly integrated in the new MHD solver as a sub-model. The model also uses a new way to estimate the sheath voltage, instead of iterating the counter-diffusing current until a solution is reached that matches the total current, it calculates it directly thus saving computational time and while maintaining accuracy.

The current model was both used with the channel arc model as a test base and then also with the full MHD model. It calculates the different current components present in the space charge sheath close to the conducting surfaces of the plasma. it gives the sheath voltage u_c with good accuracy and show some interesting results for the anode. It also allows us to see the electrode erosion across the surface of the electrode for each time step.

Further Work

Further improvement of the SAF circuit model would be to implement the MHD model that includes more of the actual physics present in an industrial arc. Further modeling of the arc footprint during tapping would also be of interest since it is one of the main operations carried out in live SAFs. This might further our understanding of the current distribution and harmonics during said operation.

Further work on the MHD model needs to be carried out, first to implement a better radiation model since it seems that the arc voltage is to high and the radiations is the a likely contributor for this. A new solver should also be developed so that a part of the solid electrode can be included in the modeling domain; this would allow for the magnetic and electric transport equations to be solved within the electrode and thus allow for a better estimation of the voltage and the current density at the boundary between it and plasma. This would allow for the cathode / anode model to be fully integrated with the MHD at that boundary and thus allow for a far more accurate estimation of the current density in the arc as well as the cathode spot radius and electrode erosion.

Bibliography

[1] H. Haraldsson, Y. A. Tesfahunegn, M. Tangstad, and G. Sævarsdottir, "Modelling of Electric Arcs for Industrial Applications, a Review," *SSRN Journal*, 2021, ISSN: 1556-5068. DOI: 10.2139/ssrn.3927158.

[2] H. V. Haraldsson, H. Traustason, Y. A. Tesfahunegn, M. Tangstad, and G. Sævarsdóttir, "Measuring and processing of electrical parameters in a submerged arc furnace," in *Materials Processing Fundamentals 2023*, 2023, pp. 161–170, ISBN: 978-3-031-22657-1. DOI: 10.1007/978-3-031-22657-1_14.

[3] H. V. Haraldsson, H. Traustason, Y. A. Tesfahunegn, M. Tangstad, and G. Saevarsdottir, "Modeling and comparison study of industrial AC-arcs," *Metallurgical and Materials Transactions B*, Jul. 24, 2024, ISSN: 1543-1916. DOI: 10.1007/s11663-024-03214-y. [Online]. Available: https://doi.org/10.1007/s11663-024-03214-y.

[4] H. V. Haraldsson, Q. Reynolds, Y. A. Tesfahunegn, and G. Saevarsdottir, "Modeling of industrial electric arcs using different plasma gas compositions," *Metallurgical and Materials Transactions B*, vol. 56, no. 2, pp. 1208–1217, Apr. 1, 2025, ISSN: 1543-1916. DOI: 10.1007/s11663-024-03397-4. [Online]. Available: https://doi.org/10.1007/s11663-024-03397-4.

[5] H. Haraldsson, Y. A. Tesfahunegn, M. Tangstad, and G. Sævarsdottir, "Modelling of industrial electric arcs with changing plasma compositions and arc lengths," *SSRN Electronic Journal*, 2024, ISSN: 1556-5068. DOI: 10.2139/ssrn.4942616. [Online]. Available: https://www.ssrn.com/abstract=4942616 (visited on 06/09/2025).

[6] A. Alzate, J. Durango, and A. Mejia, "Electric arc furnace modeling for power quality analysis," pp. 1–6, 2010. DOI: 10.1109/ANDESCON.2010.5629655.

[7] S. Golestani and H. Samet, "Generalised cassiemayr electric arc furnace models," *IET Generation, Transmission & Distribution*, vol. 10, no. 13, pp. 3364–3373, Oct. 6, 2016, ISSN: 1751-8687, 1751-8695. DOI: 10.1049/iet-gtd.2016.0405. [Online]. Available: https://digital-library.theiet.

org / content / journals / 10 . 1049 / iet - gtd . 2016 . 0405 (visited on 12/15/2020).

[8] G. Saevarsdottir, H. Larsen, and J. Bakken, "Modelling of industrial AC-arcs," *High Temperature Material Processes (An International Quarterly of High-Technology Plasma Processes)*, vol. 3, pp. 1–15, Jan. 1, 1999. DOI: 10 . 1615/HighTempMatProc.v3.i1.10.

[9] Q. G. Reynolds, "Computational modeling of arcslag interaction in DC furnaces," *JOM*, vol. 69, no. 2, pp. 351–357, Feb. 2017, ISSN: 1047-4838, 1543-1851. DOI: 10 . 1007 / s11837 - 016 - 2166 - 9. [Online]. Available: http : / / link . springer . com / 10 . 1007 / s11837 - 016 - 2166 - 9 (visited on 12/21/2020).

[10] A. D. Rocca and Q. G. Reynolds, "Large-eddy simulations of electric arcs at industrial scale," 2019, Publisher: Unpublished. DOI: 10 . 13140/RG . 2 . 2 . 24803 . 71209.

[11] J. A. Bakken, L. Gu, H. L. Larsen, and V. G. Sevastyanenko, "Numerical modeling of electric arcs," *Journal of Engineering Physics and Thermophysics*, vol. 70, no. 4, pp. 530–543, Jul. 1, 1997. DOI: 10 . 1007/BF02663569.

[12] G. Scevarsdottir, J. Bakken, V. Sevastyanenko, and L. Gu, "High-power AC arcs in metallurgical furnaces," *High Temperature Material Processes*, vol. 15, pp. 205–225, Jan. 1, 2011. DOI: 10 . 1615/HighTempMatProc . v15 . i3 . 40.

[13] G. Sævarsdóttir, H. Pálsson, M. Jónsson, and J. A. Bakken, "Electrode erosion due to high-current electric arcs in silicon and ferrosilicon furnaces," *steel research international*, vol. 77, no. 6, pp. 385–391, 2006, _eprint: https://onlinelibrary.wiley.com/doi/pdf/10.1002/srin.200606403, ISSN: 1869-344X. DOI: 10 . 1002/srin . 200606403. [Online]. Available: https : //onlinelibrary . wiley . com/doi/abs/10 . 1002/srin . 200606403 (visited on 10/23/2020).

[14] G. A. Sævarsdóttir, "High current AC arcs in silicon and ferrosilicon furnaces.," 2002.

[15] M. Tangstad and L. Kolbeinsen, *Metal production in Norway*. Oslo: Akademika Publishing, 2013, OCLC: 866576889, ISBN: 978-82-321-0241-9.

[16] G. Saevarsdottir and Bakken, "Current distribution in submerged arc furnaces for silicon metal/ferrosilicon production," in *International ferroalloys congress; 12th*, 2010, pp. 717–728.

[17] A. Javidi Shirvan and I. Choquet, "A review of cathode-arc coupling modeling," *Welding in the World*, vol. 60, no. 4, pp. 821–835, Jul. 1, 2016, ISSN: 1878-6669. DOI: 10 . 1007/s40194-016-0319-7.

[18] Y. A. Tesfahunegn, T. Magnusson, M. Tangstad, and G. Saevarsdottir, "Effect of carbide configuration on the current distribution in submerged arc furnaces for silicon productiona modelling approach," in *CFD Modeling and Simulation in Materials Processing 2018*, 2018, pp. 175–185, ISBN: 978-3-319-72059-3. DOI: 10.1007/978-3-319-72059-3_17.

[19] M. Tangstad, H. Hoover, and G. Sævarsdottir, "Electrical resistivity of partially transformed silicon carbide made from coal," *SSRN Electronic Journal*, 2021, ISSN: 1556-5068. DOI: 10.2139/ssrn.3922184. [Online]. Available: https://www.ssrn.com/abstract=3922184 (visited on 01/30/2023).

[20] S. Halvorsen, H. Olsen, and M. Fromreide, "An efficient simulation method for current and power distribution in 3-phase electrical smelting furnaces," *IFAC-PapersOnLine*, vol. 49, no. 20, pp. 167–172, 2016, ISSN: 24058963. DOI: 10.1016/j.ifacol.2016.10.115. [Online]. Available: https://linkinghub.elsevier.com/retrieve/pii/S2405896316316780 (visited on 01/30/2023).

[21] S. A. Halvorsen, M. Sparta, V. K. Risinggård, and M. Fromreide, "Electrical conditions in 3-phase submerged arc furnaces: Learning from the ElMet project," *SSRN Electronic Journal*, 2021, ISSN: 1556-5068. DOI: 10.2139/ssrn.3926712. [Online]. Available: https://www.ssrn.com/abstract=3926712 (visited on 01/30/2023).

[22] H. G. Traustason, "Data acquisition of electrical parameters and interpretation of SAF data," Masters thesis, Reykjavík University, 2020.

[23] G. Saevarsdottir, P. Manolescu, T. Magnilsson, and K. Sigurjonsson, "Electrodes and control circulating currents in the delta connection, feasibility of skew tapping in the operation of submerged-arc furnaces," 2013.

[24] G. Saevarsdottir, T. Magnusson, and J. A. Bakken, "Electric arc on a coke bed in a submerged arc furnace," 2007.

[25] A. Hauksdottir, T. Soderstrom, Y. Thorfinnsson, and A. Gestsson, "System identification of a three-phase submerged-arc ferrosilicon furnace," *IEEE Transactions on Control Systems Technology*, vol. 3, no. 4, pp. 377–387, 1995. DOI: 10.1109/87.481962.

[26] A. Lorenzo, M. Lage, J. Bullon, *et al.*, "Measurement of electrical parameters in high-current arc furnaces," in *2007 IEEE International Symposium on Industrial Electronics*, 2007, pp. 1565–1568. DOI: 10.1109/ISIE.2007.4374836.

[27] T. Gerritsen, P. E. Tracy, and F. N. M. Saber, "Electrode voltage measurement in electric furnaces : Analysis of error in measurement and calculation," 2015.

[28] S. Documentation, *Simulation and model-based design*, 2020. [Online]. Available: https://www.mathworks.com/products/simulink.html.

[29] Y. A. Tesfahunegn, T. Magnusson, M. Tangstad, and G. Saevarsdottir, "The effect of side arcs on current distributions in a submerged arc furnace for silicon production," in *Materials Processing Fundamentals 2020*, Cham: Springer International Publishing, 2020, pp. 177–188, ISBN: 978-3-030-36556-1.

[30] A. M. Valderhaug, "Modelling and control of submerged-arc ferrosilicon furnaces," Doctoral thesis, Norges teknisk-naturvitenskapelige universitet, 1992.

[31] H. L. Larsen, G. Liping, J. A. Bakken, J. K. Tuset, I. G. Page, and H. Tveit, "A numerical model for the AC arc in the silicon metal furnace," in *International ferroalloys congress; 7th*, Backup Publisher: Norwegian Ferroalloy Industry, Norwegian Ferroalloy Research Organization; 1995, pp. 517–528, ISBN: 82-595-8649-5. [Online]. Available: https://www.tib.eu/de/suchen/id/BLCP%3ACN017100017.

[32] O. Zikanov, *Essential computational fluid dynamics*, Online-Ausg. Hoboken, N.J: Wiley, 2010, 1 p., ISBN: 978-0-470-42329-5 978-1-283-25818-0.

[33] "OpenFOAM." (Dec. 31, 2023), [Online]. Available: https://www.openfoam.com/ (visited on 04/22/2024).

[34] A. Westermoen, "Modelling of dynamic arc behaviour in a plasma reactor," Ph.D. dissertation, The Norwegian Institute of Technology, Trondheim, Norway, 2007.

[35] Q. G. Reynolds, "Toward computational models of arc dynamics in silicon smelters," in *Proceedings of the 14th International Conference on CFD in Oil & Gas, Metallurgical and Process Industries*, 2020, pp. 99–106, ISBN: 978-82-536-1684-1.

[36] G. Saevarsdottir, M. T. Jonsson, and J. Bakken, "A novel approach to cathode / anode modelling for high-current AC arcs," in *16th International Symposium on Plasma chemistry*, Jun. 2003.

[37] N. A. Barcza, "The development of large-scale thermalplasma systems," The Southern African Institute of Mining and Metallurgy, 1986.

[38] M. S. Benilov and A. Marotta, "A model of the cathode region of atmospheric pressure arcs," *Journal of Physics D: Applied Physics*, vol. 28, no. 9, pp. 1869–1882, Sep. 14, 1995, ISSN: 0022-3727, 1361-6463. DOI: 10.1088/0022-3727/28/9/015. [Online]. Available: https://iopscience.iop.org/article/10.1088/0022-3727/28/9/015 (visited on 08/20/2024).

[39] M. S. Benilov and G. V. Naidis, "Ionization layer at the edge of a fully ionized plasma," *Phys. Rev. E*, vol. 57, pp. 2230–2241, 2 Feb. 1998. DOI: 10.1103/PhysRevE.57.2230. [Online]. Available: https://link.aps.org/doi/10.1103/PhysRevE.57.2230.

[40] M. S. Benilov and G. V. Naidis, "Ionization layer at the edge of a fully ionized plasma," *Phys. Rev. E*, vol. 57, pp. 2230–2241, 2 Feb. 1998. DOI: 10.1103/PhysRevE.57.2230. [Online]. Available: https://link.aps.org/doi/10.1103/PhysRevE.57.2230.

[41] T. Magnussen, "Basic parameters in the operation and design of submerged arc furnaces, with particular reference to production of high-silicon alloys," *Journal of the Southern African Institute of Mining and Metallurgy*, vol. 118, no. 6, 2018, ISSN: 22256253, 24119717. DOI: 10.17159/2411-9717/2018/v118n6a11.

[42] Q. Reynolds, *Quinnreynolds/minplascalc*, original-date: 2018-11-06T07:45:24Z, May 15, 2024. [Online]. Available: https://github.com/quinnreynolds/minplascalc (visited on 06/05/2024).

[43] G. Liping, "Transport phenomena in silicon vapour infiltrated argon arcs and anodic metal pools," Ph.D. dissertation, The Norwegian Institute of Technology, Trondheim, Norway, 1993.

Paper I

Infacon XVI: International Ferro-Alloys Congress,
Edited by A.N. Wærnes, G. Tranell, M. Tangstad, E. Ringdalen, and C. van der Eijk
SINTEF/NTNU/FFF, Trondheim, 27-29 September 2021

Modelling of electric arcs for industrial applications, a review

Haraldsson H [1], Tesfahunegn Y.A [1], Tangstad M [2], Sævarsdóttir G [1]
[1] Department of Engineering, Reykjavík University, Iceland, hakonh12@ru.is
[2] Department of Materials Science and Engineering, Norwegian University of Science and Technology, Norway

Keywords: MHD, Electric Arc Furnace, 3-phase, AC-arcs, plasma, simulation

Abstract – Electric arcs are a necessary heat source in many industrial processes that take place in Submerged Arc Furnaces (SAFs). Arcs exhibit non-linear electrical characteristics and behave in a complex manner. Therefore, an improved understanding of their behaviour enables better control of furnace operation. Modelling of industrial arcs is a multiphysics process that involves simultaneously solving several coupled physical phenomena, such as electromagnetics, fluid dynamics and heat transfer, including a radiative heat transfer from the plasma arc. Coupling fluid dynamics and electromagnetics is known as Magnetohydrodynamics (MHD). There are also simpler approaches to arc modelling, either based on simplified physical principles or empirical behaviour. A number of MHD models for electric arcs have been presented in the literature, but most of them involve simplifications such as axial-symmetry to reduce the simulation time, pertain to currents much lower than for industrial arcs, focus on DC arcs rather than arcs carrying AC current or don´t have the plasma properties of the actual gas in the furnace. In a recently started project, the ambition is to create a full-scale 3D MHD model for an industrial AC arc at the conditions to be found in Si-metal furnaces. As much can be learned from previous arc modelling, this paper will review different arc modelling approaches and develop a classification framework to categorize the modelling methods, both the more intricate MHD models as well as the simpler modelling approaches. Among the available simplified models, one will be selected and coupled with a submerged arc furnace electrical circuit model. The complete circuit model parameters such as resistances and inductances are updated using a 3D submerged arc furnace that has been developed in ANSYS Maxwell using an eddy current solver.

INTRODUCTION

In many metallurgical processes, the energy needed to heat raw materials is supplied by an alternating current (AC), passing through and heating the materials in the furnace. In the case of a submerged arc furnaces (SAFs), much of the current will at some point pass through an electric arc, which burns in a gas-filled volume. The extremely hostile environment inside SAFs makes any direct observation of the arc impossible. This means that an accurate numerical simulation model of the electric arc is important for enhanced understanding and improved furnace operation. Modelling industrial arcs is a multiphysics process that simultaneously solves several coupled physical phenomena, such as electromagnetics, fluid dynamics, and heat transfer. Coupling fluid dynamics and electromagnetics is known as Magnetohydrodynamics (MHD). There are also simpler approaches to arc modelling, either based on simplified physical principles or empirical methods.

Most studies focus, at least in part, on how the electric properties around the arc change with different arc conditions. The most common and simplest model in use for industrial arcs is the Cassie-Mayr model used in (Alzate et al., 2010) and in the model introduced in this paper. Vervenne et al., 2007 and Junwen et al., 2010 used a dynamic numerical model. The next step

up in complexity are channel arc models (Saevarsdottir et al., 1999), where the arc implemented as a cylindrical conductor, the arc characteristics are then found based on power balances between electric input and various output losses. The most complete and complex are the magnetohydrodynamics models, for direct current (DC) arcs (Reddy, 2010), (Reynolds, 2017) and, (A Della Rocca and Q G Reynolds, 2019), for alternating current (AC) arcs (Bakken et al., 1997), (Saevarsdottir et al., 1999) and,(Scevarsdottir et al., 2011). All the models are embedded as circuit elements into circuit models, that supply current or voltage to the arc model, be it Cassie, Channel or MHD.

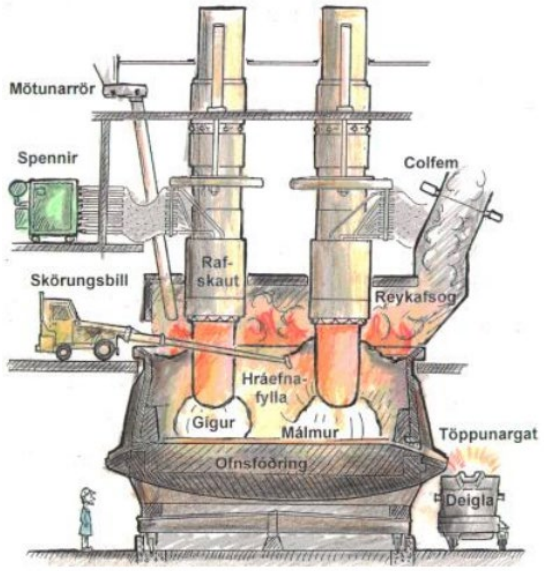

Figure 1: An illustrated figure of a SAF in operation, drawn by Thorsteinn Hannesson **(Hannesson, 2015)**.

This paper will review different arc modelling approaches and develop a classification framework to categorize the modelling methods, both the more intricate MHD models as well as the simpler modelling approaches. Among the available simplified models, one will be selected and coupled with a submerged arc furnace electrical circuit model. The complete circuit model parameters such as resistances and inductances are updated based on a 3D submerged arc furnace model that has been developed in ANSYS Maxwell using an eddy current solver (Tesfahunegn et al., 2018).

REVIEW OF MODELLING METHODS

Simulating an industrial electrical arc can be quite complex if the full set of physical equations are used. There are, however, many simpler methods that can be applied to get a less accurate but still acceptable solution; this can be especially important to determine areas of most interest before committing a more computationally expensive method. This section describes some of the recent methods used to simulate electrical arcs, from the simple to the more complex.

Arc description

Before describing the arc modelling techniques, it is appropriate to explain the general physical characteristics of arcs. This section will illustrate the physics of electric arcs and focus on DC

arcs since they can be considered a steady-state and offer an easy way to explain the basics of arcs, this will then be followed by a description of AC-arcs.

Electric arcs are defined as an electrical discharge sustained by a current flowing through a gaseous media (plasma) between two electrodes. It can be divided into 5 zones or regions based on the electrical potential distribution. In the border regions, (1 – 2) at the cathode and (4 – 5) at the anode, the electrical field strength increases sharply while in the majority of the arc, (3), the centre has a rather constant field, in low current arcs the electron emission is generally started by field emission, however, in high current arcs thermionic emission dominates due to the large amount of current flowing through the electrodes.

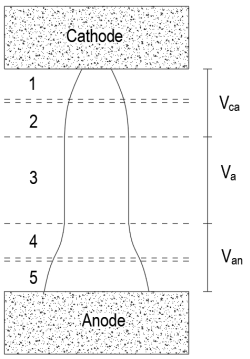

Figure 2: The arc regions and simplified voltage drop in an industrial arc.

The electrode regions 1-2 and 4-5

The regions closer to the electrode (1 and 5) are usually called the sheath or space charge layers. These are the transition regions between metallic and gaseous conduction and are made up of positive ions. The regions next to the plasma column (2 and 4) are called pre-sheath or ionization layers, where charged species are created by ionization (Javidi Shirvan and Choquet, 2016). In high-current industrial arcs these layers are less well defined, as the energy impacting anode and cathode surfaces produces a surplus of electrons through thermionic emission (Saevarsdottir et al., 2003).

The arc region 3

This region comprises a homogeneous plasma column with an almost constant electric field and temperature along the centre axis. Here local thermal equilibrium [LTE] conditions can be assumed for modelling purposes.

AC-arcs dynamic description

The problem with simulating dynamic or AC-arcs is the current and voltage are continuously changing polarity. It can be assumed that an AC-arc will try to reach an equilibrium state like a DC-arc with the same instantaneous current. This makes it possible to use a DC model where the current and voltage are then varied to simulate the change in the arc between time steps; this is briefly described in (Bakken et al., 1997), where it is proposed that they be used as nonlinear circuit elements.

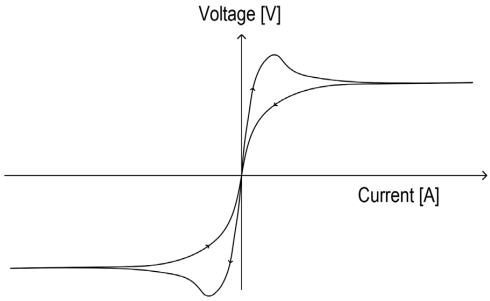

Figure 3: An example of expected arc voltage / current behaviour**.**

Arc modelling methods

Electric circuit description

The simplest description of arc behaviour can be estimated from its electrical characteristics. Industrial high current arcs are generally present within an electric arc furnaces and to determine the behaviour of the arc itself, the total electric circuit needs to be known. This includes transformers 1-3 which have voltage, current, resistances and impedances (V_{Ti}, i_{Ti}, R_{Ti} and L_{Ti}), as well as electrodes 1-3 which have resistance (R_{ei}) and the phase inductances including the mutual inductances (L_{ei}). The current that passes between the electrodes in a SAF mostly travels through the arc. The arc and the cavity surrounding it are represented by the part of the electrode present in the cavity (R_{eci}), the arc resistance (R_{ai}) and the resistance of the metal pool (R_{mi}) . There is, however, some part that goes into the raw material charge filling up the furnace (R_{ci} represents this) and, the resistance of the furnace base (R_{bi}) is also included , figure 4 shows the simplified electric circuit of a traditional three-phase SAF. The physical properties of the charge materials differ with location in the furnace, as intermediate reactions change their composition and temperature changes with depth.

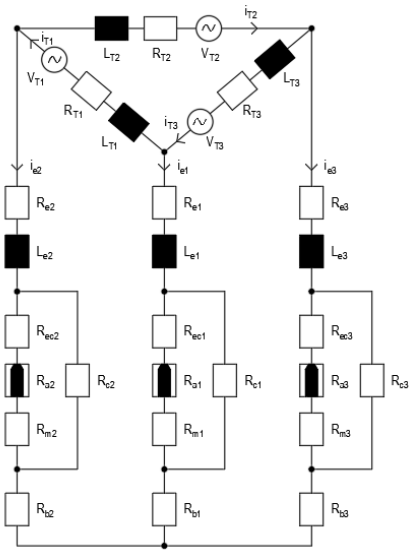

Figure 4: Electric circuit used for the dynamic model (Valderhaug, 1992).

The complete dynamic electrical model consists of a three-phase electrical and arc models, as detailed in (Valderhaug, 1992). It assumes all electrodes are symmetrical. The phase current equations are:

$$\frac{di_{e1}}{dt} = \frac{(L_2+L_3)v_{T1}+L_2v_{T2}-[(L_2+L_3)R_1+L_2R_3]i_{e1}+[L_3R_2-L_2R_3]i_{e2}-(L_2+L_3)\widetilde{v_{AC1}}+L_3\widetilde{v_{AC2}}+L_2\widetilde{v_{AC3}}}{L_1L_2+L_2L_3+L_3L_1} \quad [1]$$

$$\frac{di_{e2}}{dt} = \frac{-L_3v_{T1}+L_1v_{T2}+[(L_3R_1-L_1R_1]i_{e1}-[(L_1+L_3)R_2+L_1R_3]i_{e2}+L_3\widetilde{v_{AC1}}-(L_1+L_3)\widetilde{v_{AC2}}+L_1\widetilde{v_{AC3}}\}}{L_1L_2+L_2L_3+L_3L_1} \quad [2]$$

$$\frac{di_{e3}}{dt} = -\left(\frac{di_{e1}}{dt} + \frac{di_{e2}}{dt}\right) \quad [3]$$

Here L_i are lumped inductances that include contribution from mutual inductance:

$$L_i = L_{ei} + \frac{L_{Ti}}{3} \quad [4]$$

And R_i are the lumped resistances:

$$R_i = R_{ei} + \frac{[R_{eci}+R_{ai}+R_{mi}]R_{ci}}{R_{eci}+R_{ai}+R_{mi}+R_{ci}} + R_{bi} \quad [5]$$

$\widetilde{v_{ACi}}$ is defined as:

$$\widetilde{v_{ACi}} = \frac{R_{ci}}{R_{eci}+R_{ai}+R_{mi}+R_{ci}} v_{ACi} \quad [6]$$

V_{ACi} is the combined anode and cathode voltage drop. Equations 1 – 3 can then be used in conjunction with the various models described below to investigate the electric characteristics of SAFs.

The Cassie and Mayr models

The next step in the complexity ladder are the Cassie and Mayr models. The models describe the electric arc as an electrical circuit element, characterized by the arc voltage, the arc current, and the arc resistance per length unit (arc conductance per unit length).

- The Cassie's model is suitable to describe high-current AC arcs and can be applied to the simulation of arcing in an electric furnace
- The Mayr's model is best suitable for descriptions of low-current AC arcs or investigations of arc conditions near current-zero-passing.

The derivation of Cassie's model and Mayr's model is based on the assumption that the change with time in the arc's inner energy is equal to the difference between the electrical power input and the power dissipation in the arc column. The characteristic arc resistance per unit length is:

$$\frac{d\widehat{R_a}(t)}{dt} = \frac{1}{\theta_a}\left[1 - \left(\frac{E_a(t)}{E_0}\right)^2\right] R_a(t) \quad [7]$$

Where θ_a is a time constant that characterizes the arc dynamics given by:

$$\theta_a = \frac{1}{g_0 E_0^2} \quad [8]$$

The total arc column resistance for an arc length or height of h_a is then given by:

$$R_a(t) = h_a\widehat{R_a}(t) \quad [9]$$

This allows the model to be incorporated in a more complex electric circuit analysis such as where all three phases are implemented. This can be helpful to analyse harmonic content generated by the arc in industrial applications, this is done in (Golestani and Samet, 2016) for electric arc furnaces (EAFs) to evaluate harmonics and flicker effects from a steel manufacturing plant.

As has been discussed about the dynamic behaviour of arcs inside submerged arc furnaces, it can be difficult to model since the material properties cannot be measured directly. In this paper a dynamic model of transient electrical states is derived based on the equivalent circuit presented in (Valderhaug, 1992), (see figure 4 above). To get a better understanding of the electrical properties of a SAF, a 3D model of an actual 32 MW furnace was constructed in Ansys maxwell solver to investigate the effects of carbide configuration on current distribution in the SAF, this model could also be used to estimate the inductances of different materials and components present inside the SAF, see (Tesfahunegn et al., 2020) for details. Detail procedure on how to calculate the resistance and inductance of the furnace is presented by (Tesfahunegn et. al., 2020).

These were then used to implement a more detailed simulation in MATLAB SIMULINK of the voltage and current behaviour of the arc, a similar method is used in (Junwen Dai et al., 2010) for a DC arc and in (Vervenne et al., 2007) for a AC steel making furnace. The parameters shown in table 3 were measured in the maxwell solver as averages for each component and all three phases are assumed symmetrical (see table 1). The voltage V_{Ti} is assumed to be 130 V with a frequency of 50 Hz and the arc length h_a is 10 cm.

Table 1: Calculated values from ANSYS Maxwell solver and parameters used in the Cassie-Mayr model.

R_{Ti}	0.005 mΩ
L_{Ti}	0.018 μH
R_{ei}	0.038 mΩ
L_{ei}	0.097 μH
R_{ci}	0.82 mΩ
R_{mi}	0.002 mΩ
R_{bi}	0.002 mΩ
R_{eci}	25% of R_e
θ_a	1 ms
G_{min}	0.1 nS

The resistances and inductances are calculated according to the method described in ((Tesfahunegn et al., 2020). The detail dimension of the furnace are described in the paper due to proprietary right.

A combined Cassie-Mayr model is then used to estimate the conductance of the arc and thus the arc voltage and current. The arc conductance G_i is given by:

$$\frac{dG_i}{dt} = \frac{G_{min} - G_i + \left[1 - exp\left(-\frac{i_{ai}^2}{I_0^2}\right)\right]\frac{v_{ai} i_{ai}}{(A + B h_a)} + \left[exp\left(-\frac{i_{ai}^2}{I_0^2}\right)\right]\frac{i_{ai}^2}{P_0}}{\theta_a} \quad [10]$$

where: G_i is the arc conductance of phase i, G_{min} the conductance between any two electrodes when the electric arc is absent, θ_a is the arc time constant, i_{ai}, v_{ai} are the arc current and voltage on phase i, P_0 momentarily power loss, I_0 is current value used to determine which model is

dominant set to $3\ kA$, h_a arc length, A is a constant containing the sum of anode and cathode voltage drops and B is the voltage drop per unit of arc length. This is then used to calculate the arc voltage and current over an entire period, as shown in figure 5 below.

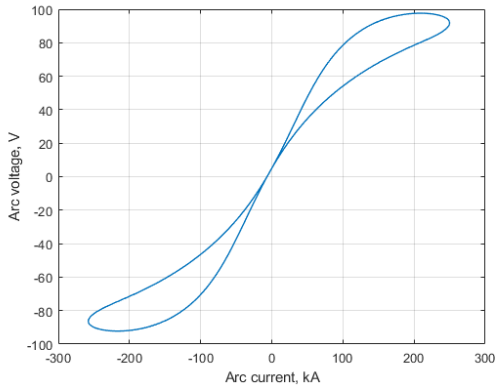

Figure 5: The V-I characteristic from the new mathematical model used to test the 3D furnace model.

The model can then be used to investigate power quality such as harmonic distortions, flicker effects and phase shifts. This is also done in (Alzate et al., 2010) using a similar numerical model and real parameters from a functioning steel mill. The next step will be to compare the model to data gathered in (Traustason, 2020) of an operational SAF and to implement a channel arc model as a substitute for the simpler model presented here.

Channel arc models

This type of model is physically based on a real arc with significant simplifications. It is assumed that the arc is an ionized gas channel, which is symmetrical around the axis. This allows for a variety of simplifying assumptions to be made within the channel. The simplest is to assume homogeneous current distribution throughout the channel diameter, but other distributions such as parabolic or gaussian can also be used. Here there needs to be an area where the arc expands from the cathode towards the arc channel. In the region where the current expands, it will have a radial component, which interacts with the magnetic field and forms a Lorentz force component directed towards the anode. This generates flow, contributing to convection in the arc.

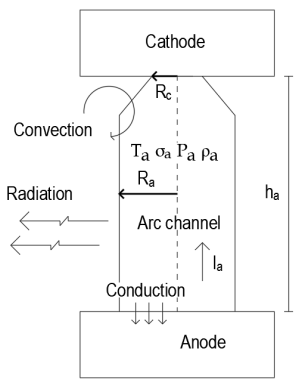

Figure 6: A DC channel arc model.

Generally, the variables used are the arc temperature T_a, electrical conductivity σ_a, pressure P_a and mass density ρ_a. The radiative heat transfer from the arc plasma is included as well. They

then vary based on the type of distribution. r_C is the arc radius at the cathode and r_a is the arc radius in the main arc area. In a steady state arc, the electric power that the arc generates must be transferred completely to the surroundings of the arc:

$$P_{el} = P_{loss} \quad [11]$$

where

$$P_{el}(r_a, T_a, I_a) = \frac{\mathrm{h}_a {i_a}^2}{\sigma_a(T_a)\pi r_a^2} + (V_{an} + V_{ca})I_a \quad [12]$$

Here h_a is the arc length i_a is the arc current, r_a is the arc radius and $\sigma_a(T_a)$ is the temperature dependent conductivity. The arc then dissipates power by three mechanisms, i.e., radiation, convection, and conduction. A model developed in (Saevarsdottir et al., 1999) takes all three into account. The convective heat transfer to the arc surroundings is given as:

$$P_{con} = 2\pi \int_0^{R_a} r\, \rho_a\big(T(r)\big)\, v_a(r) \left[h\big(T(r)\big) - h(T_F)\right] dr \quad [13]$$

Where $h(T)$ is the specific enthalpy of the arc, $h(T_F)$ is the enthalpy of the surroundings and $v_a(r)$ is the gas velocity distribution. The maximum gas velocity is along the arc axis and is given by:

$$v_{a,max} = \frac{i_a}{\pi r_a}\sqrt{\frac{K_1 \mu_0}{2\rho_a}\left(\frac{r_a^2}{r_c^2} - 1\right)} \quad [14]$$

K_1 determines the current density profile, $K_1 = 1$ is a uniform profile while $K_1 = 5/3$ is a parabolic one. And then the mean distribution is then:

$$\overline{v_a} = K_2 v_{a,max} \quad [15]$$

Here K_2 decides the velocity profile. The radiative heat transfer from the arc is given by:

$$P_{rad} = \pi r_a^2 h_a\, \overline{u}\big(R_{eff}, \overline{T}_a\big) \quad [16]$$

Here $\overline{u}\big(R_{eff}, \overline{T}_a\big)$ is the tabulated mean radiation density as function of mean arc temperature and effective radiation radius based on the radiative properties for the plasma composition. Heat transfer to the anode due to conduction is given by:

$$P_e = i_a\left(\Phi_{an} + \frac{5k_B\overline{T_a}}{2e} + V_{an}\right) \quad [17]$$

Φ_{an} is the material work function for the anode, k_B is the Boltzmann constant and e is the electron charge.

Dynamic channel arc models

These models use modified versions of DC channel arc models, where the instantaneous arc current $i(t)$ is used to calculate the dynamic arc radius $R_{ac}(t)$. This arc radius is then used to calculate the parameters described for the DC case, the precise method is described in (Sævarsdóttir, 2002), results for voltage vs current from the model presented in (Sævarsdóttir et al., 2006) can be seen in figure 7 below.

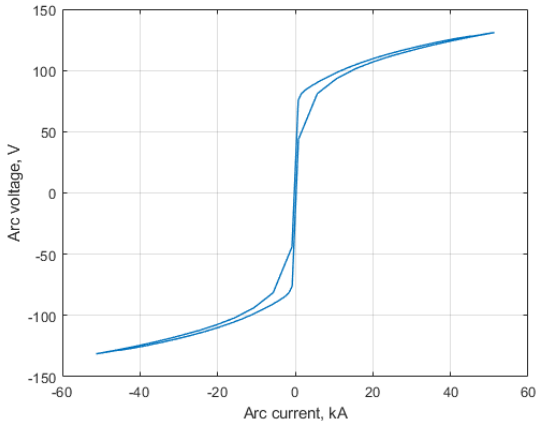

Figure 7: The V-I characteristic from the channel arc model in (Sævarsdóttir et al., 2006).

Magnetohydrodynamics [MHD] models

MHD is the most complete way to model any plasma and is thus a good way get an estimate of electric arcs. This method involves solving sets of differential equations that govern the physics inside the arc plasma and in theory should give rather detailed information about all the major arc variables. Generally, models consist of the following set of equations:

Maxwell equations:

$$\nabla \cdot \vec{D} = q \quad [18]$$

$$\nabla \times \vec{H} - \frac{d\vec{D}}{dt} = \vec{j} \quad [19]$$

$$\nabla \cdot \vec{B} = 0 \quad [20]$$

$$\nabla \times \vec{E} + \frac{d\vec{B}}{dt} = 0 \quad [21]$$

where $\vec{D} = \epsilon_0 \vec{E}$, $\vec{H} = \vec{B}/\mu_0$, q is the electric charge per unit volume, ϵ_0 is electric permittivity, $\vec{j}$ is the current density, and μ_0 is the magnetic permeability if vacuum.

Navier Stokes with Lorentz force:

$$\nabla \cdot (\rho v) = 0 \quad [22]$$

$$\rho(v \cdot \nabla)v = \nabla p - \nabla \tau + F_L \quad [23]$$

Energy equation with Joule heating:

$$\rho(v \cdot \nabla h) = \nabla \cdot \lambda \nabla T + \frac{\vec{j}^2}{\sigma} + \frac{5}{2}\frac{k_B}{e}\vec{j} \cdot \nabla T - P_R \quad [24]$$

Now ρ is the mass density, v is the speed, p is the pressure, τ is the viscous pressure tensor, F_L is the Lorentz force, T is the temperature, and P_R is the radiation power loss.

There are, however, many different approaches taken in creating MHD models for industrial arcs. In (Larsen et al., 1995) and (Bakken et al., 1997) these assumptions are described for a 2D axially symmetrical model of an electric arc in a SAF. Figure 8 shows the modelling domain

for one of the three electrodes, A-B is the center of the arc, B-C is the metal pool boundary, C-D-C is the charge boundary and E-A is the part of the elctrode inside the cavity. In (Reddy, 2010) a 2D and 3D model of a DC-arc is simulated using a time-explicit finite difference method and in (Rong et al., 2014) the effects of turbulence on the arc are investigated. The most common approach to solving a MHD problem is by using already existing commercial software such as ANSYS Fluent, OPENFOAM, or COMSOL this is done by changing out the source terms in the software making it possible to calculate Plasma flow instead of conventional fluid. Generally, MHD models try to represent the physical geometry of the system under study as closely as possible. A detailed description if the actual discretisation employed for finite volume MHD for industrial DC arcs is given in (A Della Rocca and Q G Reynolds, 2019).

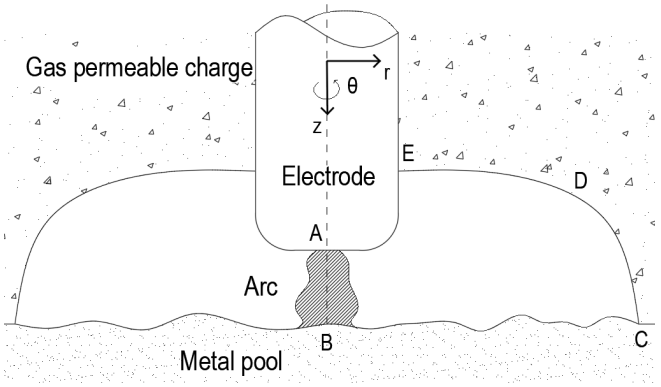

Figure 8: A sketch of a typical AC silicon furnace crater and the modelling domain (Larsen et al., 1995).

One of the main challenges that arise is the lack of precise data about the physical properties of the plasma gas itself. In (Reynolds, 2015) the effects from dust inside the furnace are investigated and, in (Andresen et al., 1995) a dynamic model for the chemical processes in silicon SAFs was developed along with the boundary conditions that need to be defined, this is especially true at the cathode and anode where electron transfer occurs. A detailed description of the cathode/anode modelling is given in (Javidi Shirvan and Choquet, 2016) for low power DC arcs, the effects of different boundary conditions on anode temperature for a free burning arc are modelled in (Xu et al., 2014), and in (Saevarsdottir et al., 2003) a more focused method is developed for high-power industrial arcs, and finally in (Sævarsdóttir et al., 2006) the effects of electrode erosion are studied as well as the likelihood of multiple arcs appearing on the same electrode.

Another concern is how to estimate the magnetic field in the model since it is generally assumed to be the only driving force in the simulation. An numerical estimation of the magnetic forces in SAFs is given in (Makarov et al., 2014). In (Loic et al., 2009) a finite volume method is used for the magnetic field so that it can be solved using the same mesh as the CFD, in (Kazak and Semko, 2011) a 3D model of a steel arc furnace is developed in ANSYS CFX and ANSYS Multiphysics is used to estimate the magnetic field, in (Lindmayer and Springstubbe, 2002) a 3D model is developed where the effects of ferromagnetic materials on arc motion can be investigated. In (Ruempler et al., 2019) arc in switching equipment is studied and a 3D simulation model developed where ANSYS Fluent and Emag are coupled together using MpCCI to solve a full MHD system. In (Kiyoumarsi et al., 2009) a 3D model if an AC-arc furnace is constructed to calculate the magnetic flux density and magnetic field intensity, and in (Tesfahunegn et al., 2018) a complete 3D model of a ferrosilicon SAF is developed, both for

a single arc and many side arcs, in fluent electric potential solver to estimate the conductance and inductance in the various materials inside the SAF.

SORTING FRAMEWORK

All the papers discussed in this review, and a few other older papers, have been categorised into a sorting framework to make it easier for readers to get an overview of what these papers contain. It is hoped that this could make it easier for future research in the field to be conducted. The categories in the framework are based on the sections presented in this review as well as others related to solution method, number of dimensions, software used and current type. The framework is presented as a table in an appendix.

CONCLUSIONS

This paper offers an overview of some of the more recent papers on electric arc modelling (primarily for SAFs) and tries to explain the basic methods used in them, it also presents a sorting framework for easy reference of these papers. These methods differ significantly in implementation and complexity ranging from direct explicit calculations to complex three dimensional models where multiple coupled partial differential equations are solved. The simpler methods are usually implemented in MATLAB or similar platforms whereas as the amount of detail increases commercial solvers become more commonly used.

A Cassie-Mayr model is presented as a tool to test a new 3D model created in Ansys Maxwell that calculates the electric properties of a full size SAF. Future plans for this model are to use the current model to investigate power quality in the SAF and then a complete MHD model will be constructed in Fluent and then coupled to the Maxwell model for a complete simulation of a SAF in operation.

ACKNOWLEDGEMENTS

The Icelandic Research Fund is greatly acknowledged for their funding of this work.

REFERENCES

A Della Rocca, Q G Reynolds, 2019. Large-eddy simulations of electric arcs at industrial scale. https://doi.org/10.13140/RG.2.2.24803.71209

Alzate, A., Durango, J., Mejia, A., 2010. Electric arc furnace modeling for power quality analysis, in: 2010 IEEE ANDESCON Conference Proceedings, ANDESCON 2010. pp. 1–6. https://doi.org/10.1109/ANDESCON.2010.5629655

Andresen, B., Tuset, J.K., Page, I.G., Tveit, H., 1995. Dynamical Model for the High-Temperature Part of the Carbothermic Silicon Metal Process, International ferroalloys congress; 7th, INFACON 7, in: INFACON 7, INFACON, International Ferroalloys Congress; 7th, INFACON 7. Norwegian Ferroalloy Research Organization;, pp. 535–544.

Bakken, J.A., Gu, L., Larsen, H.L., Sevastyanenko, V.G., 1997. Numerical modeling of electric arcs. J Eng Phys Thermophys 70, 530–543. https://doi.org/10.1007/BF02663569

Golestani, S., Samet, H., 2016. Generalised Cassie–Mayr electric arc furnace models. IET Generation, Transmission & Distribution 10, 3364–3373. https://doi.org/10.1049/iet-gtd.2016.0405

Hannesson, T., 2015. Furnace ilustration [WWW Document]. URL https://www.elkem.is/globalassets/iceland/si-process.pdf (accessed 5.10.21).

Javidi Shirvan, A., Choquet, I., 2016. A review of cathode-arc coupling modeling in GTAW. Weld World 60, 821–835. https://doi.org/10.1007/s40194-016-0319-7
Junwen Dai, Ruixiang Hao, Xiaojie You, Hu Sun, Xianjin Huang, Yan Li, 2010. Modeling of plasma arc for the high power arc heater in MATLAB, in: 2010 5th IEEE Conference on Industrial Electronics and Applications. Presented at the 2010 5th IEEE Conference on Industrial Electronics and Applications, pp. 463–468. https://doi.org/10.1109/ICIEA.2010.5517144
Kazak, O., Semko, O., 2011. Modelling magnetohydrodynamic processes in DC arc steelmaking furnace with bottom electrodes. Ironmaking & Steelmaking 38, 353–358. https://doi.org/10.1179/1743281211Y.0000000004
Kiyoumarsi, A., Nazari, A., Ataei, M., Beheshti, H.K., Karimi, H., 2009. Three dimensional analysis of an AC electric arc furnace, in: 2009 35th Annual Conference of IEEE Industrial Electronics. Presented at the 2009 35th Annual Conference of IEEE Industrial Electronics, pp. 3697–3702. https://doi.org/10.1109/IECON.2009.5415134
Larsen, H.L., Liping, G., Bakken, J.A., Tuset, J.K., Page, I.G., Tveit, H., 1995. A Numerical Model for the AC Arc in the Silicon Metal Furnace, International ferroalloys congress; 7th, INFACON 7, in: INFACON 7, INFACON, International Ferroalloys Congress; 7th, INFACON 7. Norwegian Ferroalloy Research Organization;, pp. 517–528.
Lindmayer, M., Springstubbe, M., 2002. Three-dimensional-simulation of arc motion between arc runners including the influence of ferromagnetic material. Components and Packaging Technologies, IEEE Transactions on 25, 409–414. https://doi.org/10.1109/TCAPT.2002.804604
Loic, R., Mazauric, V., Delannoy, Y., Meunier, G., 2009. Dedicating Finite Volume Method (FVM) to Electromagnetic Plasma Modeling: Circuit Breaker Application. Magnetics, IEEE Transactions on 45, 1262–1265. https://doi.org/10.1109/TMAG.2009.2012587
Makarov, A., Rybakova, V., Galicheva, M., 2014. Electromagnetism and the Arc Efficiency of Electric Arc Steel Melting Furnaces. Journal of Electromagnetic Analysis and Applications 06, 184–192. https://doi.org/10.4236/jemaa.2014.67018
Reddy, B., 2010. Mathematical and computational modelling of the dynamic behaviour of direct current plasma arcs. Journal of the South African Institute of Mining and Metallurgy.
Reynolds, Q., 2015. Interaction of dust with the DC plasma arc - A computational modelling investigation. Journal of the Southern African Institute of Mining and Metallurgy 115, 395–407. https://doi.org/10.17159/2411-9717/2015/v115n5a7
Reynolds, Q.G., 2017. Computational Modeling of Arc–Slag Interaction in DC Furnaces. JOM 69, 351–357. https://doi.org/10.1007/s11837-016-2166-9
Rong, M., Ma, R., Chen, J., Hou, C., Sun, Y., 2014. Numerical Investigation on Arc Behavior in Low-Voltage Arc Chamber Considering Turbulence Effect. IEEE Transactions on Plasma Science 42, 2716–2717. https://doi.org/10.1109/TPS.2014.2334694
Ruempler, Ch., Chechare, R., Zacharias, A., 2019. Arc Modeling in Industrial Applications. PPT 6, 200–207. https://doi.org/10.14311/ppt.2019.2.200
Saevarsdottir, G., Jonsson, M.T., Bakken, J., 2003. A novel approach to cathode / anode modelling for high-current AC arcs, in: 16th International Symposium on Plasma Chemistry.
Saevarsdottir, G., Larsen, H., Bakken, J., 1999. Modelling of industrial AC-arcs. High Temperature Material Processes (An International Quarterly of High-Technology Plasma Processes) 3, 1–15. https://doi.org/10.1615/HighTempMatProc.v3.i1.10
Sævarsdóttir, G., Pálsson, H., Jónsson, M., Bakken, J.A., 2006. Electrode Erosion due to High-Current Electric Arcs in Silicon and Ferrosilicon Furnaces. steel research international 77, 385–391. https://doi.org/10.1002/srin.200606403
Sævarsdóttir, G.A., 2002. High current AC arcs in silicon and ferrosilicon furnaces. (Doctoral thesis). Norges teknisk-naturvitenskapelige universitet.
Scevarsdottir, G., Bakken, J., Sevastyanenko, V.G., Gu, L., 2011. High-power AC arcs in metallurgical furnaces. High Temperature Material Processes 15, 205–225. https://doi.org/10.1615/HighTempMatProc.v15.i3.40
Tesfahunegn, Y.A., Magnusson, T., Tangstad, M., Saevarsdottir, G., 2018. Effect of Carbide Configuration on the Current Distribution in Submerged Arc Furnaces for Silicon Production—A Modelling Approach, in: Nastac, L., Pericleous, K., Sabau, A.S., Zhang, L., Thomas, B.G. (Eds.), CFD Modeling and Simulation in Materials Processing 2018, The Minerals, Metals & Materials Series. Springer International Publishing, Cham, pp. 175–185. https://doi.org/10.1007/978-3-319-72059-3_17
Tesfahunegn, Y.A., Magnusson, T., Tangstad, M., Saevarsdottir, G., 2020. The Effect of Side Arcs on the Current Distributions in Submerged Arc Furnaces for Silicon Production, in: Lee, J., Wagstaff, S., Lambotte, G., Allanore, A., Tesfaye, F.. (Eds.), Materials Processing Fundamentals 2020, The Minerals, Metals & Materials Series. Springer International Publishing, Cham, pp. 177–188. https://doi.org/10.1007/978-3-030-36556-1_16

Traustason, H.G., 2020. Data acquisition of electrical parameters and interpretation of SAF data (Masters thesis). Reykjavík University.
Valderhaug, A.M., 1992. Modelling and control of submerged-arc ferrosilicon furnaces (Doctoral thesis). Norges teknisk-naturvitenskapelige universitet.
Vervenne, I., Reusel, K.V., Belmans, R., 2007. Electric arc furnace modelling from a "power quality" point of view, in: 2007 9th International Conference on Electrical Power Quality and Utilisation. Presented at the 2007 9th International Conference on Electrical Power Quality and Utilisation, pp. 1–6. https://doi.org/10.1109/EPQU.2007.4424209
Xu, B.A., Chen, B., Chen, Q., Dou, L., 2014. Modeling of Free-Burning Arc and Effects of Boundary Conditions on the Anode Temperature Field [WWW Document]. Applied Mechanics and Materials. https://doi.org/10.4028/www.scientific.net/AMM.551.429

Hákon Valur Haraldsson
PhD student, Reykjavík University

Hákon received a BSc degree in applied electrical engineering from Reykjavik University in 2017, a MSc degree in electrical energy engineering at the same university and is now working on a PhD in MHD modelling of AC arcs in SFAs. He did his bachelors thesis on Field emission in micro vacuum devices and his master thesis in on large scale simulations of the Icelandic power system in relation to electric vehicles. He is also a master electrician and has worked as an engineer designing electrical systems for various projects in Iceland. Current research interests are in electron emission modelling, impact of electric vehicles, power system simulation and CFD modelling.

APPENDIX

The sorting framework

As mentioned in the main text the papers presented in this review have been sorted based on certain categories so that selecting applicable for different interests is easier. The categories chosen are explained in the table below:

Table 1.A: The different categories present in the sorting framework.

Paper Name	The name of the paper
Literature Review	Is the paper a literature review of some sort
Explicit simulation	This is usually some other method than MHD but mostly applies to when no actual model is used, or a method is used to estimate arcs before using MHD.
Channer arc	Papers that include channel arc models
Cassie-Mayr	Papers that use Cassie-Mayr models
MHD	Is the main used in the paper.
FLUENT	The Ansys fluent software is used to model the problem
CFX	The Ansys CFX software is used to model the problem
COMSOL	COMSOL Multiphysics is used
Open FOAM	The Open FOAM software is used to model the problem
Solver coupling	This is when the paper goes into some method that is used to connect different solvers together.
Arc furnace	Is the area of study some sort of arc-furnace (either a submerged or a regular one). Rather interesting to our research.
1D	Is the simulation in 1D, rather rare but does happen
2D	Is the simulation in 2D, probably the most common approach
3D	Is the simulation in 3D, this is of most interest
AC-arc	Is the arc an AC arc
DC-arc	Is the arc an DC arc

Table 2.A: The sorting framework for all the papers presented in the review.

Paper Name	Literature Review	MHD	Explicit simmulation	Cassie / Mayr	Cathode / Anode	Electric Circuit	Channel arc	FLUENT	CFX	COMSOL	OpenFOAM	Electric arc furnace	1D	2D	3D	AC-arc	DC-arc	Circute breaker	Power Quality
A NUMERICAL MODEL FOR THE AC ARC IN THE SILICON METAL FURNACE			x			x									x				
Arc Simulation Model for Three-Phase Electro-Metallurgical Furnaces		x	x			x								x	x	x			
Dedicating Finite Volume Method to Electromagnetic																			
Plasma Modeling: Circuit Breaker Application		x						x						x	x		x		
Effect of Carbide Configuration on the Current Distribution in Submerged																			
Arc Furnaces for Silicon Production – A Modelling Approach								x				x		x	x				
Electric Arc Furnace Modelling from a "Power																			
Quality" Point of View												x				x	x		x
Electrode erosion due to High -Current eletric arcs in silicon and																			
ferrosilicon furnaces		x	x									x	x	x		x			
Electromagnetism and the Arc Efficiency of																			
Electric Arc Steel Melting Furnaces												x				x	x		
High-Power AC Arcs in Metallurgical Furnaces		x	x					x				x	x			x			
Magnetohydrodynamics in Electric Arc																			
Furnace Steelmaking		x										x				x	x		
MODELLING OF INDUSTRIAL AC-ARCS			x		x	x						x	x			x	x		
Numerical Modeling Of Electric Arc			x		x		x						x	x		x	x		
Process Modeling and Optimization of a Submerged Arc												x		x	x				
Furnace for Phosphorus Production		x																	
Three Dimensional Analysis of an AC Electric Arc Furnace												x	x	x	x	x	x		
Three-Dimensional Simulation of Arc Motion Between Arc Runners																			
Including the Influence of Ferromagnetic Material									x				x	x		x			
Generalised Cassie–Mayr electric arc furnace models			x	x	x							x			x				x
A review of cathode-arc coupling modeling in GTAW	x	x	x		x														
A Review of Commonly Used DC Arc Models	x																	x	
ARC MODELING IN INDUSTRIAL APPLICATIONS		x				x		x										x	
DYNAMICAL MODEL FOR THE HIGH-TEMPERATURE PART OF THE																			
CARBOTHERMIC SILICON METAL PROCESS.								x				x		x				x	
Influence of the power supply on the behaviour of DC plasma arcs — a																			
modelling study			x			x					x								
Large-eddy simulations of electric arcs at industrial scale		x																x	
Mathematical and computational modelling of the dynamic behaviour of																			
direct current plasma arcs			x									x	x	x		x		x	
Modeling of Free-burning Arc and Effects of Boundary Conditions on the																			
Anode Temperature Field		x						x					x					x	
Modeling of Plasma Arc for the High Power																			
Arc Heater in MATLAB			x															x	
Modelling magnetohydrodynamic processes in DC arc steelmaking																			
furnace with bottom electrodes		x							x			x						x	
Numerical Investigation on Arc Behavior in Low-Voltage Arc Chamber																			
Considering Turbulence Effect			x															x	
Three-dimensional modeling of the plasma arc in arc welding			x											x				x	
Three-dimensional simulation of the plasma arc welding process			x											x				x	
Understanding Plasma Fluid Dynamics Inside Plasma Torches Through																			
Advanced Modeling		x						x					x					x	
A novel approach to chathode abode modelling for high current AC arcs																			
Effect of Electrode Shape on the Current Distribution in Submerged Arc			x		x														
Furnaces for Silicon Production- A Modelling Approach												x		x	x	x	x		

Paper II

Measuring and Processing of electrical parameters in a Submerged Arc Furnace

Hákon valur Haraldsson[1,2*], Halldór Traustason[1], Yonatan A. Tesfahunegn[1], Merete Tangstad[2] and Gurún Sævarsdóttir[1,2]

[1*]Department of Engineering, Reykjavík University, Reykjavík, Iceland.

[2]Department of Materials Science and Engineering, Norwegian University of Science and Technology, Trondheim, Norway.

*Corresponding author(s). E-mail(s): hakonh12@ru.is;
Contributing authors: halldor.traustason@pcc.is; yonatant@ru.is; merete.tangstad@ntnu.no; gudrunsa@ru.is;

Abstract

Electric arcs are necessary for high Si yield in submerged arc furnaces (SAFs) for Si/FeSi production, and a certain fraction of heat dissipation in the arc enables optimal operating conditions. Direct measurement of the arc characteristics is impossible due to hostile conditions inside the SAF, so controlling the heat dissipation is both a science and an art. The arcs exhibit non-linear electrical characteristics and behave in a complex manner. Hence, by implementing a data acquisition (DAQ) system to collect current and voltage waveforms, typically on the electrodes or transformer connections combined with appropriate signal processing offers an estimate of the actual arc parameters, enabling improved understanding of the arcing in the furnace, and improving furnace operation. In this paper a DAQ system gathering data from a FeSi SAF will be discussed, the data is processed and used to determine various furnace conditions including arc and charge current as well as harmonics.

Keywords: Submerged arc furnace, arc footprint, arc harmonics, electric arc

1 Introduction

The furnace used to produce silicon is called a submerged arc furnaces (SAF) because the electrodes that carry the electric current are submerged in the raw materials used in the production process. In some processes operated in submerged arc furnaces such as in ferromanganese production, there is actually no arc in the furnace and all the heat is dissipated as the current passes through the materials in the furnace, such as the coke bed below the electrodes. For silicon and ferrosilicon production, however, the presence of an arc is essential. In this case, much of the current will pass through an electric arc, which burns in a cavity or crater which is filled with gas not solid materials, this is thought to be due to the high viscosity of the SiO_2 and the formation of a SiC crust around the cavity. Liquid silicon forms in a pool below the arcs and is tapped into ladles using tap holes. The extremely hostile environment inside SAFs makes any direct observation of the arc impossible.

A submerged arc furnace is a fairly large machine usually spanning a few floors in the building its situated in. In simple terms the furnace converts electricity and internal energy if carbon materials to heat which melts the raw materials, thus creating usable metals. The furnace itself is circular and varies from approximately 5 m to 11 m in diameter and from 3 m to 5 m in height. Raw materials are added from the top and will descend slowly in the furnace while they are heated. A diagram of a SAF can be seen in figure 1 below.

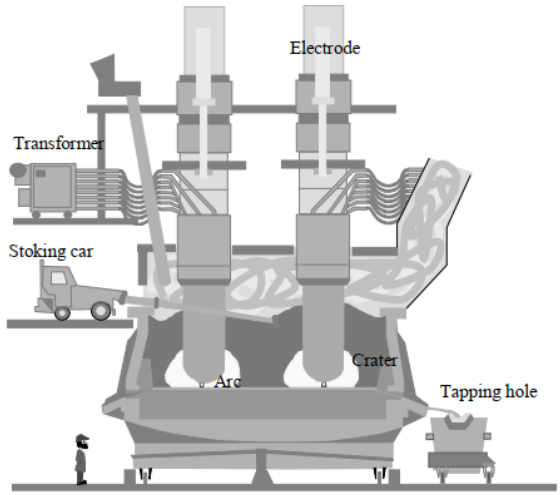

Fig. 1 A schematic drawing of a SAF in operation.

Since the arc can not be measured directly estimating its parameters can be difficult. In an operating furnace we can only measure the voltage and current going into each electrode, but by creating a complete electric circuit model of the furnace and knowing its parameters, either by simulation or measurements, we can use the measured voltage and current waveforms in each

electrode to indirectly estimate the arc. There are not many published studies on measuring arc parameters but previous work on this has been done in [1] and [2], in [3] measurements are used to model the effects of electrode height on arc currents. All measurements on any type of furnace require some sort of data acquisition (DAQ) system to collect and process the data. For industrial applications, reliable and accurate equipment is essential, so selecting the correct equipment can be a challenge, Lorenzo et al.[4] detail this for a Spanish ferroalloy company, and, Gerritsen et al.[5] describe some of the methods used and impact of error in the measurements. These should not be confused with direct arc modeling, which is a different approach [6].

In this paper, we will describe the DAQ system that was implemented on a FeSi SAF in Elkem Iceland. We will discuss the SAF properties required for data processing to estimate actual SAF parameters. Finally we will describe how the data is processed from raw measurements to actual useful parameters that are used to estimate current distribution, arc footprint and arc harmonics in the furnace

Inside the furnace the electrodes are submerged in the raw materials, below each electrode there is a cavity where the arc is burning. This cavity or crater is filled with gas not solid materials, this is thought to be due to the high viscosity of the SiO_2 and the formation of a SiC crust around the cavity. Liquid silicon forms in a pool below the arcs and is tapped into ladles using tap holes.

2 Electric circuit description of a SAF

A 3-phase SAF generally consists of 3 transformers placed concentrically around the furnace with 120° between them, this is done to minimize mutual inductance between them. The transformers are connected to 3 electrodes that conduct electric power to the furnace through bus bars and flexibles. This setup is called a knapsack configuration and is shown on figure 2.

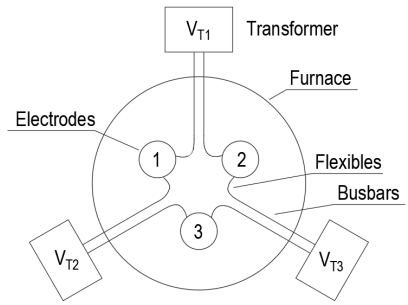

Fig. 2 A SAF in knapsack configuration.

When discussing a SAF from an electrical standpoint the main focus is on the currents present in the electrode, and what electrical parameters affect them. The electrode current is the total current that travels down the electrode

from the delta connection connecting the transformers, before it diverges to different paths. To understand what is happening we must see what the total electrical characteristics of the SAF are. Industrial high current arcs are generally present within the electric arc furnaces and to determine the behaviour of the furnace and the arc itself, a complete electric circuit must be implemented.

The circuit should include most of the actual components present, transformer resistances R_{Ti}, impedances L_{Ti} and mutual inductance between them ($M_{Ti,Ti+1}$ and $M_{Ti,Ti+2}$), as well as the resistances of the electrodes (R_e) and the phase inductance including the mutual inductance (L_e and $M_{ei,ei+1}$ and $M_{ei,ei+2}$). Mutual inductance due to currents in the bus bars and flexibles are normally lumped into the phase inductance, which is accurate if the furnace is reasonably symmetrical.

We consider the electrode current to split up into two parts, the current going into the arc and then the current in the charge material. R_c represents the charge resistance and V_a the arc voltage drop. This is a simplification but gives a reasonable estimate since other components are rather small in a well operating furnace. The physical properties of the charge materials differ with location in the furnace, as intermediate reactions change their composition and temperature changes with depth both of . Figure 3 shows the electric circuit of a three-phase SAF and where each component is located in it.

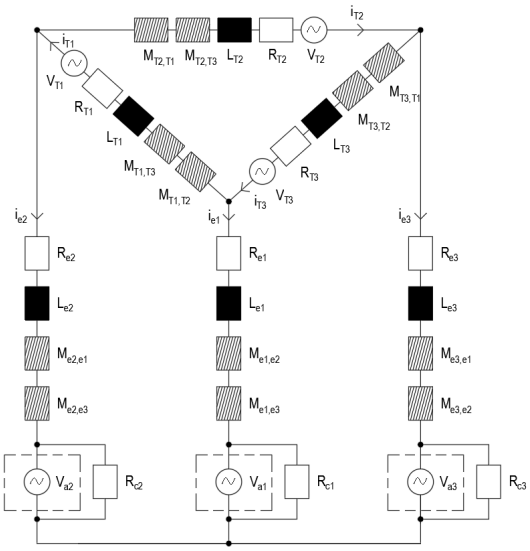

Fig. 3 The electric circuit used to describe a SAF. [7]

3 Estimating SAF parameters

3.1 The DAQ system

The data acquisition system for SAF samples both the voltage and current in each electrode as well as a few of the higher harmonics that are present in the signal. Here the measurement frequency f_S is 3000 Hz which gives about 60 samples per period. This sampling rate allows for the estimation of harmonics up to 1500 Hz which is the 30th harmonic of 50 Hz.

The DAQ system consists of three voltage sensors that measure the electrode voltage through step-down modules since it is too high to measure directly, the current sensors measure the current in each electrode using the hall effect. A detailed description can be found in [8] where the DAQ systems design and implementation are described in detail.

3.2 Data processing

A method has been developed to estimate the current that passes through the arc and charge material. The simplified circuit presented in figure 4 shows the model used to process the measured current and voltage waveforms. The model is similar to the section surrounding the arc in figure 3 but most circuit elements have been combined and the furnace resistance is included. Current and voltage measurements for each electrode are defined as i_{phi} and V_{phi}. Here the subscript i denotes the electrode numbering. The total phase voltage V_{phi} is a combination of the voltage induced in the furnace V_{Li}, the voltage over the arc V_{pi} (which is over the time varying arc resistance R_{ai} and the assumed constant charge resistance R_{ci} connected in parallel) and, finally the voltage over the furnace short-circuit resistance R_{si},the liquid metal resistance and, the base resistance in the furnace. V_{pi} can be considered as the power producing voltage or load voltage that contributes to the actual silicon production.

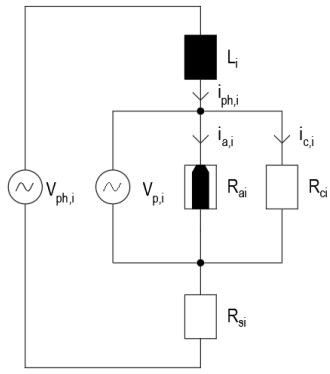

Fig. 4 The simplified circuit model used to estimate arc characteristics from the measurements.

Now the equivalent phase resistance R_{ph}, the arc resistance R_a and, the charge resistance R_c can be defined using Ohms law as:

$$R_{ph} = \frac{1}{\frac{1}{R_a} + \frac{1}{R_c}} + R_s \tag{1}$$

$$R_a = \frac{R_c(R_{ph} - R_s)}{R_s + R_c - R_{ph}} \tag{2}$$

$$R_c = \frac{R_a(R_{ph} - R_s)}{R_s + R_a - R_{ph}} \tag{3}$$

The induced voltage present in the phase voltage causes a phase shift in the current, this results in the current lagging behind the voltage by 30° to 45°. The magnitude of the phase shift varies with the size of the furnace but also with electrode movement withing the furnace. The induced voltage V_{Li} must therefore be removed from the total phase voltage V_{phi} before the resistances can be calculated. This is done by a simple time dependent differentiation of the current signal to estimate the induced voltage:

$$V_{pi} = V_{phi} - Li\frac{di_{phi}}{dt} \tag{4}$$

Here L_i is the total inductance present in the electrode, this value is found by iteration until the phase shift is negligible. With the phase shift removed the total phase resistance for each electrode R_{phi} can be determined. The phase resistance or zero crossing resistance is the resistance when both the phase current and the power producing voltage cross the zero point simultaneously. R_{phi} is found by plotting the Lissajous curve for i_{phi} and V_{pi} and then the slope is estimated as the curve passes zero. To find R_c we need both R_s and R_a, the short-circuit resistance is either known from the modeling, such as in [9], or can be assumed to be around 5% of the phase resistance similar to what is done in [8]. Determining the arc resistance R_a can be difficult since you ideally need measurements from when the furnace being measured when only an arc is present with out any charge materials present, this is important since different furnaces will have different parameters. Previous measurements carried out in the same furnace when a pure arc was present were used and determined the arc resistance to be around 2.5 to 4 mΩ [2]. This will give an upper and lower limit for the charge resistance R_c, and consequently both the arc resistance R_a and the arc current i_a will have similar limits, here we will show the upper limit only for simplicity of the graphs. Now all that is needed to determine the range for the arc current i_a which is the voltage over the arc V_a given as:

$$V_{ai} = V_{pi} - i_{phi}R_s \quad \Rightarrow \quad i_{ai} = \frac{V_{ai}}{R_{ai}} \tag{5}$$

4 Results

The ability to estimate furnace parameters both after or preferably during operation will allow for better control of the overall operation of a furnace. The data used in this paper for all three electrodes can be seen in figure 5 where the RMS values for current and voltage have been averaged over one second periods. From these figures, we can easily observe the intensely variable nature of the furnace's electric properties.

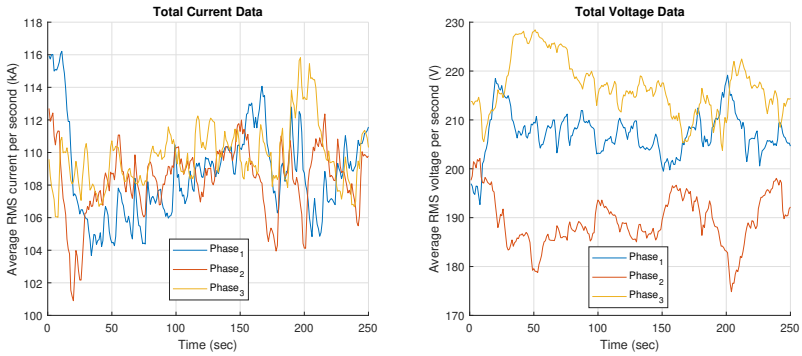

Fig. 5 Total RMS electrode current and voltage data averaged over one second periods.

Now we can pick a piece of the data to investigate in more detail. First, we need to remove the induced voltage in the electrodes; figure 6 shows the voltage vs. current profile before and after the induced voltage is removed and the fit used to estimate the zero passage resistance using equation 4.

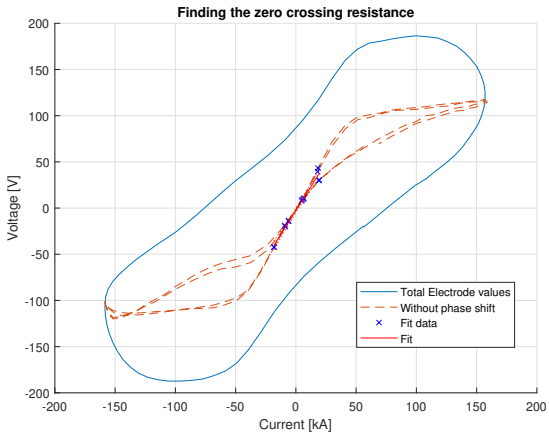

Fig. 6 To find the zero crossing phase resistance we do a linear fit around the center of the voltage vs current curve.

Now we can find out the charge resistance R_c using equation 3 and, since it is assumed constant over each period the change in the phase resistance must be due to the arc resistance R_a. We can now dived the electrode current into charge and arc currents and in figure 7 we can see all three current for two periods. Here a large part is going into the arc so we estimate it is probably rather short and that this will increase the harmonic distortions in the furnace as a result.

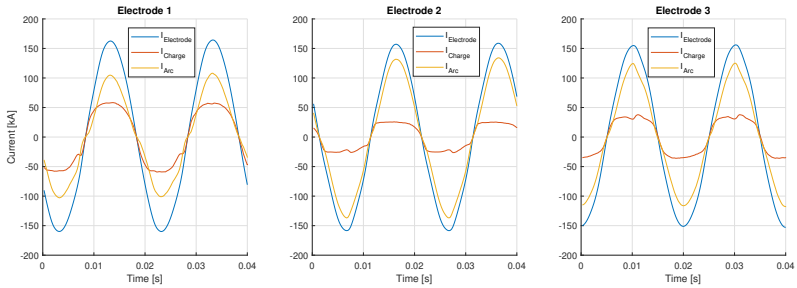

Fig. 7 Current distribution for all three electrodes. The arc and charge currents vary somewhat between them.

Another factor of interest is the arc footprint or the voltage and current graph area. This area has the units kVA so it tells us how much power is present in the arc over a whole period but the shape of the curve can also be connected to furnace operations. Theses can be tapping, how the charge material is distributed and so forth. Figure 8 shows all three arc footprints and the area for arc 2 is 5566.2 kVA.

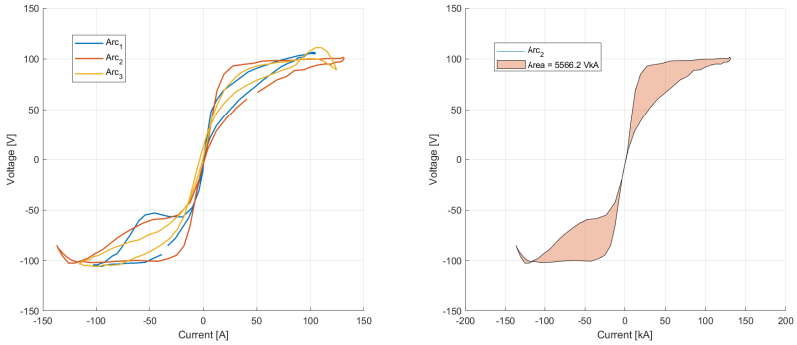

Fig. 8 The arc footprints for all three arcs and the footprint area for arc 2.

More data during various furnace operations is needed to connect these footprints to what is actually happening in the furnace, ideas would be to properly observe during tapping, charge refilling and electrode operation and to catalog the arc footprints to get a better understanding of the electric behaviour during these events.

The final thing looked into in this paper is are the harmonics, these are very important to consider since they can if used along with the rest of the parameters help give a better image if what is going on as well as being important on their own. Minimizing the total electrode harmonics is important so that the total harmonic distortion (THD) doesn't go over the limit allowed by the electric utility supplying power to the furnace. Seeing what frequency components are present in which current can also give an idea of the situation at each electrode and in the charge material. This can be arc length and material properties in the charge and metal bath below the electrodes. Figure 9 shows the current harmonics in the furnace for electrode 2 and all the arcs, we can see which frequency components are present in the furnace currents in the given period.

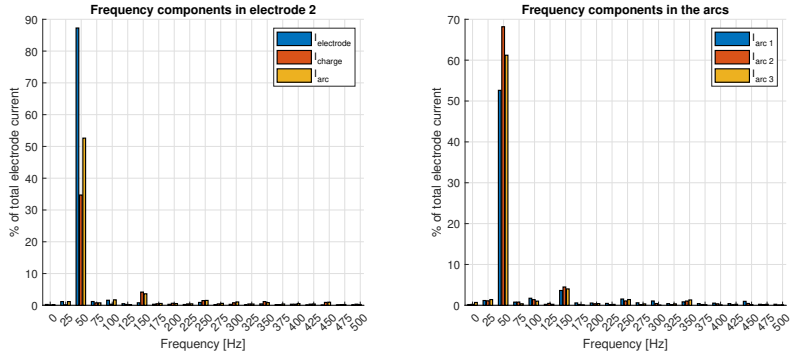

Fig. 9 The frequency components present in electrode 2 and in all three arcs as a percentage of total current in each electrode.

5 Conclusion

We have used data gathered using a DAQ system implemented in Elkems FeSi plant in Iceland to estimate various furnace parameters. The data is initially a set of voltage measurements that must be converted to actual voltage and current values based on the selected furnace, and measurement equipment. Using this data and previous measurements done on the furnace we have devised a method of estimating the furnace current distribution profile for arc and charge currents.

The method described allows us to estimate all electrode current and voltage parameters for each time period. Using reference data for a pure arc, we can find the constant charge resistance based on each electrode's slope of the Lissajous curve. This, in turn, allows us to estimate the arc resistance, which is very variable during each period.

By having a better idea of what is going on inside the furnace in relation to the arc and charge currents should allow for smother furnace operation. Which should improve silicon yield and lower the specific energy consumption.

More measurements are however needed during operations to collect more data on current behaviour, preferably during tapping, filling and general electrode operation.

Acknowledgments. The Icelandic Research Fund is greatly acknowledged for their funding of this work.

References

[1] Saevarsdottir, G., Magnusson, T., Bakken, J.A.: Electric arc on a coke bed in a submerged arc furnace. (2007)

[2] Saevarsdottir, G., Bakken: Current distribution in submerged arc furnaces for silicon metal /ferrosilicon production, international ferroalloys congress; 12th, INFACON 12. In: INFACON 12, INFACON, International Ferroalloys Congress; 12th, INFACON 12, pp. 717–728. Norwegian Ferroalloy Research Organization;. Backup Publisher: Norwegian Ferroalloy Industry. https://www.pyro.co.za/InfaconXII/717-Saevarsdottir.pdf

[3] Hauksdottir, A.S., Soderstrom, T., Thorfinnsson, Y.P., Gestsson, A.: System identification of a three-phase submerged-arc ferrosilicon furnace. IEEE Transactions on Control Systems Technology **3**(4), 377–387 (1995). https://doi.org/10.1109/87.481962

[4] Lorenzo, A., Lage, M., Bullon, J., Rivas, J., Fondado, A., Torres, A., Farina, J., Rodriguez-Andina, J.J.: Measurement of electrical parameters in high-current arc furnaces. In: 2007 IEEE International Symposium on Industrial Electronics, pp. 1565–1568 (2007). https://doi.org/10.1109/ISIE.2007.4374836

[5] Gerritsen, T., Tracy, P.E., Saber, F.N.M.: Electrode voltage measurement in electric furnaces : Analysis of error in measurement and calculation. (2015)

[6] Haraldsson, H., Tesfahunegn, Y.A., Tangstad, M., Sævarsdottir, G.: Modelling of Electric Arcs for Industrial Applications, a Review. SSRN Journal (2021). https://doi.org/10.2139/ssrn.3927158. Accessed 2022-08-30

[7] Saevarsdottir, G., Larsen, H., Bakken, J.: Modelling of industrial AC-arcs **3**, 1–15. https://doi.org/10.1615/HighTempMatProc.v3.i1.10

[8] Traustason, H.G.: Data Acquisition of Electrical Parameters and Interpretation of SAF Data

[9] Tesfahunegn, Y.A., Magnusson, T., Tangstad, M., Saevarsdottir, G.: Effect of carbide configuration on the current distribution in submerged arc

furnaces for silicon production—a modelling approach. In: Nastac, L., Pericleous, K., Sabau, A.S., Zhang, L., Thomas, B.G. (eds.) CFD Modeling and Simulation in Materials Processing 2018. The Minerals, Metals & Materials Series, pp. 175–185. Springer. https://doi.org/10.1007/978-3-319-72059-3_17

Paper III

ORIGINAL RESEARCH ARTICLE

Modeling and Comparison Study of Industrial AC-Arcs

HÁKON VALUR HARALDSSON, HALLDÓR TRAUSTASON, YONATAN A. TESFAHUNEGN, MERETE TANGSTAD, and GUDRUN SAEVARSDOTTIR

Electric arcs are a necessary heat source in many industrial processes that take place in Submerged Arc Furnaces (SAFs). Arcs exhibit non-linear electrical characteristics and behave in a complex manner. Therefore, an improved understanding of their behavior enables better control of furnace operation. Modeling of industrial arcs is a multiphysics process that involves simultaneously solving several coupled physical phenomena, such as electromagnetics, fluid dynamics, and heat transfer, including a radiative heat transfer from the plasma arc. Coupling fluid dynamics and electromagnetics is known as Magnetohydrodynamics (MHD). For practical applications, however, there are also simpler approaches to arc modeling, either based on simplified physical principles or empirical behavior. In this paper, a combined Cassie–Mayr model (CMM) and a channel arc model (CAM) are implemented and coupled with a submerged arc furnace electrical circuit model. The complete circuit model parameters such as resistances and inductances are estimated using modeling of a full size furnace, and then, actual measurements from a SAF are used to validate the models by comparing current and voltage waveform. Both models are then used to estimate harmonic distortion in a SAF for different arc current ratios, which should help operators to estimate the arc current in real time thus be able to lower and raise the electrode to keep operating conditions constant.

https://doi.org/10.1007/s11663-024-03214-y

I. INTRODUCTION

IN many metallurgical processes, the energy needed to heat the raw materials is supplied by an alternating current (AC), passing through and heating the materials in the furnace. In some processes operated in submerged arc furnaces (SAFs) such as in ferromanganese production, there is no arc in the furnace and all the heat is dissipated as the current passes through the materials in the furnace, such as the coke bed below the electrodes. In other processes, such as silicon and ferrosilicon production, the presence of an arc is essential, Figure 1 shows a typical SAF. In this case, much of the current passes through an electric arc, which burns in a gas-filled volume. The extremely hostile environment inside SAFs makes any direct observation of the arc impossible. Therefore, an accurate numerical simulation model of the electric arc can be a helpful tool for enhanced understanding and improved furnace operation. Physical modeling of arcs is a multiphysics process that simultaneously solves several coupled phenomena, such as electromagnetics, fluid dynamics, and heat transfer. Coupling fluid dynamics and electromagnetics is known as Magnetohydrodynamics (MHD). There are also simpler approaches to arc modeling, either based on simplified physical principles or empirical methods. Some are based on a simplified version of the physics of the arcs, such as channel arc models (CAM), and others are more empirically based, such as the AC Cassie-Mayr model (CMM) used in this paper.

A few similar studies that also focus on how the electric properties around the arc change with different arc conditions can be put into three categories based on complexity. The most common and simplest model in use for industrial arcs is the Cassie–Mayr model used in References 1 and 2 as well as the model introduced in this paper. In References 3 and 4 used a dynamic numerical model. The next step up in complexity is

HÁKON VALUR HARALDSSON and GUDRUN SAEVARSDOTTIR are with the Department of Engineering, Reykjavík University, Reykjavík 101, Iceland and also with the Department of Materials Science and Engineering, Norwegian University of Science and Technology, Trondheim 7491, Norway. Contact e-mail: hakonh12@ru.is HALLDÓR TRAUSTASON and YONATAN A. TESFAHUNEGN are with the Department of Engineering, Reykjavík University. MERETE TANGSTAD is with the Department of Materials Science and Engineering, Norwegian University of Science and Technology.

Manuscript submitted May 13, 2024; accepted July 6, 2024.

Published online: 24 July 2024

channel arc models,[5] where the arc implemented as a cylindrical conductor, the arc characteristics are then found based on power balances between electric input and various output losses. The most complete and complex are the magnetohydrodynamics models, for direct current (DC) arcs[6,7] and for alternating current (AC) arcs.[8–11] For a better overview of arc modeling, see Reference 12. Generally, these models are embedded as circuit elements into complete circuit models, that supply current or voltage to the arc model, be it Cassie, Channel, or MHD.

In this paper, one three-phase circuit model and two arc models are presented. One is a combined Cassie-Mayr model that numerically simulates dynamic arc behavior based on certain parameters and the second is an improved channel arc model based on an older model created in Reference 5. The CAM uses pre-tabulated physical values to estimate the dynamic behavior of an AC-arc. Both models are simulated in a three-phase electric circuit model of a submerged arc furnace (SAF) modeled in SIMULINK.[13] The values of the circuit elements are estimated using modeling as well as actual measurements from an operational silicon plant in Iceland. These measurements are then used to validate the arc models by comparing the current and voltage waveform. Finally, the models are used to simulate a furnace where the charge resistance is varied so that the amount of current going into the arc changes from 0 to 100 pct. The total harmonic distortion is then calculated for each simulation to see how it changes with increasing arc power. This should give operators an idea about how the arc current-to-charge current ratio changes with harmonics and should allow for better furnace control since that has a large impact on furnace yield.[14]

A. *Arc Description*

Before describing the arc model, it is appropriate to explain the general physical principles of electric arcs. This section illustrates the physics of DC electric arcs since they can be considered as a steady-state system, which offers an easy way to explain the basic principles of arcs, then followed by a description of AC-arcs.

Electric arcs are defined as electrical discharge sustained by a current flowing through a gaseous media (plasma) between two electrodes. It can be divided into 5 zones or regions, Figure 2, based on the electrical potential distribution. In the border regions, (1-2) at the cathode and (4-5) at the anode, the electrical field strength increases sharply, in particular for low-current arcs, while in the majority of the arc, (3), the center has a rather constant field. In low-current arcs, the electron emission is generally started by field emission; however, in high current arcs, thermionic emission dominates due to the heat load from the electric arc and large amount of current flowing through the electrodes. In this case, a high field strength at the anode and cathode is not necessary. We classify the voltage drops across the border regions as V_{ca} for the cathode, V_{an} for the anode, and, then the middle region is V_a for the arc voltage.

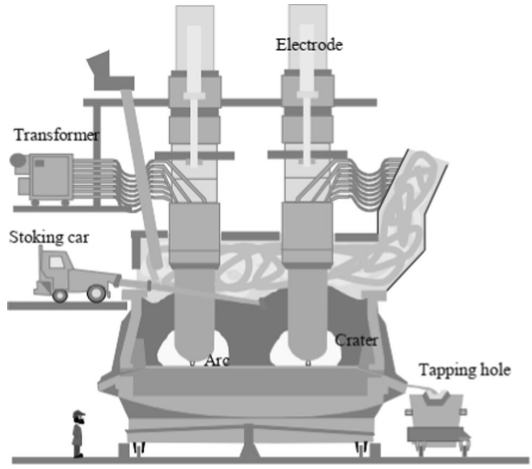

Fig. 1—A schematic drawing of a SAF in operation.

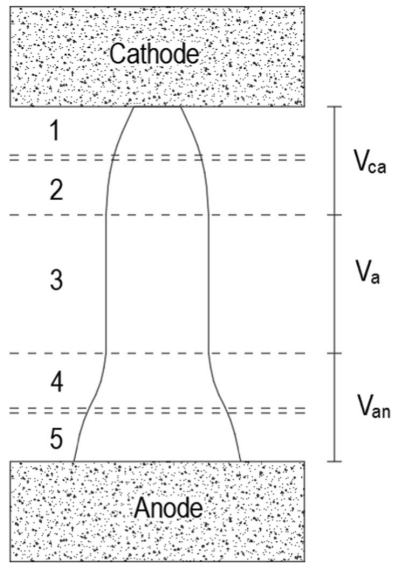

Fig. 2—The arc regions and simplified voltage drop in an industrial arc.

The regions closer to the electrode (1 and 5) are usually called the sheath or space charge layers. These are the transition regions between metallic and gaseous conduction and are made up of positive ions. The regions next to the plasma column (2 and 4) are called pre-sheath or ionization layers, where charged species are created by ionization.[15] In high-current industrial arcs, these layers are less well defined, as the energy impacting anode and cathode surfaces produces a surplus of electrons through thermionic emission.[16]

B. *AC-Arcs Dynamic Description*

When simulating AC-arcs, the current and voltage vary periodically and change polarity. It can be assumed that an AC-arc will try to reach an equilibrium state like a DC-arc with the same instantaneous current. This makes it possible to use a DC model where the current and voltage are then varied to simulate the change in the arc between time steps. Also, special consideration must be given to the time interval the current passes through zero, as the absence of current eliminates the heat source necessary to maintain the ionized plasma state necessary for the arc to re-ignite. This must be addressed in some way in the AC-arc model (Figure 3).

II. ELECTRIC CIRCUIT DESCRIPTION OF A SAF

The behavior of a SAF can be estimated from its electrical characteristics. Industrial high current arcs are generally present within the electric arc furnaces. Therefore, a complete electric circuit must be implemented to determine the behavior of the furnace and the arc itself. A 3-phase SAF generally consists of 3 transformers placed concentrically around the furnace with 120° between them; as a result, the mutual inductance is minimized. The transformers are connected to 3 electrodes that conduct electric power to the furnace through bus bars and flexibles. This setup is called a knapsack configuration and is shown in Figure 4.

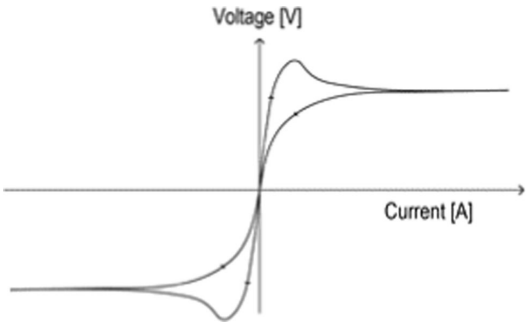

Fig. 3—An example of expected arc voltage/current behavior.

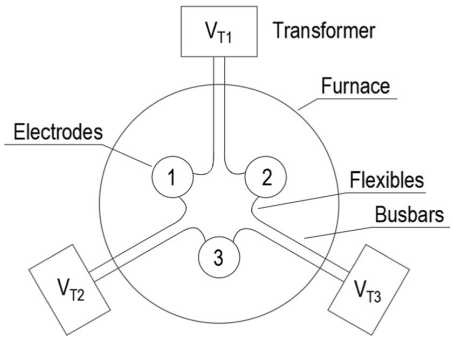

Fig. 4—A SAF in knapsack configuration.

We recreated and added to the model presented in Reference 10, and we also changed the parameters to fit with our other work. The circuit model should include most of the components, transformer currents i_{Ti}, voltages V_{Ti}, resistances R_{Ti}, impedances L_{Ti}, and mutual inductance between them ($M_{\mathrm{Ti,Ti+1}}$ and $M_{Ti,Ti+2}$), as well as the resistances of the electrodes (R_e) and the phase inductance including the mutual inductance (L_e and $M_{ei,ei+1}$ and $M_{ei,ei+2}$). Mutual inductance due to currents in the bus bars and flexibles is not included in this model. The current i_{ei} that passes between the electrodes in a SAF mostly travels through the arc. There is, however, some part that goes into the raw material charge filling up the furnace (R_c), we call this current the charge current i_{ci}, Figure 5 shows the electric circuit of a three-phase SAF where each of the components mentioned before are located in it. Throughout this paper, we will use i as a stand in for the electrode numbers 1-3 since writing all the numbers every time will become repetitive and is unnecessary since the models can work for any electrode. The physical properties of the charge materials differ with location in the furnace, as intermediate reactions change their composition and temperature changes with depth. However, this variation is not considered in the model.

The purpose of the model is to determine the electric conditions in a SAF, particularly the arc and charge current, as well as the harmonics generated by the arc. The complete dynamic electrical model then consists of a three-phase electrical- and arc model. We determine the phase current equations by applying Kirchoff's current law and summing up the voltage drop in the three current loops T_1e_1, T_2e_2 , and T_3e_3. To find the transformer current, we have to solve three coupled equations, written in matrix form as

$$\begin{bmatrix} -L_{T1}-L_1-L_2 & L_2-M_{T1,T2} & L_1-M_{T1,T3} \\ L_2-M_{T2,T1} & -L_{T2}-L_2-L_3 & L_3-M_{T2,T3} \\ L_1-M_{T3,T1} & L_3-M_{T3,T2} & -L_{T3}-L_3-L_1 \end{bmatrix} \begin{bmatrix} \frac{i_{T1}}{dt} \\ \frac{i_{T2}}{dt} \\ \frac{i_{T3}}{dt} \end{bmatrix} = \begin{bmatrix} V_{T1}-V_{a1}+V_{a2}+(R_{T1}+R_{e1}+R_{e2})i_{T1}-R_{e1}i_{T3}-R_{e2}i_{T2} \\ V_{T2}-V_{a2}+V_{a3}+(R_{T2}+R_{e2}+R_{e3})i_{T2}-R_{e2}i_{T1}-R_{e3}i_{T3} \\ V_{T3}-V_{a3}+V_{a1}+(R_{T3}+R_{e3}+R_{e1})i_{T3}-R_{e3}i_{T2}-R_{e1}i_{T1} \end{bmatrix} \quad [1]$$

where the inductance L_{1-3} includes the mutual inductance between the electrodes as well as the electrode inductance itself:

$$\begin{aligned} L_1 &= L_{e1}-M_{e1,e2}-M_{e3,e1}+M_{e2,e3} \\ L_2 &= L_{e2}-M_{e2,e3}-M_{e1,e2}+M_{e3,e1} \\ L_3 &= L_{e3}-M_{e3,e1}-M_{e2,e3}+M_{e1,e2} \end{aligned} \quad [2]$$

Now we use the current law to find the electrode currents i_{e1}, i_{e2} , and i_{e3}:

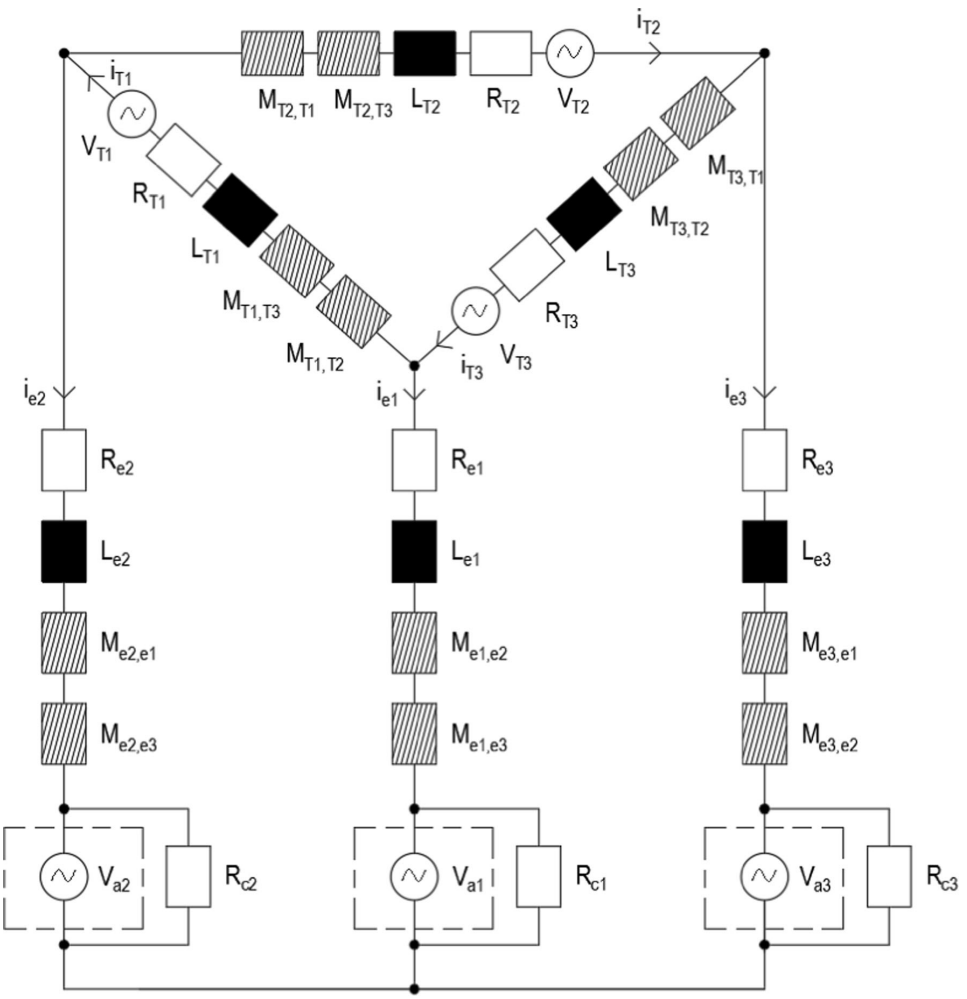

Fig. 5—Electric circuit used for the dynamic models, similar to the one in Ref. [5] but includes updated parameters and additions.

$$\begin{aligned} i_{e1} &= i_{T3} - i_{T1} \\ i_{e2} &= i_{T1} - i_{T2} \\ i_{e3} &= i_{T2} - i_{T3} \end{aligned} \qquad [3]$$

Notice how the arc voltages V_{ai} are used in the coupled equations but not arc resistance R_a and charge resistance, this is because we assume that the voltage is the same over both these resistances. The arc voltages are estimated by a dedicated arc model and this allows us to investing the charge current in more detail later, this model can be any arc model that uses electrode current as input since that allows us to use the model to solve the circuit equations above.

A. *Multiple Arcs Submodel*

We suspect that most furnaces electrodes have more than one arc per electrode,[17] to include multiple arcs we implemented a new multi arc submodel, where the resistance from an arc is calculated for each time step using the arc model. The arcs are assumed to be identical and parallel connected to each other as well as the charge resistance, see Figure 6. This setup allows for only one instance of the chosen arc model to be run at a time since the current is determined by simple current division for both the arc and charge currents. Future improvements of this submodel should include a more detailed method for estimating multiple arcs.

III. THE CASSIE–MAYR MODEL

The first model we developed for use with our new circuit model was a combined Cassi–Mayr model [CMM]. Both Cassie and Mayr models include the electric arc as a non-linear electrical circuit element, characterized by the arc voltage V_a, the arc height H_a, the arc current i_a, and the arc resistance per unit length $\widehat{R_a}$

- The Cassie model is suitable to describe high-current AC-arcs and can be applied to the simulation of arcing in an electric furnace
- The Mayr model is best suitable for descriptions of low-current AC-arcs or investigations of arc conditions near current-zero-passing.

The derivation of Cassie's model and Mayr's model is based on the assumption that the change with time in the arc's inner energy is equal to the difference between the electrical power input and the power dissipation in the arc column. The characteristic arc resistance per unit length for the Cassie model is[2]

$$\frac{d\widehat{R_a}}{dt} = \frac{R_a}{\theta_a}\left[1 - \left(\frac{V_a}{V_0}\right)^2\right] \qquad [4]$$

where θ_a is the time constant that characterizes the arc dynamics and, V_0 is steady-state static arc voltage defined here as $((V_{an} + V_{ca}) + V_d * H_a)$, where V_d is the chosen voltage per arc length and H_a is the arc height or length. And for the Mayr model, it is very similar:

$$\frac{d\widehat{R_a}}{dt} = \frac{R_a}{\theta_a}\left[1 - \left(\frac{V_a i_a}{P_0}\right)\right] \qquad [5]$$

Here P_0 is the momentary arc power loss. The total arc resistance is then given by

$$R_a = H_a\widehat{R_a} \qquad [6]$$

In this paper, a new combined Cassie–Mayr model was developed to estimate the conductance of the arc and thus the arc voltage and current. The change in arc conductance G_i is given by

$$\frac{dG_i}{dt} = \frac{G_{min} - G_i + \left[1 - exp\left(-\frac{i_{ai}^2}{I_0^2}\right)\right]\frac{V_{ai}i_{ai}}{(V_0)} + \left[exp\left(-\frac{i_{ai}^2}{I_0^2}\right)\right]\frac{i_{ai}^2}{P_0}}{\theta_a} \qquad [7]$$

where: G_i is the arc conductance, G_{min} is the conductance between any two electrodes when the electric arc is absent, and I_0 is a current value used to determine which model is dominant. We now have a model that can be inserted into the 3-phase circuit model.

IV. THE CHANNEL ARC MODEL

The second model developed was a channel arc model [CAM], it is a reconstruction of the model in Reference 5 but we will explain the model in detail here as well since notations have been changed and the method

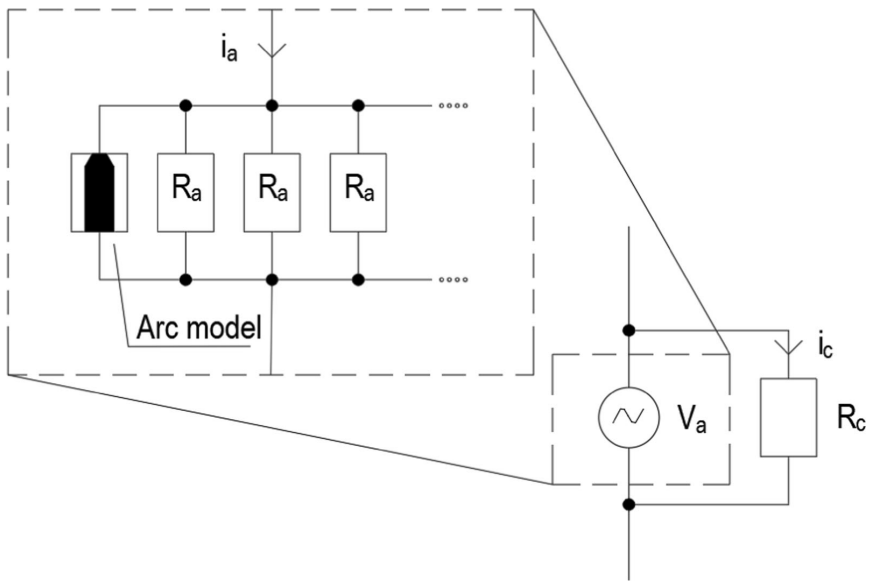

Fig. 6—The current is divided between arcs by modeling them as a parallel resistances connected to the charge resistance.

slightly as well. Here, we assumed that the arc is an ionized gas channel, which is symmetrical around the central arc axis. This allows for a variety of simplifying assumptions to be made within the channel. The simplest is to assume homogeneous current distribution throughout the channel diameter, but other distributions such as parabolic or gaussian can also be used. There is also an area where the arc expands from the cathode toward the arc channel. In the region where the current expands, it will have a radial component, which interacts with the magnetic field and forms a Lorentz force component directed toward the anode. This generates flow, contributing to convection in the arc. Figure 7 visually shows the model parameters and the variables used in the model.

The variables used in the model are the arc temperature T_a, electrical conductivity σ_a, pressure p_a , and mass density ρ_a. The radiative heat transfer, convection, and conduction to the anode from the arc plasma are included as well. These variables then vary based on the type of heat distribution within the arc. r_c is the arc radius at the cathode and r_a is the arc radius in the main arc area. While the arc is in a steady state, the electric power P_{el} that the arc generates must be transferred completely to the surroundings, P_{loss}, of the arc and it can be assumed that

$$P_{el} = P_{loss} \quad [8]$$

The electric power delivered to the arc must both include the energy loss in the arc column and the cathode anode layers and is given as

$$P_{el} = \frac{H_a {i_a}^2}{\sigma_a \pi r_a^2} + (V_{an} + V_{ca}) i_a \quad [9]$$

As mentioned above, the arc then dissipates power by three mechanisms, *i.e.*, radiation, convection, and conduction. The convective heat transfer to the arc surroundings is then given as

$$P_{con} = 2\pi \int_0^{r_a} r \rho_a(T_a(r))\ v_a(r)\ [h(T_a(r)) - h(T_F)]\ dr\,, \quad [10]$$

where $h(T_a)$ is the specific enthalpy of the arc, $h(T_F)$ is the enthalpy of the surroundings, and $v_a(r)$ is the gas velocity distribution. The maximum gas velocity is along the arc axis and is given by

$$v_{a,max} = \frac{i_a}{\pi r_a} \sqrt{\frac{K_1 \mu_0}{2\rho_a} \left(\frac{r_a^2}{r_c^2} - 1 \right)} \quad [11]$$

The constant K_1 determines the current density profile, $K_1 = 1$ is a uniform profile, while $K_1 = 5/3$ is a parabolic one.[21] The cathode spot radius is estimated with $r_c = \sqrt{i_a/\pi j_c}$, where j_c is a preselected current density. And then the mean velocity distribution is found with

$$\overline{v_a} = K_2 v_{a,max} \quad [12]$$

Here, K_2 decides the velocity profile. Finally, the radiative heat loss from the arc is given by

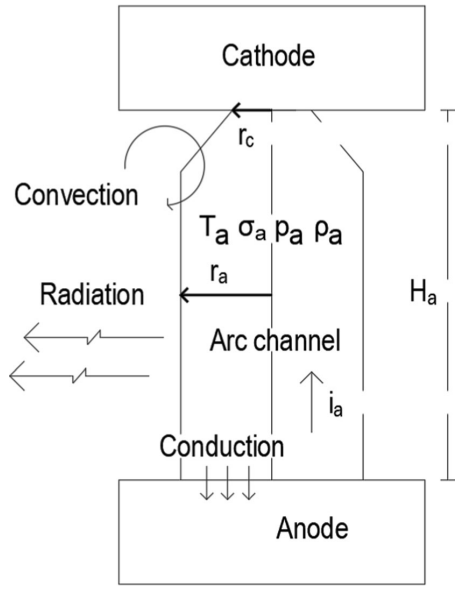

Fig. 7—A visual representation of the parameters present in the channel arc model.

$$P_{rad} = \pi r_a^2 H_a\ \overline{u}\left(r_{eff}, \overline{T}_a\right) \quad [13]$$

Here, $\overline{u}\left(R_{eff}, \overline{T}_a\right)$ is the tabulated mean radiation density as function of the mean arc temperature $\overline{T}_a$ and effective radiation radius r_{eff} based on the radiative properties for the plasma composition. Heat transfer to the anode due to conduction is given by

$$P_{an} = i_a \left(\Phi_{an} + \frac{5 k_B \overline{T_a}}{2e} + V_{an} \right) \quad [14]$$

Φ_{an} is the material work function for the anode, K_B is the Boltzmann constant, and e is the electron charge. In the end, we will need a final relation to add to the energy balance (8) so we can determine the arc radius and mean temperature. We assume that the power loss P_{loss} will be minimized which means that the arc will find the path of least resistance:

$$P_{con} + P_{rad} + P_{an} = P_{loss} = P_{el} = V_a i_a \rightarrow Minimum \quad [15]$$

A. *Dynamic Channel Arc Model*

To make the model capable of simulation alternating current arc, we use the already discussed DC model as a submodel for the new dynamic model, where the instantaneous arc current $i_a(t)$ is used to calculate the dynamic arc radius r_{ac} and mean temperature $\overline{T}_{ac}$. This is done by first estimating the DC arc radius r_{dc} and the mean temperature $\overline{T}_{dc}$, the mass of the DC arc can then be calculated by

$$M_{dc} = \pi r_{dc}^2 H_a \overline{\rho}_a \quad [16]$$

Since the AC-arc will always attempt to approach the temperature and radius of the steady-state DC model for any given current i(t), the change of mass over time can be estimated by

$$\frac{dM}{dt} = \frac{1}{\tau}(M_{dc} - M) \quad [17]$$

here τ is a time constant, around 1 ms. The change of mass can both be positive and negative since the arc can both lose and gain mass. The surrounding gas, which is pulled into the arc, has a temperature T_F, estimated around 2300 K. The gas released from the arc has the mean temperature $\overline{T}_{ac}$. The change of arc energy due to mass change P_m is then

$$\frac{dM}{dt} > 0 \Rightarrow P_m = h(T_F)\frac{dM}{dt} \quad [18]$$

$$\frac{dM}{dt} < 0 \Rightarrow P_m = \overline{h}(\overline{T}_{ac})\frac{dM}{dt} \quad [19]$$

here the $\overline{h}(\overline{T}_{ac})$ is the mean enthalpy of the arc for the mean instantaneous temperature $\overline{T}_{ac}$. The energy balance for the AC-arc can then be defined as

$$\frac{dE}{dt} = P_{el} - P_{loss} + P_m\,, \quad [20]$$

where P_{el} and P_{loss} are the arc losses calculated for the current AC-arc time step using the DC submodel. The arc mass M(t) and energy E(t) can then be found by explicit integration over time. When the total mass and energy are known, they can be used to find the mean enthalpy of the arc, and from that the mean ac-arc temperature $\overline{T}_{ac}$ is estimated:

$$\frac{E(t)}{M(t)} = \overline{h}(\overline{T}_{ac}) \quad \Rightarrow \quad \overline{T}_{ac} \quad [21]$$

Then, the AC-arc radius is found using

$$r_{ac}(t) = \sqrt{\frac{M(t)}{\pi H_a \overline{\rho}_a}} \quad [22]$$

The final step is then to find the dynamic arc voltage V_{ac} for the circuit model we use equation (23) by equating the new AC values and finding the new electric power in the arc:

$$P_{el,ac} = \frac{H_a {i_a}^2}{\sigma_a \pi {r_{ac}}^2} + (V_{an} + V_{ca})i_a \rightarrow V_{ac} = \frac{P_{el,ac}}{i_a} \quad [23]$$

Table I. Parameters for the SAF Circuit Model

Parameters	Values
V_{Ti}	230 V
R_{Ti}	0.03 mΩ
L_{Ti}	2.25 μH
$M_{Ti,Ti+1}$	0.375 μH
R_{ei}	0.09 mΩ
L_{ei}	2.09 μH
$M_{ei,ei+1}$	0.349 μH
R_c	2.1 mΩ

V. MODELING RESULTS

Above we have described the models we used and their methodologies. Setting up the simulation is a bit complex since we have a total of three models with varying degrees of complexity and amount of input needed. In this section, we will describe these inputs as much as possible and then how the needed parameters were estimated.

A. *Circuit Model Parameters*

The circuit model requires quite a few parameters to run, some are easier to get than others. The transformer resistances and inductance's can be measured by conventional means. In the current model, the distributed resistances and inductances in the furnace are lumped into circuit elements L_i, R_i, based on a complete furnace model reported in References 18 and 9.

We assume for this study that the transformers are symmetrical and thus have the same resistances and inductances, same for the electrodes. This is probably not the case in a live SAF but will give a good starting point and makes the setup easier. The values are presented in Table I.

Table II. Parameters for the Cassi–Mayr Model and the Channel Arc Model

CMM		CAM		Used in Both	
V_d	13 V/cm	j_c	25 MA/m^2	V_{an}	5 V
I_0	1 kA	K_1	1	V_{ca}	5 V
G_{min}	3 S	K_2	1/2	H_a	7 cm
P_0	50 kW	Φ_{an}	4.75 eV	number of arcs	2
θ_a	0.1 ms	T_F	2273 K		
		τ	1 ms		

B. *Model Verification*

As we have discussed the previous sections, there are many parameters that have to be chosen for each of the arc models so that they can simulate a real arc. Those used in the CMM are not physically based but serve as a fitting parameters to be adjusted to obtain the deserved result. For the CAM, you need a completer set of material properties and radiation energy absorption data for the desired arc plasma composition (SiO + CO in this case) for the model to work. The parameters for the arc models are given in Table II below. The arc height is set to 7 cm since that industrial arcs in Si-furnaces are thought to be around 5 - 10 cm and the number of arcs was 2 in the model since the simulations did not fit well if more or less were used.

The simulations were validated with measurements in an industrial furnace. One of Elkem Iceland's ferrosilicon furnaces was equipped with a data acquisition system [DAQ].[19] This system measured the three-phase current and voltage waveforms, independently for each electrode of the furnace. One of the most interesting factors is how much current goes through the arc and the charge material respectively. The method used in Reference 10, was implemented to estimate both current and voltage in each electrode. The implementation used in this paper is explained in detail in Reference 20. We tried to pick a time period where the currents in the three electrodes were the same since we had already set the circuit model to be symmetric, we chose the time at 141 seconds for this purpose, Figure 8.

For validation the models were run and adjusted to get the best fit and then we compared together the electrode, arc and charge currents for both models and the SAF measurements [MEAS], Figure 9 left. All the modeled currents fit very well to the measured values, the total electrode current is around 150 kA while the arc and charge currents are 100 kA and 50kA respectively. The general shape is also a very good fit. The second thing to compare is the arc voltage waveform, Figure 9 right, which also conforms to an acceptable level with the arc voltage being around 100 V and slightly square. For the case in question, around 2/3 of the phase current passes through the arcs, dissipating heat at extremely high temperatures.

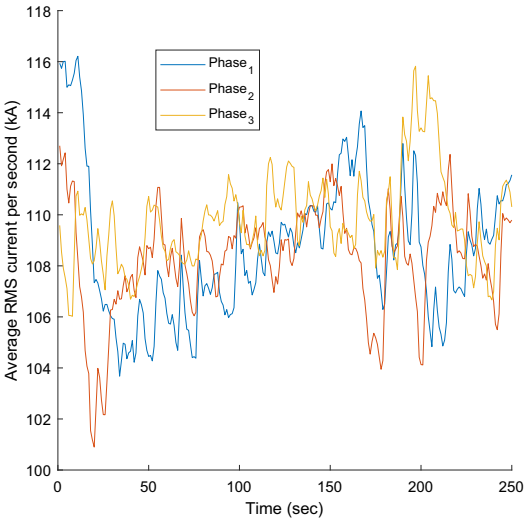

Fig. 8—Total RMS electrode current data averaged over one second periods, here we use the same data set as in Ref. 20 but a different part of the data.

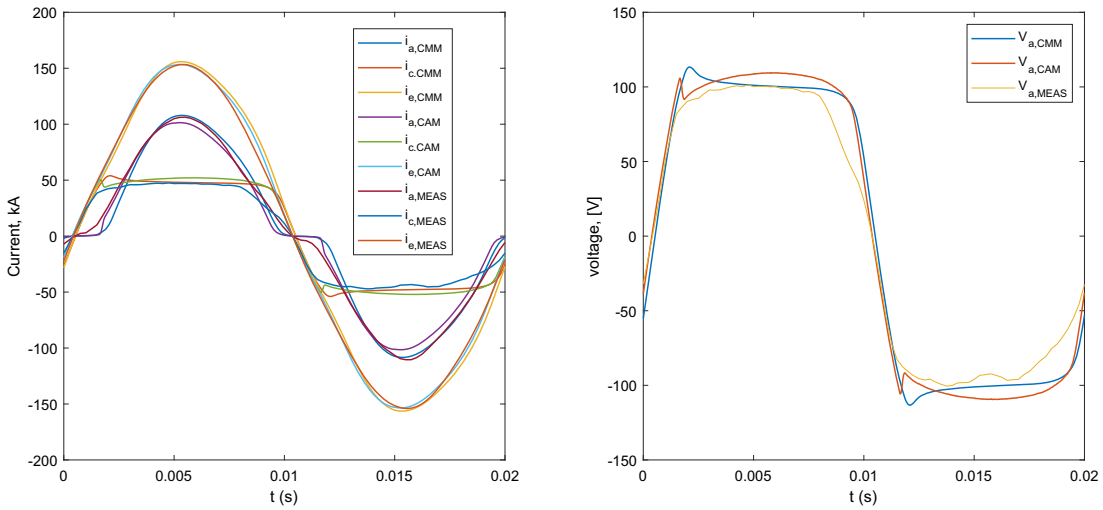

Fig. 9—Electrode, arc and charge current (left), and arc voltage (right). Model data is marked CMM and CAM are the models and the measurements are marked [MEAS].

Finally it can be interesting to look the I-V curve of the arc or the arc footprint. We can see from Figure 10 how the footprints for the models and the SAF look. There is a good comparison for the models but we can also see that the real arc behaves a lot more erratically, but this is normal. We can now say that both the circuit model and the two arc models are working as desired.

C. *Harmonics in the Electrode*

The electrical control of a SAF consists of a combination of Power control, where the power dissipation is managed by changing transformer tap position. The phase current and/or resistance is changed by adjusting electrode holder position and thus moving the electrode tip up and down. The electrode tip position determines how power dissipation is distributed in the furnace. When the electrode is moved up or down, the contact area between the electrode and surrounding materials changes, and the availability of potential arcing sites, as well as the resulting length of the arc, changes accordingly.[14]

The question is then when to lower or raise the electrode so that we can keep the correct balance between the arc and charge current. Since the arc is the main generator of furnace harmonics, Figure 11, we should see a change in the total harmonic distortion [THD] as more or less current goes through the arc. So we propose here that by measuring the THD should give you an idea of the amount of current going through the arc and thus inversely the charge.

To investigate the variations in the harmonics, we used both models to simulate different values of the charge resistance R_c. This was done by scaling the charge resistance from a low to a high value. It changes the current that goes through the arc from about 0 to 90 pct in several steps. To estimate the harmonics, we decided to use the standard THD pct generally used for power systems, given by

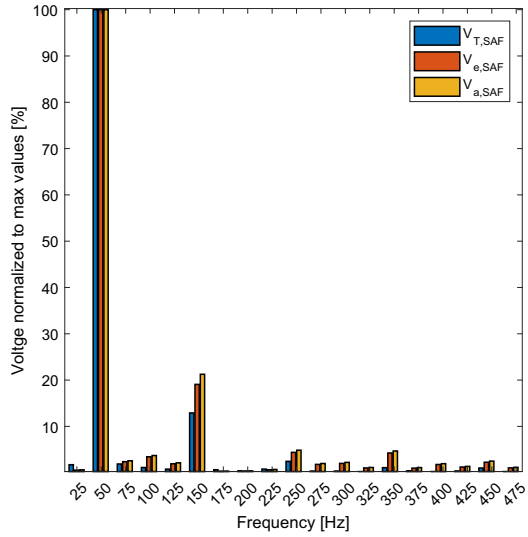

Fig. 11—Normalized frequency components for the transformer, electrode, and arc voltages for the measured values from the SAF. The arc can be observed to have the highest amount of over tones.

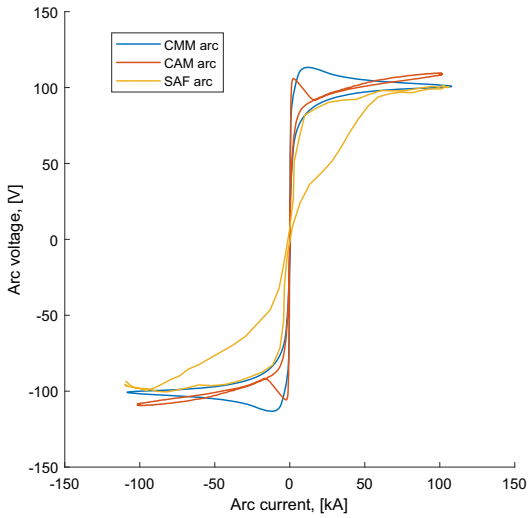

Fig. 10—Arc footprints for the arc voltage and current from the SAF measurements and both simulation models.

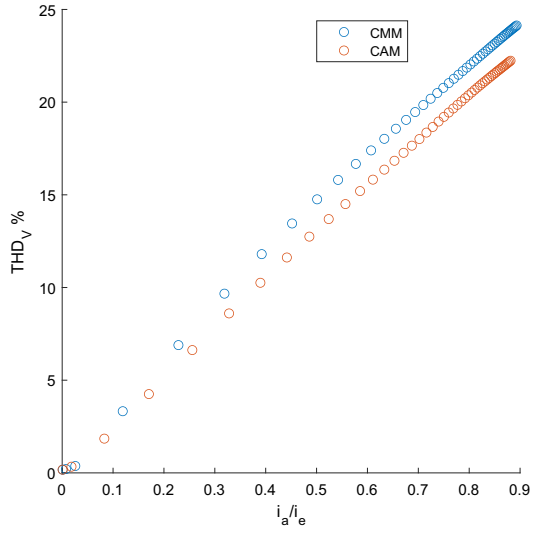

Fig. 12—Total harmonic voltage distortion as a function of the current going to the arc for both models.

$$THD = \frac{\sqrt{H_2 + H_3 + H_4 + ... \quad H_n}}{H_1}, \qquad [24]$$

where H_i is the harmonic component number i and i is the multiple of the base frequency, in this case 50 Hz. The results from both models for the voltage harmonics are shown in Figure 12.

We can observe that as more power goes through the arc, the THD_V pct increases, almost linearly from 0 to 22-24 pct. This simple figure shows us where we want to have the voltage THD in order to have the desired arc current ratio, this will in turn ensure that the right amount of power goes into driving reactions to make silicon and in to melting the furnace charge materials. So if we would want to keep the ratio at 0.6 for example and we see that the THD is getting above 17 pct, we can raise the electrode and thus increase the arc resistance.

VI. CONCLUSION

Two models, Cassie–Mayr and a channel arc model, were constructed to simulate electric arcing in a submerged arc furnace. They were validated with industrial data, indicating that around 2/3 power dissipates in the arc for the case considered. The models were connected to a complete three-phase AC circuit, which represents a SAF and includes an new multi arc submodel. The model uses parameters from a full-scale SAF electrical model and from actual measurements conducted in a ferrosilicon plant in Iceland. This allows for verification of the model presented by estimating most of the model parameters with the ones measured in the SAF.

The models can simulate a wide range of arcs present in many industrial applications, this is possible for both DC- and AC-arcs. The circuit used to represent the SAF also has the ability to use any arc model as well as multiple arcs, this allows for an easy comparison between different arc models using the same base electrical conditions. The models seem to conform acceptably to the actual arcs measured, after the arc model parameter has been determined.

An investigation into the effects of varying charge resistances was conducted by changing the appropriate parameter in the circuit model (R_c) from very low to high. The results show that total harmonic distortions increase with a higher portion of total current going into the arc and should give operators and idea of how the current distribution can be estimated based on the harmonics.

Further improvement of the SAF circuit model would be to implement an arc model that includes more of the actual physics present in an industrial arc, this work is currently underway. A new Magnetohydrodynamics (MHD) model is being developed, this model will use values from the 3D model created in Ansys Maxwell that calculates the electric properties of a full size SAF. It will also be possible to connect it to the same electric circuit as the previous model. Further modeling of the arc footprint during tapping would also be of interest since it is one of the main operations carried out in live SAFs. This might further our understanding of the current distribution and harmonics during said operation.

ACKNOWLEDGMENTS

The Icelandic Research Fund is greatly acknowledged for their funding of this work.

FUNDING

Open access funding provided by NTNU Norwegian University of Science and Technology (incl St. Olavs Hospital - Trondheim University Hospital).

CONFLICT OF INTEREST

On behalf of all authors, the corresponding author states that there is no conflict of interest.

REFERENCES

1. A. AIlzate, J. Durango, and A. Mejia: *IEEE ANDESCON Conference Proceedings*, 2010, pp. 1–6.
2. S. Golestani and H. Samet: *IET Gener.Transm. Distrib*. 2016, vol. 10, pp. 3364–73.
3. I. Vervenne, K.V. Reusel, and R. Belmans: *9th International Conference on Electrical Power Quality and Utilisation*, 2007, pp. 1–6.
4. J. Dai, R. Hao, X. You, H. Sun, X. Huang, and Y. Li: *5th IEEE Conference on Industrial Electronics and Applications*, 2010, pp. 463–68.
5. G. Saevarsdottir, H. Larsen, and J. Bakken: *High Temperature Material Processes (An International*, 1999, vol. 3, pp. 1–15.
6. Q. Reynolds, R. Jones, and E. Reddy: *J. South Afr. Inst. Min. Metall*., 2010, vol. 110, pp. 733–42.
7. A.D. Rocca and Q. Reynolds: *Unpublished*, 2019.
8. J.A. Bakken, L. Gu, H.L. Larsen, and V.G. Sevastyanenko: *J. Eng. Phys. Thermophys*., 2010, vol. 70, pp. 530–43.
9. G. Saevarsdottir: *Norges teknisk-naturvitenskapelige universitet*, 2002.
10. G. Saevarsdottir and J. Bakken: *12th International ferroalloys congress*, 2010, pp. 717–28.
11. Q. Reynolds: *Proceedings of the 14th International Conference on CFD in Oil & Gas, Metallurgical and Process Industries*, 2020, pp. 99–106.

12. H. Haraldsson, Y.A. Tesfahunegn, M. Tangstad, and G. Sævarsdottir: *SSRN J.*, 2021.
13. Simulink, Simulation and Model-Based Design: https://www.mathworks.com/products/simulink.html, Accessed July 2024.
14. T.E. Magnussen: *J. Southern Afri. Inst. Min. Metall.*, 2018, vol. 118, pp. 631–36.
15. A.J. Shirvan, and I. Choquet: *Weld. World*, 2016, vol. 60, pp. 821–36.
16. G. Saevarsdottir, M.T. Jonsson, and J. Bakken: *16th International Symposium on Plasma chemistry*, 2003.
17. G. Saevarsdottir, J. Bakken, V.G. Sevastyanenko, and L. Gu: *High Temp. Mater. Process.*, 2011, pp. 205–25.
18. Y.A. Tesfahunegn, T. Magnusson, M. Tangstad, and G. Saevarsdottir: *CFD Model. Simul. Materi. Process.*, 2018, pp. 175–85.
19. H.G. Traustason: *Reykjavik University*, 2020.
20. H.V. Haraldsson, H. Traustason, Y.A. Tesfahunegn, M. Tangstad, and G. Saevarsdottir: *Mater. Process. Fundam.*, 2023, pp. 161–70.
21. L.H. Larsen: *Norges teknisk-naturvitenskapelige universitet*. Doctoral Thesis, NTNU, 2002.

Paper IV

ORIGINAL RESEARCH ARTICLE

Modeling of Industrial Electric Arcs Using Different Plasma Gas Compositions

HÁKON VALUR HARALDSSON, QUINN REYNOLDS, YONATAN A. TESFAHUNEGN, and GUDRUN SAEVARSDOTTIR

Electric arcs are an important heat source in submerged arc furnaces that are used in the pyrometallurgical production of silicon. They are therefore of great interest to study so that the production process can be improved and made more efficient. Modeling of industrial arcs is a multiphysics problem that involves simultaneously solving several coupled physical phenomena, such as electromagnetics, fluid dynamics, and heat transfer, including radiative heat transfer from the plasma arc. Coupling fluid dynamics and electromagnetics is known as Magnetohydrodynamics (MHD). Two MHD model implementations developed by the authors are used to simulate alternating current arcs with different plasma gas compositions. The thermophysical properties of each composition are calculated using specialized code as well as gathered from literature. We investigate the dependence of the results on both the MHD model used and the input plasma data for three argon data sets and compare the results to data obtained from laboratory experiments. Finally, we investigate furnace conditions using different ratios of SiO to CO gases.

https://doi.org/10.1007/s11663-024-03397-4

I. INTRODUCTION

SILICON metal is typically produced in a large electric smelting vessel called a submerged arc furnace (SAF). In simple terms, the furnace converts electricity and internal energy of carbon-based materials into heat which drives chemical reactions between the raw materials, thus producing Si metal. The electrodes that carry the electric current are submerged in a deep bed of raw material used in the furnace, and heat is released via plasma arcs and resistive heating at the electrode tips. In silicon and ferrosilicon production, the electric arc is essential to provide heat at high enough temperature to separate the silicon from the oxides. In these processes, much of the current will pass through the arc, which burns in a gas-filled volume, surrounded by a solid silicon carbide (SiC) crust. The extremely hostile environment inside SAFs makes any direct observation of the arc impossible. Therefore an accurate numerical simulation model of the electric arc can be a helpful tool for enhanced understanding and improved furnace operation. Liquid silicon forms in a pool below the arcs and is tapped into ladles via taping holes located in the furnace sidewalls. High temperatures of over 10000°C in and around the arc provide the required energy to drive the chemical reactions of liquid SiO_2 with SiC to form Si metal in liquid form and CO gas.[1]

SAFs are large pieces of industrial equipment and usually span a few floors of the buildings they are situated in. The furnace itself is circular, with diameters ranging from approximately 5 to 11 m and heights from 3 to 5 m. Raw materials are added through feed chutes located in the roof of the vessel and gradually descend as they are consumed by heating and reactions occurring around the electrode tips. A diagram of a SAF can be seen in Figure 1 below.

The construction and operation of the SAF makes it almost impossible to observe or measure anything from the interior of the furnace. Simulation models that attempt to estimate the internal parameters of the SAF are therefore of great value to researchers and plant operators. The simplest models in use for industrial arcs are probably the Cassie-Mayr models (which are fully numerical) used in for example in References 2 and 3

HÁKON VALUR HARALDSSON and GUDRUN SAEVARSDOTTIR are with the Department of Engineering, Reykjavík University, Reykjavík, 101, Iceland and also with the Department of Materials Science and Engineering, Norwegian University of Science and Technology, Trondheim, 7491, Norway. Contact e-mail: hakonh12@ru.is QUINN REYNOLDS is with the Pyrometallurgy Division, Mintek, Randburg, 2194, South Africa and also with the Department of Chemical Engineering, University of Stellenbosch, Stellenbosch, 7600, South Africa. YONATAN A. TESFAHUNEGN is with the Department of Engineering, Reykjavík University.

Hákon Valur Haraldsson and Quinn Reynolds have contributed equally to this work.

Manuscript submitted July 19, 2024; accepted December 2, 2024.

Published online: 03 January 2025

and in Reference 4. They are easy to implement and have a low computational cost but are not very accurate. Slightly more complex and accurate are channel arc models described in Reference 5, where the arc is implemented as a cylindrical conductor and the arc

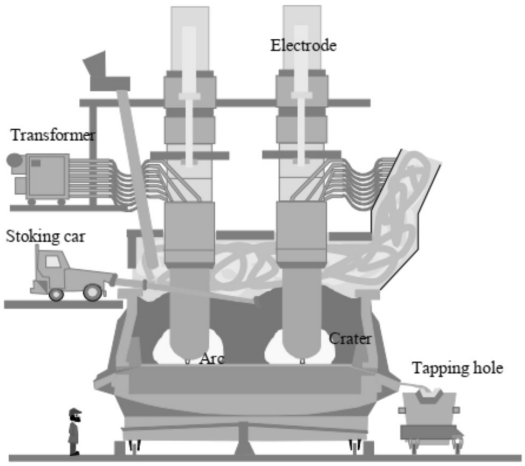

Fig. 1—A schematic drawing of a SAF in operation.

characteristics are calculated based on power balances between electric input and various output losses. The most complete and complex are the magnetohydrodynamics (MHD) models. These models provide highly detailed and accurate results but are computationally formidable—some examples for direct current (DC) arcs are References 6 and 7, and for alternating current (AC) arcs.[5,8,9]

In this paper, we will investigate the effect of the composition of the plasma gas present in the crater at the center of a silicon smelting furnace, Figure 2, on the transient electrical behavior of the arc. We start by verifying two independently developed MHD models by comparing them using three different plasma property data sets for Argon, in a geometry that corresponds to a known laboratory furnace for which experimental measurements are available. This allows us to assess the effect that different plasma property data sets have on the final results, and how well they fit the experimental data. We also simulate an industrial case using high current and two plasma property data sets for a 50/50 mixture of SiO and CO gas, again investigating the effect that different property data sets will have on large-scale arcs with the gas that is expected to be present in the crater region. Finally we simulate industrial arcs in plasmas generated from different mixtures of SiO and CO gas, and investigate how the arc conditions change as the crater gas becomes more CO- or SiO-rich.

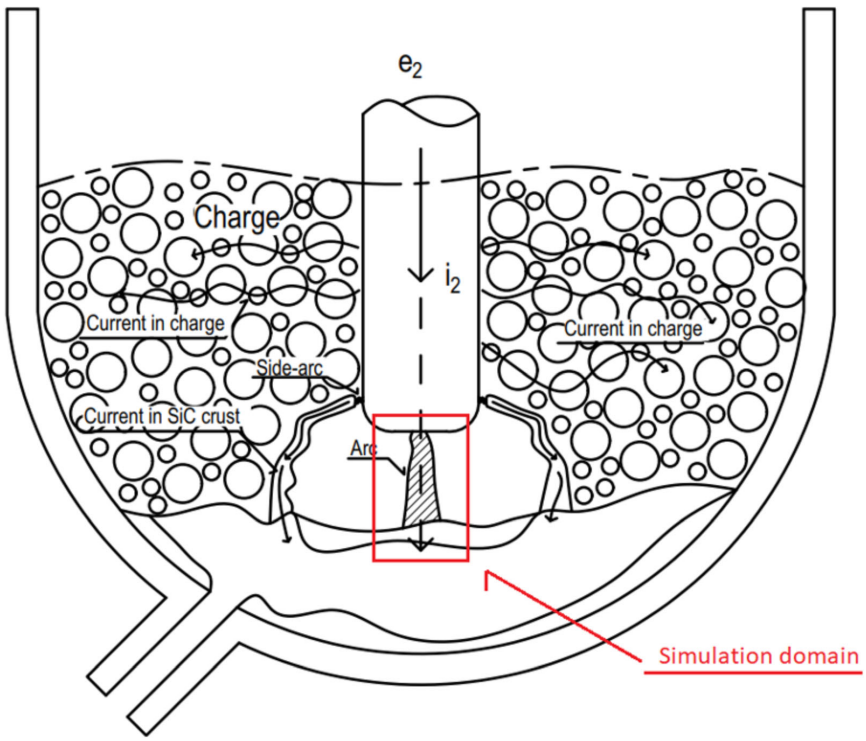

Fig. 2—The simulation domain for our MHD models is directly below the electrode in SAF.

II. PLASMA GAS COMPOSITION

One of the major challenges in simulation of arc furnaces is the lack of precise data on the compositions of the arc plasma gas. Additionally, there is a lack of thermodynamic and transport property data for this plasma gas, which is known to exist in the high-temperature regions of the arc. Argon is used as the plasma gas in many simulations and experiments due to its ease of use and comprehensive knowledge of its thermophysical properties. The main gases present inside an industrial furnace are SiO(g) and CO(g), and these can be in different ratios depending on conditions in the furnace interior.

For this paper, we have used different methods to estimate the plasma gas properties, and we will be studying the effect of different data sets on the overall simulation results. The plasma property data used as input for the simulations are the enthalpy h, density ρ, electric conductivity σ, thermal conductivity κ, and Specific heat C_p. First we compare three different data sets for Argon, and then we move to comparing two different sets for SiO + CO gas in half and half ratios. In the end we vary the ratios of SiO to CO from 0 to 100 pct in order to give an overview of how the properties change with different gas compositions.

A. *Argon Properties*

Here we have used two different calculation procedures to estimate the parameters for Argon, as well as previously tabulated data from calculations by Boulos *et al.*[10] The benefit of using Argon for verification is that its properties are well understood even at the temperatures present in an arc, and it is often used as a plasma gas in arc experiments which provide measured data for model validation. The three above mention data sets for Argon are surprisingly different but follow a similar trend, see Figure 3:

B. *Industrial Furnace Gas Properties—50/50 Mixture*

For the industrial case studies, a SiO + CO gas with an equimolar mixture ratio was chosen. This is the most likely composition of the gases present in the crater at optimal furnace operating conditions. The data sets conform for density, enthalpy, and electric conductivity but are fairly divergent for the rest except for specific heat at lower temperatures, see Figure 4:

C. *Industrial Furnace Gas Properties—All Mixtures*

Thermophysical property data for a range of plasma compositions from 0 to 100 pct SiO (the rest being made up of CO) were calculated to further investigate the effects of changing plasma composition on the industrial scale. In Figure 5, we can see how the enthalpy-temperature curves change as the SiO fraction is increased. The corresponding variation in the specific heat capacity curves is quite extreme, particularly at low to moderate temperatures, and this can be expected to have an appreciable impact on the thermal behavior of the arc. This discrepancy is likely due to how the two data sets are calculated, since atomic interaction is handled in a slightly different manner.

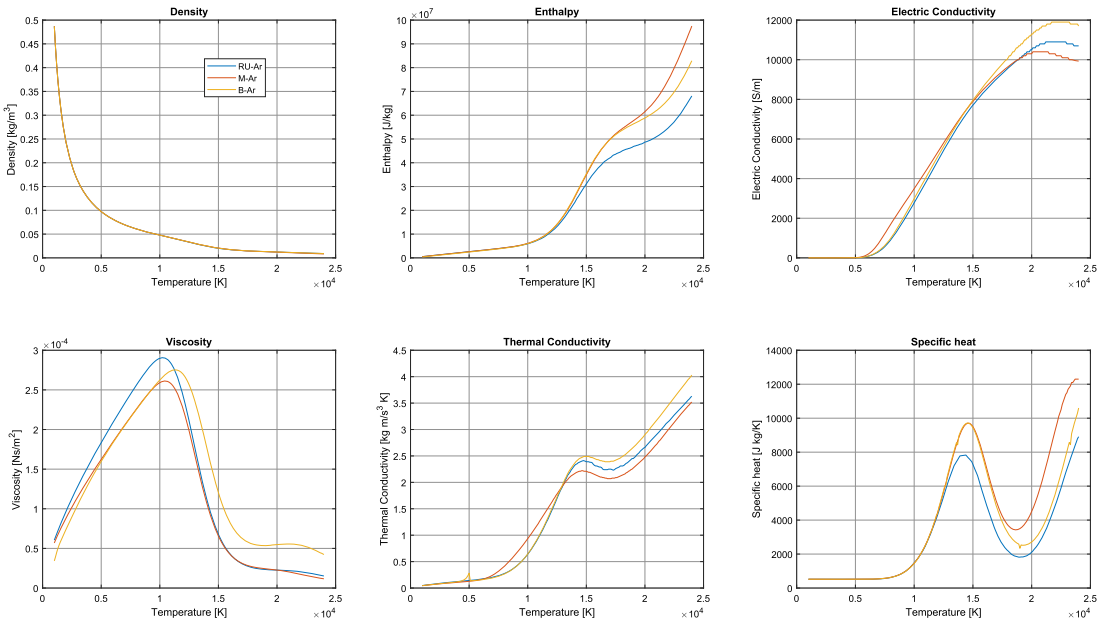

Fig. 3—Plasma properties for different argon plasma compositions. Blue is RU data, red is Mintek, and yellow is the Boulos (Color figure online).

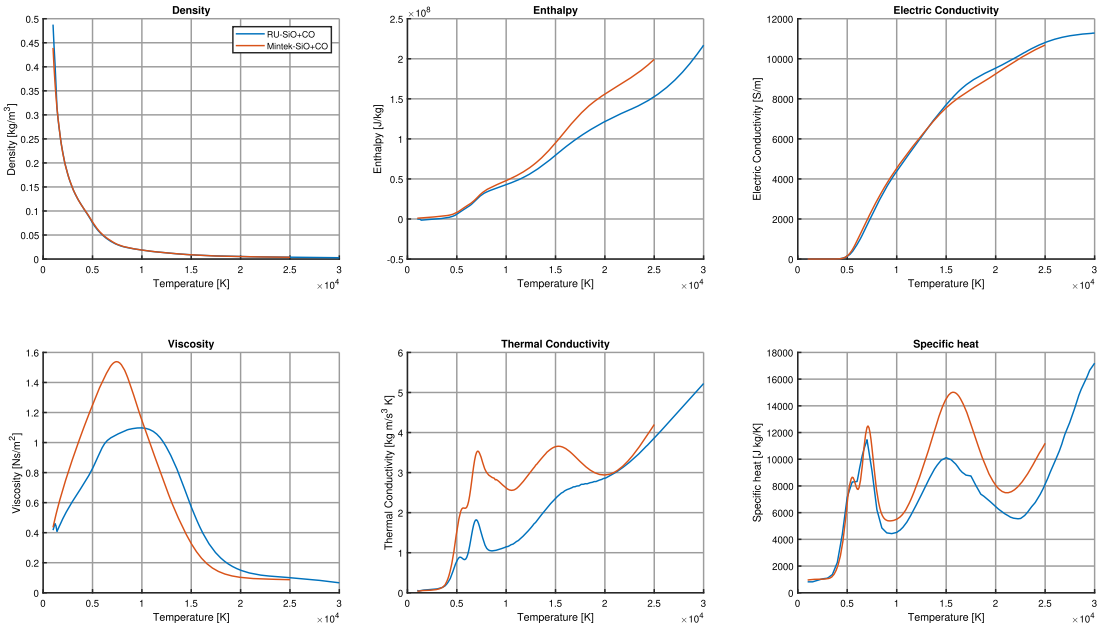

Fig. 4—Plasma properties for the industrial plasma compositions. Blue is RU data, red is Mintek (Color figure online).

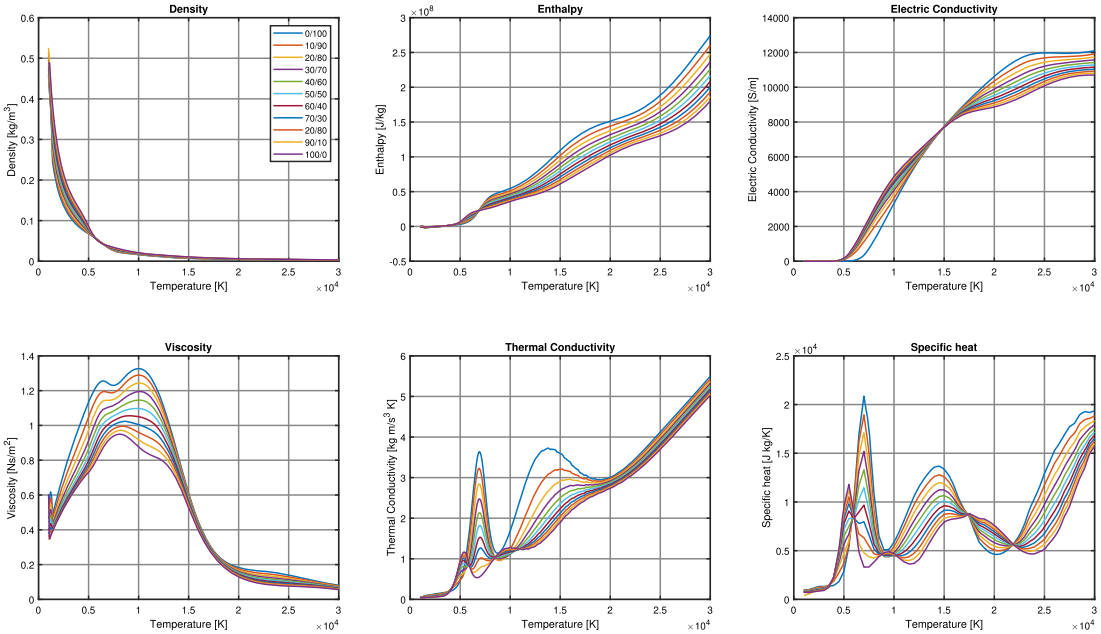

Fig. 5—Plasma properties for the different industrial plasma compositions from RU, here the ratio of SiO to CO varies from 0 to 100 pct.

III. MODEL DESCRIPTION

Detailed electric arc models are generally based on MHD, as this approach incorporates most of the relevant physics. To capture the momentum and heat transfer as well as the effect of the electromagnetic fields, Maxwell's equations are solved together with Navier Stokes and energy conservation equations. This results in a total of seven coupled partial differential equations.

The electromagnetic fields are governed by Maxwell's equations:

$$\nabla \cdot D = q \quad [1]$$

$$\nabla \times H - \frac{dD}{dt} = j \quad [2]$$

$$\nabla \cdot B = 0 \quad [3]$$

$$\nabla \times E + \frac{dB}{dt} = 0 \quad [4]$$

where $D = \epsilon_0 E$ is the flux density, $H = B/\mu_0$ is the magnetic field density, ϵ_0 is the electric permittivity, q is the electric charge, j is the current density, and μ_0 is the vacuum magnetic permeability.

Fluid flow is described using the Navier–Stokes equations for momentum conservation, and the continuity equation for mass conservation:

$$\frac{\partial \rho u}{\partial t} + \nabla \cdot (\rho u \otimes u) + \nabla P = \mu \nabla^2 u + j \times B \quad [5]$$

$$\frac{\partial \rho}{\partial t} + \nabla \cdot (\rho u) = 0 \quad [6]$$

Here ρ is the plasma density, u is the velocity field, P is the pressure field, u is the viscosity, j is the electric current density, and B is the magnetic field.

Heat transfer is described by the energy conservation equation. We have added extra terms on the right hand side to include the effects of electric current on the energy. The second term on the right is the electron energy transport term and the third is the ohmic heating. As most of the thermophysical properties of plasmas are strongly temperature dependent, this couples the energy equation tightly to the other components in the model. The general equation is:

$$\frac{\partial \rho h}{\partial t} + \nabla \cdot (\rho u h) = \nabla \cdot \kappa \nabla T + \nabla \cdot \left(\frac{5 k_B T j}{2q}\right) + \frac{j \cdot j}{\sigma} + Q_m - Q_R \quad [7]$$

Here h is the enthalpy field, κ is the plasma thermal conductivity, σ is the plasma electrical conductivity, k_B is the Boltzmann constant, and Q_R is the radiation energy loss term. Q_m includes all additional terms related to the mechanical contribution to the energy from compressibility effects.

Both models used in this paper aim to solve all of these equations, however, this is done in slightly different ways. In particular the model made by Reynolds[11] solves Eqs. [1] through [4] using a semi-explicit approach based on current conservation, and also uses simplified boundary conditions for the electric potential which define a fixed arc orientation between the electrode and work surfaces.

A. *New model implementation*

In the present work, we have developed a new MHD model implementation in the OpenFOAM-v2012®[12] open-source computational mechanics framework. We used a modified version of the standard rhoPimpleFoam solver as a base for our solver, given its existing capabilities for transient turbulent flow and heat transfer. A new MHD solver loop was added to the base code of the standard solver. For the implementation in OpenFOAM® simplifications for Eqs. [1] through [4] can be made by using the electric scalar potential ϕ and magnetic vector potential A:

$$\nabla \cdot j = 0 \quad \text{with} \quad j = -\sigma\left(\nabla\phi + \frac{\partial A}{\partial t} - u \times B\right) \quad [8]$$

$$\nabla^2 A = -\mu_0 j \quad \text{with} \quad B = \nabla \times A \quad [9]$$

With B and j, it is then possible to calculate the Lorentz force and the Ohmic heating source terms for the Navier–Stokes equation and the energy conservation equation. For each time step the electromagnetic calculation loop is iterated multiple times to increase the accuracy of the solution.

To account for the radiation heat transfer term we currently use OpenFOAM®'s built-in P1 radiation model. The main assumption of this model is that the directional dependence in the radiative transfer equation is integrated out, resulting in a diffusion equation for incident radiation. The model is described by:

$$\nabla^2(\Gamma, G) - aG = -4(e\sigma_{SB}T^4 + E) \quad [10]$$

where Γ is the diffusivity, G is the incident radiation intensity, a is the absorption coefficient, is the emission coefficient, T is the temperature, σ_{SB} is the Stefan–Boltzmann constant, and E is the emission contribution. The emission and absorption coefficients have been tabulated for different temperatures and pressure which are then input into the radiation model.

This model could, however, be changed out due to the modular nature of the solver it is possible to implement more detailed radiation models in the future. With the modifications above, we have a new MHD solver for OpenFOAM® called mhdRhoPimpleFOAM.

B. *Boundary Conditions*

In order to compare the two MHD solvers, we use the same conditions as described in Reference 11 with the exception of the electric potential ϕ. For this, we have created a new boundary condition for the MHD solvers which correctly identifies the surface that electrons are emitted from at any point in the AC cycle. As in previous work the electric potential boundary condition is based on the current density field on the emitting surface, which is set to the thermionic emission current j_k in computational cells where the temperature is the highest such that a specified total current is obtained. So, in cells where emission occurs, we have:

$$\frac{d\phi}{dn} = -\frac{j_k}{\sigma} \qquad [11]$$

In the new boundary condition, the arc is reversed by switching the emitting surface between the electrode and the work surface in order to simulate the change in voltage polarity at different points in the AC cycle. Figure 6 shows the boundary conditions for ϕ:

C. *Modeling Domain*

In order to compare the solvers and plasma data sets, simulations are run on two different geometries. The first replicates the Argon pilot furnace used for the experiments described in Reference 13 (Figure 7).

The second case is a representative geometry for an industrial-scale arc, and is constructed in such a way that it simulates part of the arc cavity in a submerged arc furnace. The upper boundary is the electrode material, the lower boundary is the work surface representing the silicon metal bath, and the sides are pressure boundaries open to inflow and outflow. Figure 2 shows which part of the cavity is being simulated.

The industrial case geometry is a cylinder with a height of 7 cm and a total radius of 30 cm. The domain height was chosen to represent a typical arc length for an operating furnace.[5,14] A 5 × 5 cm central area has a smaller mesh size to increase simulation accuracy in the arc area. In this region the dimensions of the boundary elements are 1.43 × 1.43 × 0.35 mm, with the element height gradually increasing closer to the middle of the domain. This is important due to the rapid spatial and temporal changes in the temperature field in and around the arc column during the simulation. The mesh inflation layers near the upper and lower boundaries permit better evaluation of local variations in the magnetic vector potential A in the electromagnetic field solution (Figure 8).

IV. MODELING RESULTS

A. *Verification and Validation Between Solvers for Argon Experiments*

As discussed earlier, experimental data from laboratory furnace experiments were used to verify and cross-validate our models. We compared measurement data from Reference 5 obtained from the pilot furnace experiment described in Reference 13 to simulations conducted with the two MHD models and the three Argon plasma property data sets. We observed minimal differences between the two solvers, but there was some significant variance between the different data sets. The results are shown in Figure 9 below. The measurements from the actual furnace show somewhat more chaotic behavior than all the simulations, but a similar trend can easily be observed. We can therefore say that the solvers are working as desired and conform acceptably well to measurements and to each other for this known case.

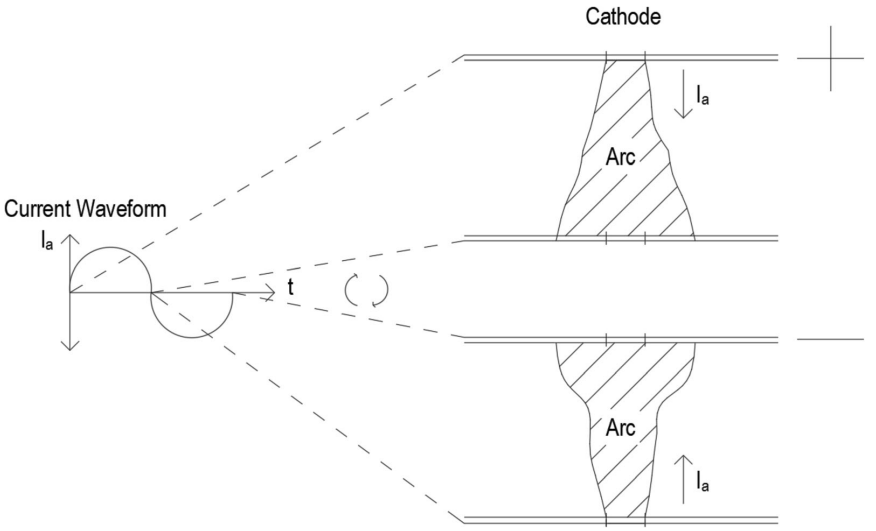

Fig. 6—The arc changes direction using the new boundary conditions for the voltage potential Φ.

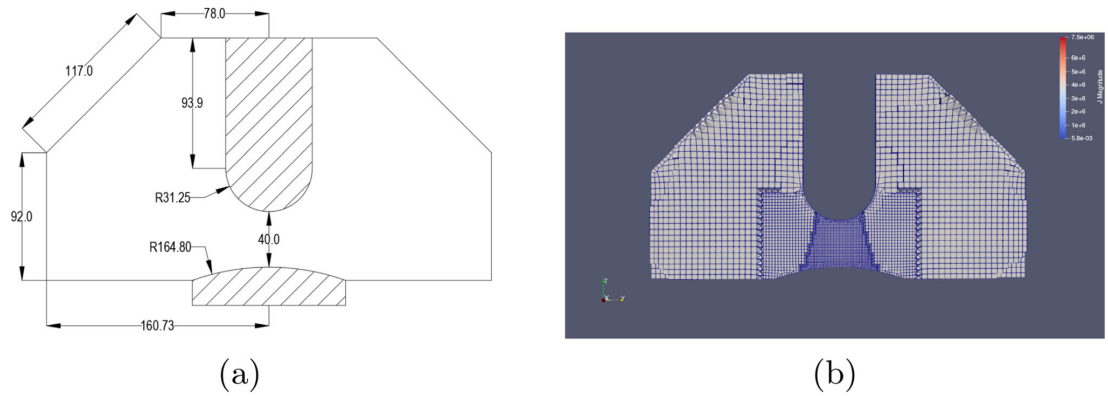

Fig. 7—(*a*) The argon furnace geometry in mm, (*b*) The mesh of the argon furnace.

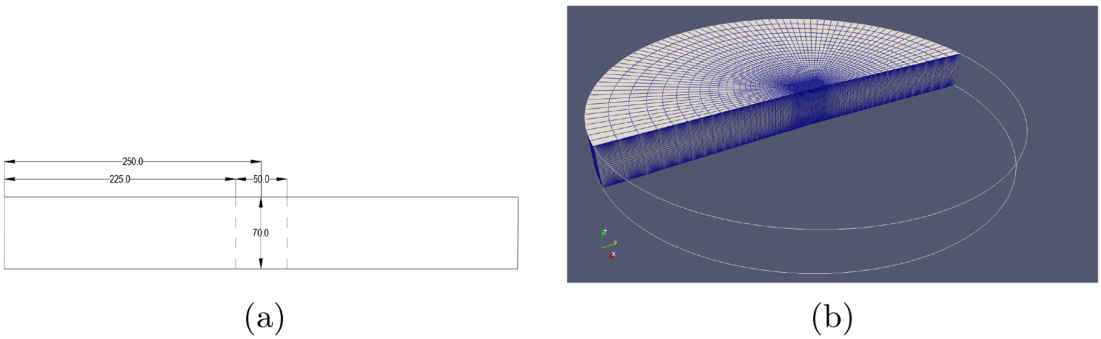

Fig. 8—(*a*) The Industrial furnace geometry in mm, (*b*) A visual representation of the mesh used in the simulation of the industrial case.

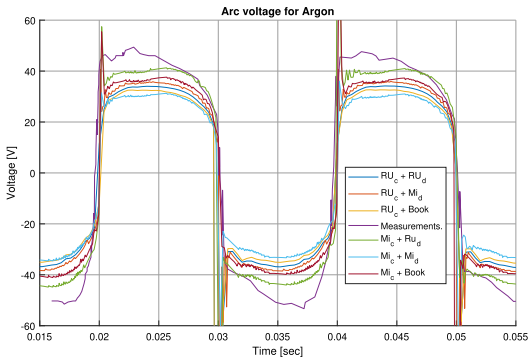

Fig. 9—Arc voltage of the three different argon plasma data sets, run with both solvers. Measurements data is plotted in purple (Color figure online).

We can, however, see that the different data sets give slightly differing results. The voltage varies from around 40 to 30 V for different data sets, or approximately 25 pct.

This difference can be attributed in part to the substantial deviations in calculated electrical conductivity of Argon plasma between 5000 and 10000 K which can be seen in Reference 3. This temperature range is very significant for the bulk of the conducting volume of the arc, and changes in plasma properties here can have a disproportionate effect on the macroscopic electrical behavior.

B. *Mesh Dependence for the Industrial Case*

The simulations for the industrial case were observed to have a large amount of noise during the transition from zero to top current. A simple mesh dependence study was performed to check if this was due to numerical or physical issues. We both reduced and increased the mesh element size from 2 to 1.1 mm, respectively, to see if that would be a noticeable change in the behavior of the noise as well as the final result. Figure 10 show the results for the mesh study and we can see that the noise appears to be dependent on mesh resolution, but the final values of the arc voltage vary only a little.

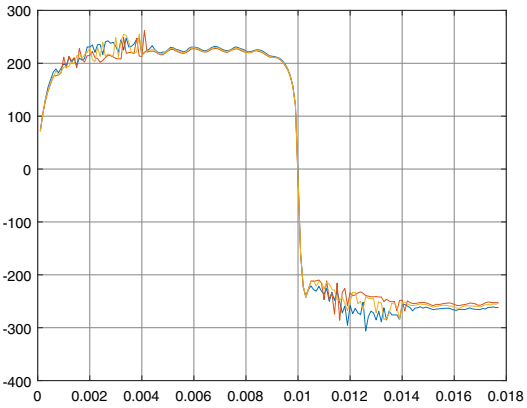

Fig. 10—Arc voltage of the three different mesh densities. The noise seems to be dependent on the mesh not the physical parameters and the final result changes little between meshes.

C. *Verification Between Solvers for Industrial Case*

With this set of cases, the aim was to test if the different solvers produce similar results at higher currents representative of industrial-scale operation. The most likely plasma composition, a 50 pct mix of SiO and CO, was used. The current has an amplitude of 50 kA, and for the boundary condition of ϕ we use the current density $j_k = 2.0 \times 10^7 A/m^2$. We can see on Figure 11 the arc voltage for both solvers and both data sets. We observed a good fit between the solvers and the data but with small differences, somewhat less than for the previous argon case. The Mintek plasma property data gives a slightly lower voltage than the RU one, and similarly for the solvers. When the RU solver is running on Mintek data and vice versa, the models produce similar results. The voltage is higher than expected from industrial silicon smelting operations, but it is likely that this is due to the oversimplified cathode boundary condition being used here; implementation of a physically realistic cathode model as seen in Reference 15 may improve matters. The simplicity of the radiation model used is also likely to be a contributing factor, as this may be exaggerating energy losses from the arc column resulting in a cooler and less conductive plasma.

D. *Effect of Plasma Composition in Industrial Case*

In this set of tests the aim was to investigate how the arc voltage in the industrial case would change with different plasma compositions. As mentioned above we varied the composition from 0 to 100 pct SiO in the SiO–CO mixture to get an indication of how the corresponding arc voltage would change; this could then be used to estimate changes in furnace conditions in a real furnace. The resulting arc voltages are shown in Figure 12. We can see that the voltage changes from approximately 263 to 240 V. This is a small variation of only roughly 8 pct—we can therefore say that changes in the composition of the arc plasma will not significantly impact the voltage in a operating silicon SAF unless the furnace transformer is constrained at or near its current or voltage limits. It is also interesting to observe that the voltage increases only when relatively low fractions of SiO are present in the arc plasma. These composition ranges are, however, not likely to occur in a live furnace. This suggests that increased furnace resistance may be more strongly correlated with upsets in the metallurgical process rather than normal operation.

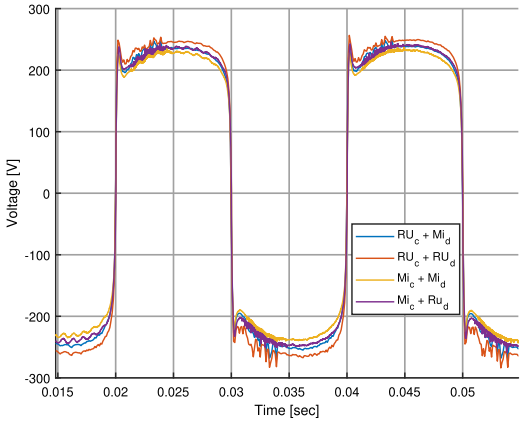

Fig. 11—Arc voltage for the industrial case where the SiO to CO ratio is 50/50. Here both solvers are used and both data sets for the plasma. (*a*) shows the larger waveform and (*b*) Zooms in on one of the tops.

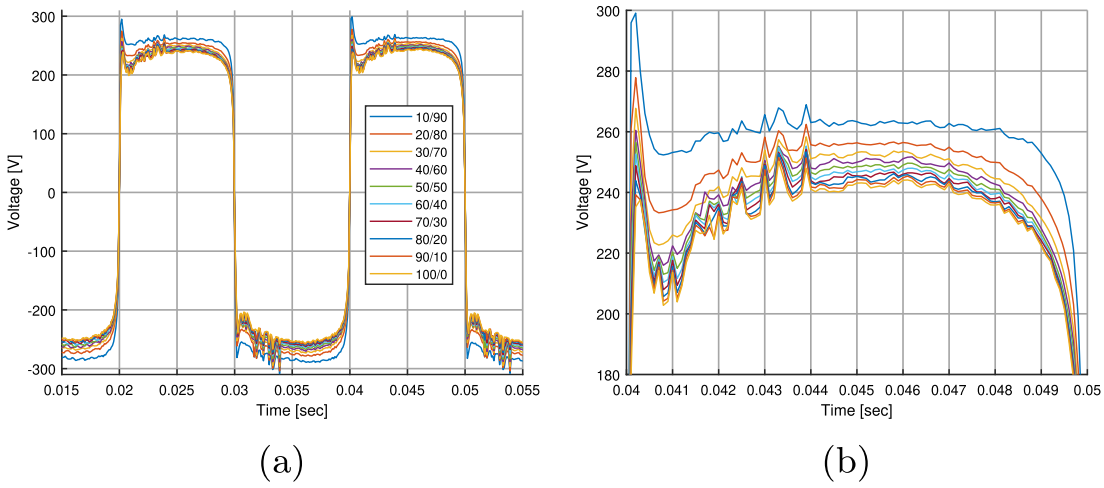

Fig. 12—Arc voltage of the ten different SiO / CO ratios of plasma data sets, run with the RU solver. (*a*) shows the larger waveform and (*b*) Zooms in on one of the tops.

V. CONCLUSION

We investigated the effect of changing compositions on the plasma gas present in a silicon submerged arc furnace using a selection of different plasma property data sets and MHD models. We have validated the models using a known geometry of an Argon furnace for which measurement data was available, we use three different data sets for argon gas for this purpose. All model and data set combinations gave qualitatively acceptable results for the argon furnace geometry, although some differences in predicted voltage were observed. This is most likely due to discrepancies in the Argon plasma electrical conductivity between data sets.

To test the models at industrial current levels we used a 50/50 mixtures of SiO and CO plasma gas, and compared the results obtained from various combinations of MHD models and plasma property data sets. The results were found to be acceptably close to each other, although we did observe the voltages to be somewhat high compared to what we would expect from real furnace operations. This is likely due to lack of detail in the modeling used, in particular the simplified thermal radiation sub-model or the arc might be to long.

Finally, the models were used to study how different mixtures of the two gases in the furnace can impact the electrical behavior of the arc. A variation of 8 pct in the peak voltage was observed, with CO-rich compositions producing more resistive arcs with higher voltages.

Some problems were encountered with the models, especially related to the formulation of the cathode boundary conditions and the radiation sub-models. Inconsistencies in the plasma data sets were also observed, and can produce significant differences in the end results. These issues will need to be given attention in future work, but overall the two MHD models tested were seen to be acceptably consistent and accurate for simulating arcs in industrial processes. We also have an improved understanding of the importance of input parameters when simulating electric arcs, and that care is needed when choosing plasma property data sets for such high temperatures.

ACKNOWLEDGMENTS

The Icelandic Research Fund is greatly acknowledged for their funding of this work. This paper is published by permission of Mintek. The authors acknowledge the Centre for High Performance Computing (CHPC), South Africa, for providing computational resources to this research project.

CONFLICT OF INTEREST

On behalf of all authors, the corresponding author states that there is no conflict of interest.

FUNDING

Open access funding provided by NTNU Norwegian University of Science and Technology (incl St. Olavs Hospital - Trondheim University Hospital).

REFERENCES

1. M. Tangstad, L. Kolbeinsen: Metal Production in Norway. Akademika Publishing. OCLC: 866576889, 2013.
2. A. Alzate, J. Durango, A. Mejia: in: 2010 IEEE ANDESCON, pp. 1–6, 2010. https://doi.org/10.1109/ANDESCON.2010.5629655.
3. S. Golestani, H. Samet: *IET Gener. Trans. Distrib.* vol. 10 (13), pp. 3364–73, 2016. https://doi.org/10.1049/iet-gtd.2016.0405.
4. H. Haraldsson, Y.A. Tesfahunegn, M. Tangstad, G. Sævarsdottir: *SSRN J.*, 2021. https://doi.org/10.2139/ssrn.3927158.
5. G. Saevarsdottir, H. Larsen, J. Bakken: *Int. Quart. High-Technol. Plasma Processes*, 1999, vol. 3, pp. 1–15. https://doi.org/10.1615/HighTempMatProc.v3.i1.10.
6. Q.G. Reynolds: *JOM: J. Miner. Metals Mater. Soc.*, 2017, vol. 69 (2), pp. 351–57. https://doi.org/10.1007/s11837-016-2166-9.
7. A.D. Rocca, Q.G. Reynolds: large-eddy simulations of electric arcs at industrial scale, 2019. https://doi.org/10.13140/RG.2.2.24803.71209.
8. J.A. Bakken, L. Gu, H.L. Larsen, V.G. Sevastyanenko: *J. Eng. Phys. Thermophys.*, 1997, vol. 70 (4), pp. 530–43. https://doi.org/10.1007/BF02663569.
9. G. Scevarsdottir, J. Bakken, V.G. Sevastyanenko, L. Gu: *High Temp. Mater. Processes*, 2011, vol. 15, pp. 205–25. https://doi.org/10.1615/HighTempMatProc.v15.i3.40.
10. S. Documentation: MathWorks, 2020. https://www.mathworks.com/products/simulink.html.
11. Q.G. Reynolds: in: *Proceedings of the 14th International Conference on CFD in Oil & Gas, Metallurgical and Process Industries*, pp. 99–106, 2007.
12. OpenFOAM. https://www.openfoam.com/ Accessed 22 April 2024.
13. H.L. Larsen, G. Liping, J.A. Bakken, J.K. Tuset, I.G. Page, H. Tveit: in *International Ferroalloys Congress; 7th, Norwegian Ferroalloy Research Organization*. Backup Publisher: Norwegian Ferroalloy Industry, pp. 517–528, 1995. https://www.tib.eu/de/suchen/id/BLCP.
14. G. Saevarsdottir, T. Magnusson, J.A. Bakken: Electric arc on a coke bed in a submerged arc furnace, 2007. https://api.semanticscholar.org/CorpusID:224792531.
15. G. Saevarsdottir, M.T. Jonsson, J. Bakken: in: *16th International Symposium on Plasma Chemistry*, 2003.

Paper V

Silicon for the chemical and solar industry XVII
Edited by M.Tangstad, H.Rong, A.Valderhaug, B.Andresen and I.G.Page
Trondheim, 10-13-September 2024

Modelling of Industrial electric arcs with changing plasma compositions and arc lengths

Hákon Valur Haraldsson[1,2], Yonatan A. Tesfahunegn[1], Merete Tangstad[2] and Gudrun Saevarsdottir[1,2]
[1] Department of Engineering, Reykjavík University, Iceland, hakonh12@ru.is
[2] Department of Materials Science and Engineering, Norwegian University of Science and Technology, Norway.

Keywords: Electric Arc, MHD, Modelling, Plasma, Composition

ABSTRACT

Electric arcs are an important heat source in submerged arc furnaces (SAFs), for silicon production. They are therefore of great interests for study so the production process, which is very complex, can be improved and made more efficient. Modelling of industrial arcs is a Multiphysics process that involves simultaneously solving several coupled physical phenomena, such as electromagnetics, fluid dynamics and heat transfer, including radiative heat transfer from the plasma arc. Coupling fluid dynamics and electromagnetics is known as Magnetohydrodynamics (MHD). A MHD model developed by the authors is used to simulate an alternating current arc with different plasma gas compositions with varying ratios of silicon monoxide and carbon monoxide as well as to investigate the effect of varying of the arc length at each of the composition ratios. These physical properties for these compositions are calculated using specialized code since no measurements exist at the temperatures present in the arc.

1. INTRODUCTION

Silicon and ferrosilicon alloys are typically produced in a submerged arc furnace (SAF), a large electric smelting vessel. Essentially, the furnace uses electricity and the energy from carbon-based materials to create heat, melt and chemically react with raw materials to yield usable metals. The electrodes, conducting the electric current, are submerged in a deep bed of raw material in the furnace, with heat provided by plasma arcs and resistive heating at the electrode tips. The electric arc is crucial for separating silicon from oxides in silicon and ferrosilicon production. During these processes, a significant portion of the current flows through the arc, burning in a cavity or "crater" around the electrode tips filled with gas. The crater forms due to the high viscosity of melted quartz (SiO_2) and the formation of solid silicon carbide (SiC) crust. Liquid silicon gathers in a pool beneath the arcs and is drained into ladles through tap-holes in the furnace walls. The exceptionally high temperatures, surpassing 10,000°C in and around the arc, provide the energy required for chemical reactions, transforming solid SiO_2 and SiC into liquid silicon metal and CO gas (Tangstad and Kolbeinsen, 2013).

The silicon making process happens in a very hostile environment that is deep inside the furnace and is, therefore, very difficult to observe or measure directly in any way, figure 1 below. This can be partly remedied by use of simulations to help estimate the conditions inside the furnace and more importantly in the arc cavity (Haraldsson et al., 2021). Simple models used are empirical ones, generally Cassie-Mayr models (Golestani and Samet, 2016)

or similar. Models that contain some physical aspects, but are still heavily numerical, are for example the Channel arc model (Saevarsdottir et al., 1999) and then there are fully physical models that take into account the full range of physics, the magnetohydrodynamic (MHD) models (Bakken et al., 1997; Reynolds, 2020; Saevarsdottir, 2002), which are generally considered the most accurate.

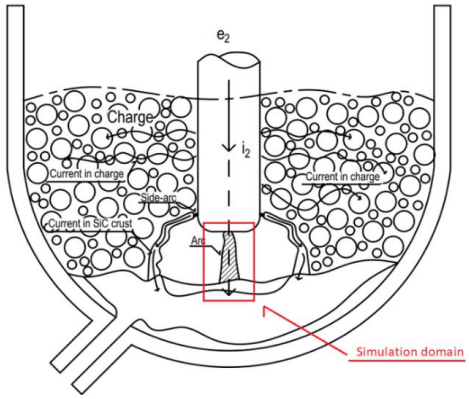

Figure 1: The simulation domain for our MHD models is directly below the electrode in SAF..

In this study we will investigate what effect varying the arc plasma composition and length will have on the arc voltage behaviour. This is a continuation on previous work on plasma compositions that is being published, but here we will change the length of the arc. We will use a MHD model that has been developed in OpenFOAM-v2012® ("OpenFOAM," 2023) to simulate an industrial AC arc of 50 kA peak current, for 5 different compositions of plasma as well as 3 variations in arc length to investigate the changes in the Arc voltage. The composition of SiO:CO gas goes from low to high SiO content in five steps. This is done to simulate extreme cases that will only happen very rarely in a furnace but will give us an idea of how input parameters affect the simulation results.

2. Modelling description

The electric arc physics can be modelled based on MHD, since this approach incorporates most of the physics present in the problem. To capture the momentum and heat transfer as well as the effect of the electromagnetic fields, Maxwell's equations are solved together with the Navier Stokes and energy conservation equations for a total of seven coupled partial differential equations. The electromagnetic fields are governed by Maxwell's equations:

$$\nabla \cdot \vec{D} = q \quad [1]$$

$$\nabla \times \vec{H} - \frac{d\vec{D}}{dt} = \vec{j} \quad [2]$$

$$\nabla \cdot \vec{B} = 0 \quad [3]$$

$$\nabla \times \vec{E} + \frac{d\vec{B}}{dt} = 0 \quad [4]$$

Where $\vec{D} = \epsilon_0 \vec{E}$ is the flux density, $\vec{H} = \vec{B}/\mu_0$ is the magnetic field density, ϵ_0 is the electric permittivity, q is the electric charge, $\vec{j}$ is the current density, and μ_0 is the vacuum magnetic permeability. Velocity and pressure fields are governed by the Navier Stokes equations, with a source term describing the Lorentz force to connect them to the electromagnetic field:

$$\frac{d\rho}{dt} + \nabla \cdot (\rho \vec{u}) = 0 \quad [5]$$

$$\frac{d\rho\vec{u}}{dt} + \rho(\nabla \cdot \vec{u})\vec{u} = \nabla p - \nabla \tau + \left(\vec{j} \times \vec{B}\right) \quad [6]$$

Here ρ is the mass density, $\vec{u}$ is the velocity, p is the pressure, τ is the viscous pressure tensor, and $\left(\vec{j} \times \vec{B}\right)$ represents the Lorentz force. Temperature is governed by the energy conservation equation. As most of the thermophysical properties of plasmas are strongly temperature dependent, this couples the energy equation tightly to the other components in the model. The general equation is:

$$\frac{d\rho h}{dt} + \rho(\vec{u} \cdot \nabla h) = \nabla \cdot \lambda \nabla T + + \frac{j^2}{\sigma} + \frac{5k_B}{q}\vec{j} \cdot \nabla T - Q_R \quad [7]$$

Here h is the specific enthalpy, T is the temperature, k_B is the Boltzmann constant, λ is the effective turbulent thermal conductivity, and Q_R is the radiation term. The second and third terms in the equation represent Ohmic heating by the passage of electric current, and the transport of thermal energy by electrons.

The MHD solver we use in this study has been created in OpenFOAM to solve the above equations in a modified turbulent and transient solver already present with the software, called *rhoPimpleFoam*. The electromagnetic equations 1 – 4 are simplified using the electric scalar potential ϕ and the magnetic vector potential $\vec{A}$:

$$\nabla \cdot \vec{j} = 0 \quad with \quad \vec{j} = -\sigma \left(\nabla \phi + \frac{\partial \vec{A}}{\partial t} - \vec{u} \times \vec{B} \right) \quad [8]$$

$$\nabla^2 \vec{A} = -\mu_0 \vec{j} \quad with \quad \vec{B} = \nabla \times \vec{A} \quad [9]$$

It is now possible to calculate the Lorentz force and the Ohmic heating terms for the Navier-Stokes equation and the energy conservation equation, by using $\vec{j}$ and $\vec{B}$. The new MHD part of the solver is iterated multiple times per times step to help with convergence. Currently, the solver uses a built in P-1 radiation model that is supplied with OpenFOAM. This model underestimates the radiation and will be replaced in future versions of the solver. We call this new solver *mhdRhoPimpleFoam*. A more detailed description of the implementation is under publication in different journal.

2.1 Modelling Parameters

In this study we are using different molar ratios of $SiO_{(g)}$ + $CO_{(g)}$ for the plasma gas present in the arc cavity Previous works indicate that temperatures in the cavity should be between 2000 K outside the arc up to 30000 K inside it. Varying the ratio will change the physical properties of the gas considerably and this should allow us

to investigate its effects on the arc behaviour. One of the problems with investigating arcs in an industrial setting is the lack of data on the gas, this data has been obtained by special software (Liping, 1993) and can be seen below in figure [2]. The plasma property data used as input for the simulations are the enthalpy h, density ρ, electric conductivity σ, thermal conductivity κ and, Specific heat C_p.

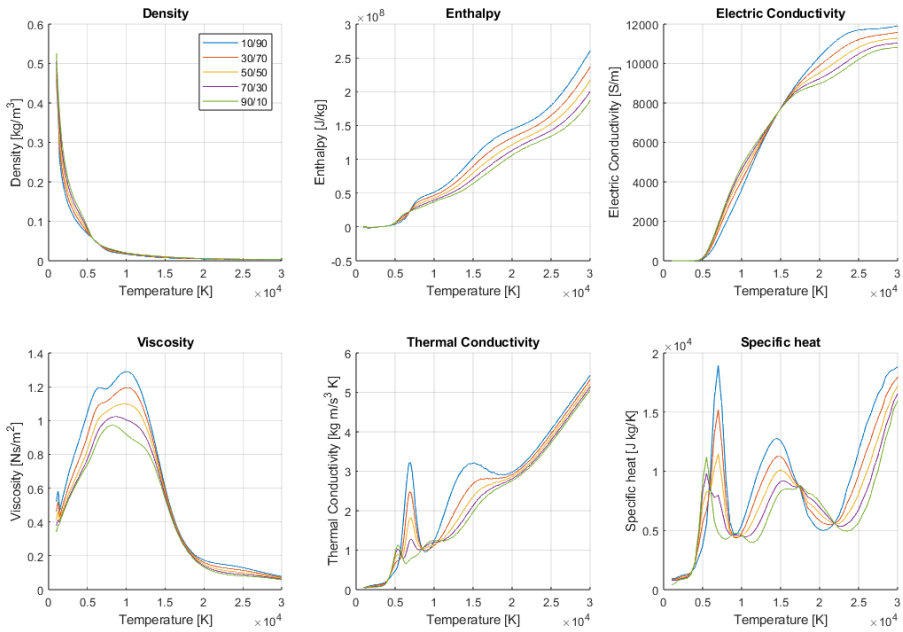

Figure 2: Plasma properties for the different molar ratios of gas. In the legend 10/90 stands for 10% SiO(g) and 90% CO(g) for example.

For the simulation it is important to note the main parameters for the boundary conditions. The temperature boundary is set to the sublimation point of the materials in question 4100 K for the carbon electrode and 3000 K for the anode. We assumed the anode to be liquid silicon in this case, some sources indicate that the liquid silicon is pushed to the sides by pressure from the arc and that the anode should be made up of SiC + FeSi material but for this study we used this simplification. The electric potential ϕ (the voltage) is set by picking the max current density j_k, here $2.0x10^7\ A/m^2\ is\ used$, and then we divide that by the conductance σ at the surface:

$$\phi = -\frac{j_k}{\sigma} \qquad [10]$$

2.2 Modelling Domain

The geometry used represents the part of the arc cavity that is of most interest. The upper boundary is the electrode material, the lower boundary is the work surface representing the silicon metal bath, and the sides are pressure boundaries open to inflow and outflow. Figure [1] shows what part of the cavity is being simulated.

We consider three cases with different arc length (height) values, 4, 7, and 10 cm, with a domain radius of 30 cm. In total three models were constructed that correspond to the three arc lengths. These heights should allow us to investigate most of the possible act lengths that can be assumed to be present in a real furnace (Saevarsdottir et al., 1999, 2007). A 5 x 5 cm central area has a smaller mesh size to increase simulation accuracy in the arc area, the dimensions of the surface elements are 2.0 x 2.0 mm, and the depth is 0.49 mm but gets gradually larger closer to the middle. This is important due to the rapid spatial and temporal changes in the temperature field in and around the arc column during the simulation.

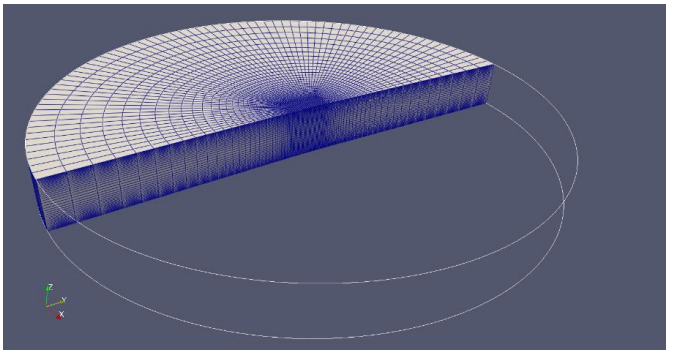

Figure 3: A visual representation of the geometry mesh used in for the simulations.

The simulations for the industrial case were observed to have a large amount of noise during the transition from zero to top current. A simple mesh dependence study was performed to check if this was due to numerical or physical issues. We reduced the mesh element size from 2 mm to 1.1 mm in two steps to see if that would be a noticeable change in the behaviour of the noise as well as the result. We observed that the noise appears to be mostly dependent on the mesh size and that the final voltage results did not change noticeably between the three meshes.

3. Modelling results

The main parameter we are looking at for the results is the Arc voltage and how it behaves for the different conditions. We ran a total of 15 cases where the arc was simulated for a total of 0.08 seconds in simulation time, or 4 periods for 50 Hz AC current. The arc current is set to 50 kA peak to peak AC, which close to the expected range in an industrial furnace but is quite a high current for MHD simulations. We observed that the arc voltage seams to be most dependent on the arc length, but the plasma composition does also have a small effect on the outcome. Figure [4] below shows the results for the arc voltage for all the runs. We can see that the different composition runs cluster around each other for each length.

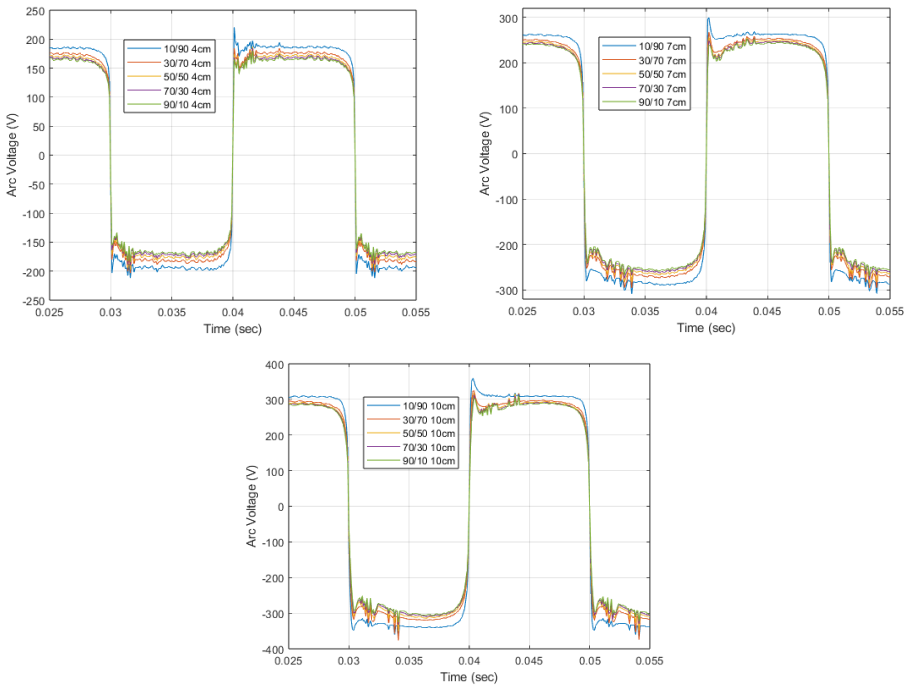

Figure 4: Arc voltages for the 15 simulations for all 5 compositions and 3 lengths. Sorted based in arc length.

To make some practical sense of the results normalized the RMS voltage for all the runs, see figure [5]. The voltage is normalized to the centre value or 50% $SiO_{(g)}$ and 7 cm arc length since this is the simulation case that is in the middle of the chosen parameters. We can then observe how much the voltage varies from that value; this should help in estimating what conditions are present in any furnace as long as the normal operating value for the arc voltage is known. This will of course vary from furnace to furnace.

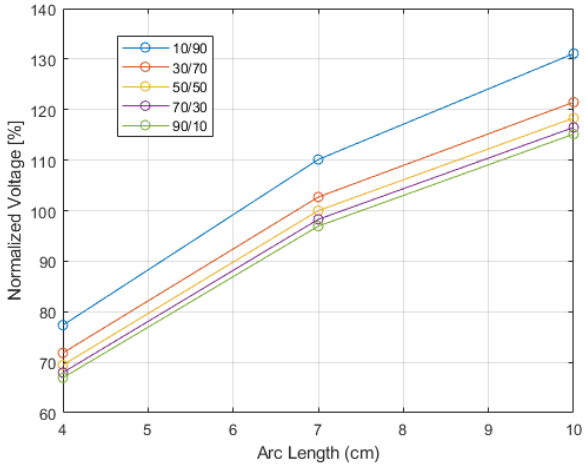

Figure 5: The normalized RMS arc voltages for all simulations, shows the effect of length and composition on the results.

What we can see from the results is that the voltage increases with length and decreasing SiO amount in the cavity. The arc length changes the voltage by about 50% while the composition changes it by about 10% – 15%. This makes it obvious that the length has the most impact on the voltage.

4. CONCLUSIONS

We have simulated an industrial arc of 50 kA by using a MHD model for five different plasma gas compositions and three arc lengths. We observed that the arc voltage varies mostly due to the length of the arc but also slightly based on the composition of the plasma.

It seems that industrial arcs operating under ideal conditions are not very affected by the exact composition present in the plasma, this is perhaps due the high current that drives the arc. Further investigation into the reason for this should be conducted and further simulations at both higher and lower currents are warranted, as well as more detailed modelling of the anode material.

ACKNOWLEDGEMENTS

The Icelandic Research Fund is greatly acknowledged for their funding of this work.

5. REFERENCES

Bakken, J.A., Gu, L., Larsen, H.L., Sevastyanenko, V.G., 1997. Numerical modeling of electric arcs. J Eng Phys Thermophys 70, 530–543. https://doi.org/10.1007/BF02663569

Golestani, S., Samet, H., 2016. Generalised Cassie–Mayr electric arc furnace models. IET Generation, Transmission & Distribution 10, 3364–3373. https://doi.org/10.1049/iet-gtd.2016.0405

Haraldsson, H., Tesfahunegn, Y.A., Tangstad, M., Sævarsdottir, G., 2021. Modelling of Electric Arcs for Industrial Applications, a Review. SSRN Journal. https://doi.org/10.2139/ssrn.3927158

Liping, G., 1993. Transport phenomena in silicon vapour infiltrated argon arcs and anodic metal pools. The Norwegian Institute of Technology, Trondheim, Norway.
OpenFOAM [WWW Document], 2023. URL https://www.openfoam.com/ (accessed 4.22.24).
Reynolds, Q.G., 2020. Toward computational models of arc dynamics in silicon smelters, in: Proceedings of the 14th International Conference on CFD in Oil & Gas, Metallurgical and Process Industries, International Conference on CFD in Oil & Gas, Metallurgical and Process Industries. Presented at the 14th International Conference on CFD in Oil & Gas, Metallurgical and Process Industries, SINTEF Academic Press, Trondheim, Norway, pp. 99–106.
Saevarsdottir, G., Larsen, H., Bakken, J., 1999. Modelling of industrial AC-arcs. High Temperature Material Processes (An International Quarterly of High-Technology Plasma Processes) 3, 1–15. https://doi.org/10.1615/HighTempMatProc.v3.i1.10
Saevarsdottir, G.A., 2002. High current AC arcs in silicon and ferrosilicon furnaces. (Doctoral thesis). Norges teknisk-naturvitenskapelige universitet.
Saevarsdottir, G.A., Magnusson, T., Bakken, J.A., 2007. Electric Arc on a Coke Bed in a Submerged Arc Furnace, in: INFACON XI 2007: Innovations in the Ferroalloys Industry. Presented at the 11th International Ferroalloys Congress INFACON XI, IFAPA, New Delhi, India, pp. 572–582.
Tangstad, M., Kolbeinsen, L., 2013. Metal production in Norway. Akademika Publishing, Oslo.

Hákon Valur Haraldsson

PhD student, Reykjavík University

Hákon received a BSc degree in applied electrical engineering from Reykjavik University in 2017, a MSc degree in electrical energy engineering at the same university and is now working on a PhD in MHD modelling of AC electric plasma arcs in SFAs. He did his bachelors thesis on Field emission in micro vacuum devices and his master thesis in on large scale simulations of the Icelandic power system in relation to electric vehicles. Current research interests are in electron emission modelling, impact of electric vehicles, power system simulation and CFD modelling.
